Title

System-level performance investigation of eVTOL concepts using large-scale DEP-focused design optimizations

Author

Ha, Tae

Publication Date

2020

Peer reviewed|Thesis/dissertation

UNIVERSITY OF CALIFORNIA SAN DIEGO

System-level performance investigation of eVTOL concepts using large-scale DEP-focused design optimizations

A thesis submitted in partial satisfaction of the
requirements for the degree of Master of Science

in

Engineering Sciences (Mechanical Engineering)

by

Tae Hyun Ha

Committee in charge:

Professor John T. Hwang, Chair
Professor Thomas R. Bewley
Professor Robert R. Bitmead

2020

The thesis of Tae Hyun Ha is approved, and it is acceptable in quality and form for publication on microfilm and electronically:

____

____

____
Chair

University of California San Diego

2020

TABLE OF CONTENTS

LIST OF FIGURES

LIST OF TABLES

ACKNOWLEDGEMENTS

I would like to acknowledge Professor John T. Hwang for his support as chair of my committee and director of the Large-Scale Design Optimization (LSDO) Lab. None of this would be possible without his guidance and efforts.

I would also like to gratefully acknowledge support from Hyundai Motor Company (HMC). The committee chair also served as a consultant for HMC. The terms of this arrangement have been reviewed and approved by the University of California San Diego in accordance with its conflict of interest policies.

Chapter 3 section 5.2 in full, is currently being prepared for submission for publication of the material. Ruh, Marius; Hwang, John T. The thesis author was not the primary investigator and author of this material.

Chapter 3 section 6, in full, is currently being prepared for submission for publication of the material. Ivanov, Alex; Joshy, Anugrah J; Hwang, John T. The thesis author was not the primary investigator and author of this material.

Chapters 4 through 5, in full are currently being prepared for submission for publication of the material. Ha, Tae; Hwang, John T. The thesis author was the primary investigator and author of this material.

ABSTRACT OF THE THESIS

System-level performance investigation of eVTOL concepts using large-scale DEP-focused design optimizations

by

Tae Hyun Ha

Master of Science in Engineering Sciences (Mechanical Engineering)

University of California San Diego, 2020

Professor John T. Hwang, Chair

Urban air mobility is a new form of aviation that holds potential to transform commuting options in congested cities. Electric vertical takeoff and landing (eVTOL) concepts are well-suited as design choices for this field considering noise, space, and environmental benefits. This thesis demonstrates the development and application of two large-scale multidisciplinary design optimization (MDO) formulations for system-level performance investigation of eVTOL concepts using distributed electric propulsion (DEP). DEP benefits are explored through a *layout* MDO formulation that focuses on rotor placement and positioning, while a *refined* MDO formulation utilizes a 3-D geometry for physics-based modeling to incorporate propeller-wing interactions. Using Uber's eCRM-002 as a baseline design, the configuration and modifications are optimized at multiple operating conditions simultaneously, where the sizing depends largely on motor-inoperative failure cases implemented. Initial testing shows a decrease in performance when increasing rotor number; however, changing one set of rotors to be capable of tilting for both cruise and hover thrust capabilities shows potential to increase performance depending on the tilt rotor's position. Large-scale design optimization shows promise through these methods as a tool for investigating the designs of eVTOL concepts.

Chapter 1

Introduction

Research on electric aircraft has been increasing steadily for the past few years. From 2006 to around 2009, roughly one paper per year was being published concerning electric and hybrid electric aircraft design and analysis, while from 2015 to 2018, this number rose to nearly 20 per year [7]. The advantages of electric aviation are largely environmental benefits, as emissions are lower, overall efficiency of the propulsion system is multiple times higher, and noise is lower with electric motors.

The energy densities of today's batteries present a bottleneck for electric aircraft in terms of the limits they impose on range. With current-generation batteries, pure electric propulsion is not feasible for regional airliners and larger commercial aircraft due to range limitations. Hybrid-electric propulsion has the potential to increase the range to an acceptable level, but it introduces complexity and loses some of the benefits of electric propulsion, e.g., simplicity, reliability, and lower maintenance costs. As a result, much of the initial research in electric aviation focuses on urban air mobility (UAM), which is the transportation of people, goods, and services within a city using 1-4 passenger aircraft. Vertical takeoff and landing (VTOL) capability is critical for UAM, giving rise to the term, eVTOL.

There is a wide range of eVTOL concepts being considered for UAM. Given that concepts, technologies, and operational models are evolving simultaneously for UAM, a rapid computational design capability is especially beneficial. One approach is multidisciplinary design optimization (MDO), which has been an active field of research for over two decades [10]. MDO refers to the use of numerical optimization, which is the minimization of an output with respect to design variables subject to constraints. Within the field of MDO, large-scale system design optimization (LSDO) methods focus on optimization problems of high-dimensionality, where gradient-based optimization algorithms are necessary for efficient scalability, with system-level models that are typically multidisciplinary.

This thesis aims to accomplish three research objectives:

1. Develop a method for large-scale MDO of eVTOL concepts capable of exploring redundancy benefits through strict rotor *layout* comparisons that highlight design features

2. Develop a more *refined* method for large-scale MDO of eVTOL concepts using higher-fidelity models paired with a 3-D geometry to obtain designs based on results with increased validity

3. Explore the effects and determine which rotor layout design changes will potentially yield benefits for maximizing range capabilities

The thesis begins with a review on the current literature surrounding multidisciplinary design optimization use for electric aircraft and current eVTOL analysis studies and tools. After, I cover the different disciplines integrated in the upcoming optimization formulations and the models used to represent them. I then introduce the methodology approach and problem formulations along with the configuration layouts that will be used for testing. Lastly, I present the optimization results and conclusions made using the two optimization formulations.

Chapter 2

Literature Review

In this chapter, I review previous literature and studies that serve as the motivation for the work accomplished in the thesis.

eVTOL capabilities for UAM

First, I discuss eVTOL capabilities and its potential use for UAM. Thipphavong [34] et al. address several considerations that need to be taken into account for three stages of UAM integration based off of operational maturity. Among these considerations include economic value, security, safety, and community acceptance. Considering economic value, first and foremost, the main objective of UAM is to provide transportation for either people or goods in a quicker or more efficient manner than that of a ground transportation counterpart. With urban, dense areas as the main focus, a new set of aircraft conceptual designs would better suit this need compared to conventional models designed typically for larger ranges. Silva et al. [32] propose some initial designs that utilize vertical takeoff and landing capabilities and comparing side by side electric and turboshaft powered vehicles, noting that although the turboshaft models produced had lower overall gross weights, noise analysis was not considered which would be heavily affected by type of power source. Courtin et al. [9] explore the feasibility of electric short takeoff and landing (eSTOL) vehicles for UAM, noting the benefits regarding critical hazard avoidances and performance advantages compared to that of VTOL aircraft. The main clear drawback is the need for a runway, and although Courtin et al. show runway lengths of 100 to 300 feet to be sufficient for STOL aircraft, this severely impacts the versatility of an STOL design as it heavily relies on the proper infrastructure and location to even be considered an option.

DEP aircraft analysis through MDO

While conflicting in some design parameters, both STOL and VTOL concept analyses show use of distributed electric propulsion (DEP) as its main power source. Borer and Moore [5] explore DEP design by highlighting the propeller-wing interaction for NASA's X-57 Maxwell model. By designing propeller blade profiles to induce a high-velocity slipstream, overall benefits in efficiency can be obtained. To tackle the complexity of the aircraft design and analysis process with DEP in mind, an MDO approach is useful and can be integrated. Moore and Ning [27] use MDO to explore DEP effects using the Cirrus SR22, a modern short haul commuter aircraft. Hwang and Ning [21] look back at NASA's X-57 Maxwell, exploring the propeller-wing interaction again this time using MDO to include design parameters such as the velocity profile, propeller diameters, and blade profile parameters to maximize range. Part of the aim of this thesis is to expand on the methods used in this work and to apply them for system-level eVTOL concept analysis.

Current eVTOL analysis and tools

While MDO has already been in constant use for decades for general aerospace purposes, current studies involving eVTOL concept analysis (with or without MDO use) is still in its infancy comparatively. While open-source analysis tools designed specifically for eVTOL analysis currently don't exist, general conceptual aircraft design tools such as SUAVE [26] and NDARC [23] have been utilized for eVTOL analysis purposes. Vegh et al. [35] use both tools to observe results that highlight areas of uncertainty, emphasizing differences between the two tools and their modeling differences. Some specific focuses are covered such as arrival sequencing [25] by Kleinbekman, Mitici, and Wei as a first approach to optimize safe and efficient UAM operations. Ha and Hwang [16] focus on the economics side by integrating a system-level analysis and economics model in one monolithic optimization formulation to observe changes in design to maximize profit based on Los Angeles' vertiport locations. Some notable parameters are a speed premium that increases the cost of a trip based off of time saved compared to traveling on ground, an additional travel time measure for distance to closest vertiport, a minimum separation distance between each aircraft, a max tip Mach number, and an estimated cost of electricity usage; these parameters are swept across multiple optimizations, the effects of which on profit can be seen in Fig. 2.1.

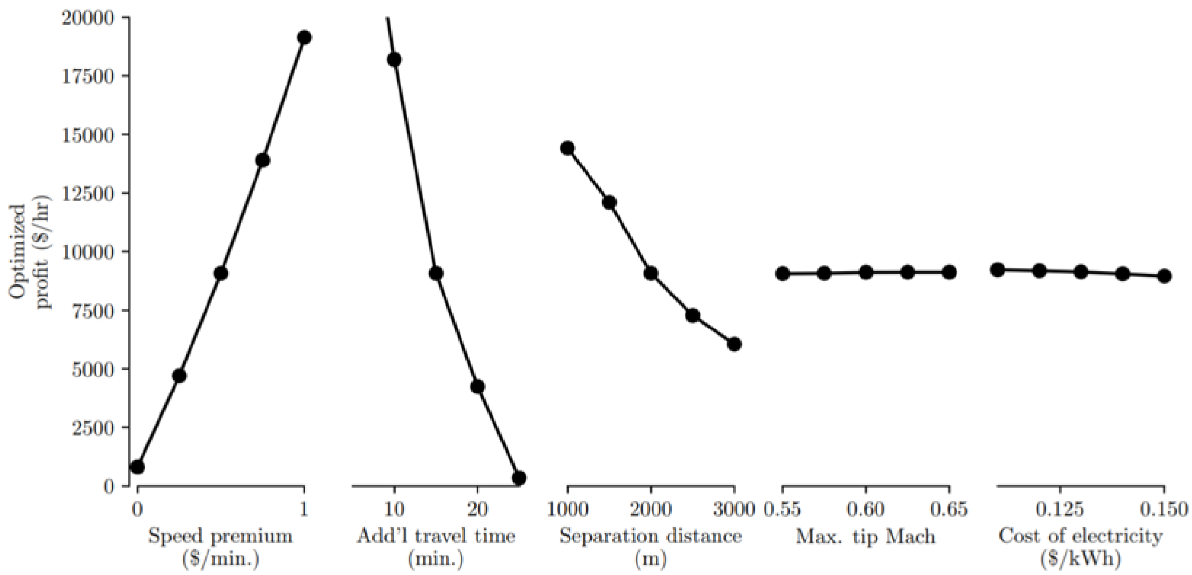

Figure 2.1. The effects of parameter sweeps on profit for a design-economics optimization formulation [16].

eVTOL configuration comparisons

While there exists a wide range of studies for eVTOL analysis in specific areas, system-level analysis and the comparison of designs are still limited. Bacchini and Cestino [2] compare three eVTOL classifications (wingless multirotor, lift + cruise, and vectored thrust) by using specific eVTOL configurations as representatives and found that the best configuration depends on the mission profile; the multirotor configuration performed more efficiently in hover, the vectored thrust configuration performed more efficiently in cruise, and the lift + cruise configuration was a compromise between the two. Saetti, Enciu, and Horn [31] perform a system-level analysis through design optimization of a single eVTOL concept, the F-Helix, a design based on the SH-4 Silvercraft light helicopter that they use as well to compare performance results. Basset et al. [3] present a new methodology used to size rotors in the case of thruster failures. While these studies compare concepts or analyze a single concept and its design features as a whole, currently no research exists to compare design features locally within a single configuration. This thesis aims to expand on system-level design formulations for eVTOL concepts with this focus in mind, while incorporating failure conditions to consider designs with built-in redundancy in the propulsion system for safety concerns.

Chapter 3

Discipline Models

In this chapter, I cover the different disciplines integrated into the upcoming optimization formulations and the models used to represent them.

3.1 Geometry

The geometry for the airframe mesh is created entirely within the Python setup, integrated directly into the OpenMDAO framework. For the remainder of the thesis, the coordinate system is defined as X pointing towards the rear of the aircraft, Y pointing towards the right wing (if looking towards the aircraft nose), and Z pointing vertically upwards. To construct the lifting surfaces, given a set of coordinates describing an airfoil shape, a least squares estimation is used to obtain a set of control points for the airfoil. Chord, twist, and XYZ positions (to represent sweep, span, and dihedral respectively) are used as inputs, and by fitting using B-splines, any number of control points could be used to define the input parameter distributions. These fitted curves describe a designated number of cross sections that expand the airfoil control points into a 2-D parametrized space. The parametrized space is then discretized into a 3-D mesh with B-spline surfaces, an example of which can be seen in Fig. 3.1 of two simple lifting surfaces with varying sweeps.

The body surfaces are obtained similarly, using width and height to vary cross sections of any arbitrary shape (a circle was used for simplicity), and XYZ positions to describe the

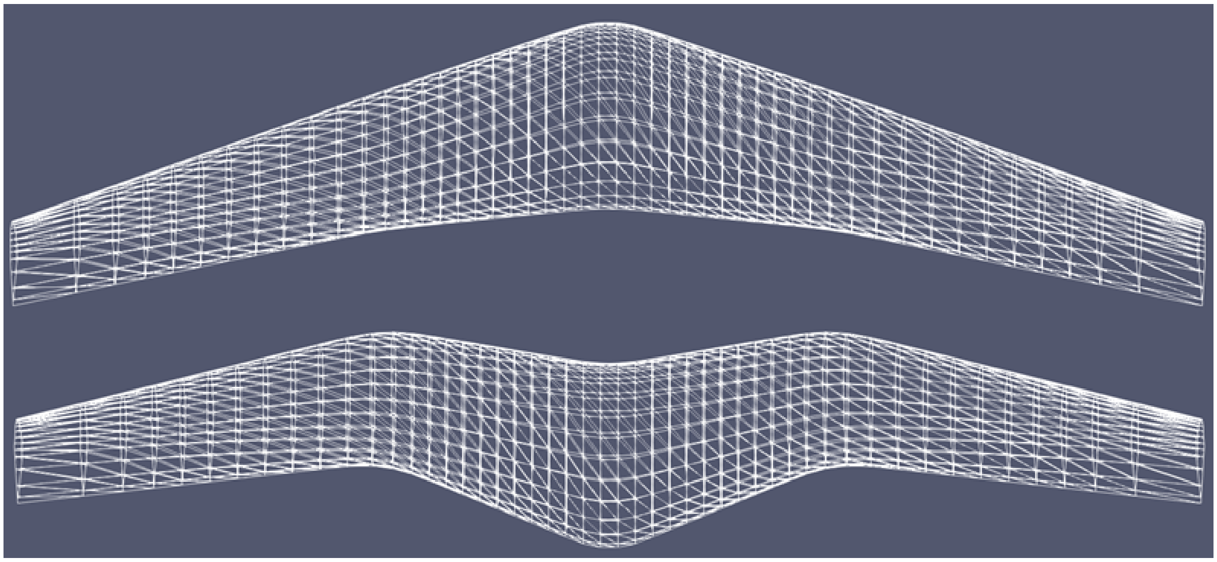

Figure 3.1. Example visualization of a change in sweep using the geometry tool.

longitudinal, lateral, and vertical positions for each cross section. These body surfaces are created and adjusted to represent the fuselage and boom components of the aircraft. For the rotors, a combination of the two geometry primitives are used, with a body surface created to represent the nacelle and several lifting surfaces created and rotated as the blade components.

Sourcing the geometry locally provides two major benefits: first, geometry parameters are easily defined and can be varied without requiring remapping during the optimization process. Second, B-spline curves and surfaces guarantee C^1 contintuity, providing exact and efficient derivatives without needing to use any finite difference methods that could quickly limit the scale of feasibility for the optimization problem.

3.2 Atmospheric

The atmospheric model uses altitude as an input to calculate temperature, pressure, density, Reynolds number, speed of sound, and dynamic pressure, the curves of which can be seen in Fig. 3.2

Temperature is assumed to vary linearly with altitude in the troposphere with no consideration of local weather. Given temperature, pressure is computed by integrating the hydrostatic

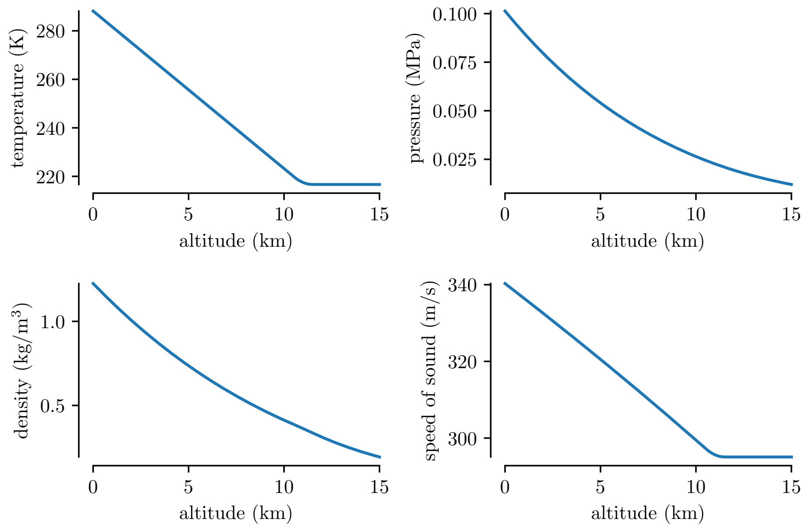

Figure 3.2. Temperature, pressure, density, and speed of sound as a function of altitude [19].

equation, replacing density with an expression involving pressure and temperature using the ideal gas law. Density is then computed using the ideal gas law, and the speed of sound and viscosity simply from temperature. Reynolds number and dynamic pressure are computed using their well-known definitions. Temperature decreases linearly with altitude up until roughly 10 km, at which the height is irrelevant to the flight capabilities of eVTOL aircraft. Pressure can be calculated by substituting density an expression using pressure and temperature via the ideal gas law into the hydrostatic equation. From there, density can be calculated, while speed of sound is calculated linearly with temperature.

3.3 Aerodynamics

3.3.1 Vortex lattice method

The vortex lattice method (VLM) is a 2-D aerodynamics analysis that predicts the lift, induced drag, and moment acting on a lifting surface. By representing a surface as a structured mesh, the method uses the flow represented as a set of horseshoe vortices and assumes the flow is incompressible, inviscid, and irrotational. These vortices have a constant strength stroughout that induce a velocity field that can be obtained using the Biot-Savart law. By assuming the net velocity at the quarter-chord of a panel has no normal component, the equation can be written as

$$\overrightarrow{v} * \hat{n} = (\overrightarrow{v}_{f_s} + \overrightarrow{v}_i) * \hat{n} = 0, \tag{3.1}$$

where $\overrightarrow{v}$ is the net velocity, $\overrightarrow{v}_{f_s}$ is the freestream velocity, $\overrightarrow{v}_r$ is the velocity components due to the vortices, and $\hat{n}$ is the normal vector for the panel. The system can be rearranged using the aerodynamic influence coefficient matrix and Γ_r as the vortex strengths, and the Biot-Savart law can be used again in the Kutta-Joukowski equation here:

$$\overrightarrow{F} = \rho \Gamma_r (\overrightarrow{v}_{f_s} + \overrightarrow{v}_i) \times \overrightarrow{l}, \tag{3.2}$$

where $\overrightarrow{F}$ is the net force on the panels, ρ is the air density, and $\overrightarrow{l}$ is the bound vortex vector for the panels.

A more detailed implementation can be seen in OpenAerostruct [22], an open-source coupled aerostructural optimization tool.

3.4 Parasitic Drag

The parasitic drag model uses the concept of an "equivalent skin friction coefficient" C_{f_e}, obtained from Raymer [30] to include both estimations of skin-friction drag as well as separation pressure drag. To model the skin-friction drag, the most important factor is the extent at which the aircraft has laminar flow across its surfaces. For portions with turbulent flow, an aircraft part can be modeled as a flat-plate where the skin-friction coefficient can be determined by

$$C_f = \frac{0.455}{(\log_{10} R)^{2.58}(1 + 0.144M^2)^{0.75}} \tag{3.3}$$

where R is Reynolds number and M is the Mach number, a correction that becomes more trivial at lower speeds. To account for the pressure drag caused by flow separation, a form factor derived from both theoretical and empirical considerations can be used. For subsonic drag, the form factor can be calculated using

$$FF = \left(1 + \frac{60}{f^3} + \frac{f}{400}\right), \tag{3.4}$$

with f calculated using the below

$$f = \frac{l}{d} = \frac{l}{\sqrt{(4/\pi)A_{max}}}, \tag{3.5}$$

where l and A_{max} represents the length and cross-sectional area of the plate respectively. Parasitic drag also increases due to mutual interference between components. Without the use of more refined aerodynamics tools, preliminary estimations simply involve a percent increase, where for parts mounted directly on the fuselage or wing, the interference factor Q is about 1.5. The fuselage has a negligible intereference factor (Q = 1.0) in most cases. The component parasite drag can be now be calculated using the skin-friction coefficient, form factor, and interference factor previously obtained using

$$C_{D_p} = C_{f_e} * Q * FF * \frac{S_{wet}}{S_{ref}}. \tag{3.6}$$

with S_{wet} and S_{ref} being the component's wetted area and reference area respectively.

3.5 Propulsion

3.5.1 Blade element momentum theory

Blade element momentum theory (BEMT) is a propulsion model that combines momentum theory, which uses a control-volume analysis and blade element theory, which is based on surrogate models produced off of known airfoil data at discretized sections of local angles of attack. By equating the two theories, the axial and tangential induced velocities can be calculated and thrust, torque, and lift can be predicted. Each propeller is separately modeled and accounted for for both slipstream influence and force and moment equilibrium. The propulsion modeling and airfoil data is implemented and used by Hwang and Ning [21] in the MDO study of NASA's X-57 experimental aircraft demonstrator for distributed electric propulsion (DEP).

Dimensionless efficiency metrics

It is useful to consider non-dimensional indicators of rotor efficiency in a way that is independent of scale, rotational speed, and so on. However, there are different metrics that are appropriate for the cruise and hover conditions.

For cruise, we can define *propulsive efficiency*, η, as

$$\eta = \frac{P_{\text{out}}}{P_{\text{req}}}, \tag{3.7}$$

where P_{out} is the output power and P_{req} is the required power. This expression can be simplified to

$$\eta = \frac{TV}{Q\omega}, \tag{3.8}$$

where T is thrust, V is forward speed, Q is torque, and ω is angular speed.

For hover, we can define a *figure of merit*, FOM, as

$$FOM = \frac{P_{\text{ideal}}}{P_{\text{req}}}, \tag{3.9}$$

where P_{ideal} is the ideal power. From momentum theory, we have

$$P_{\text{ideal}} = \frac{C_T^{3/2}}{\sqrt{2}C_P} \tag{3.10}$$

where, the thrust and power coefficients are respectively defined as

$$C_T = \frac{T}{\rho A V_{\text{tip}}^2} \quad \text{and} \quad C_P = \frac{P_{\text{req}}}{\rho A V_{\text{tip}}^3}, \tag{3.11}$$

where ρ is the atmospheric density, A is the disk area, and V_{tip} is the blade tip speed.

Validation of the BEMT model was completed by comparing results with CCBlade, a tool for analyzing wind turbine aerodynamic performance that can be reversed for propeller analysis [28]. The propeller design used was a 3-blade rotor with a 1.61 meter radius along with a linear taper chord length from 0.42 to 0.11 meters and linear twist from 34.3 to 14.3 degrees. The propeller was run at two different operating points: during cruise, the nominal RPM and speed were 1800 and 67 m/s respectively, while for hover, the nominal RPM and speed were 794 and 2 m/s respectively. Thrust, torque, power, and efficiency (or figure of merit for the hover point) were the factors of interest, and the trends generally agree for both CCBlade and our current MDO model, as can be seen in Fig. 3.3.

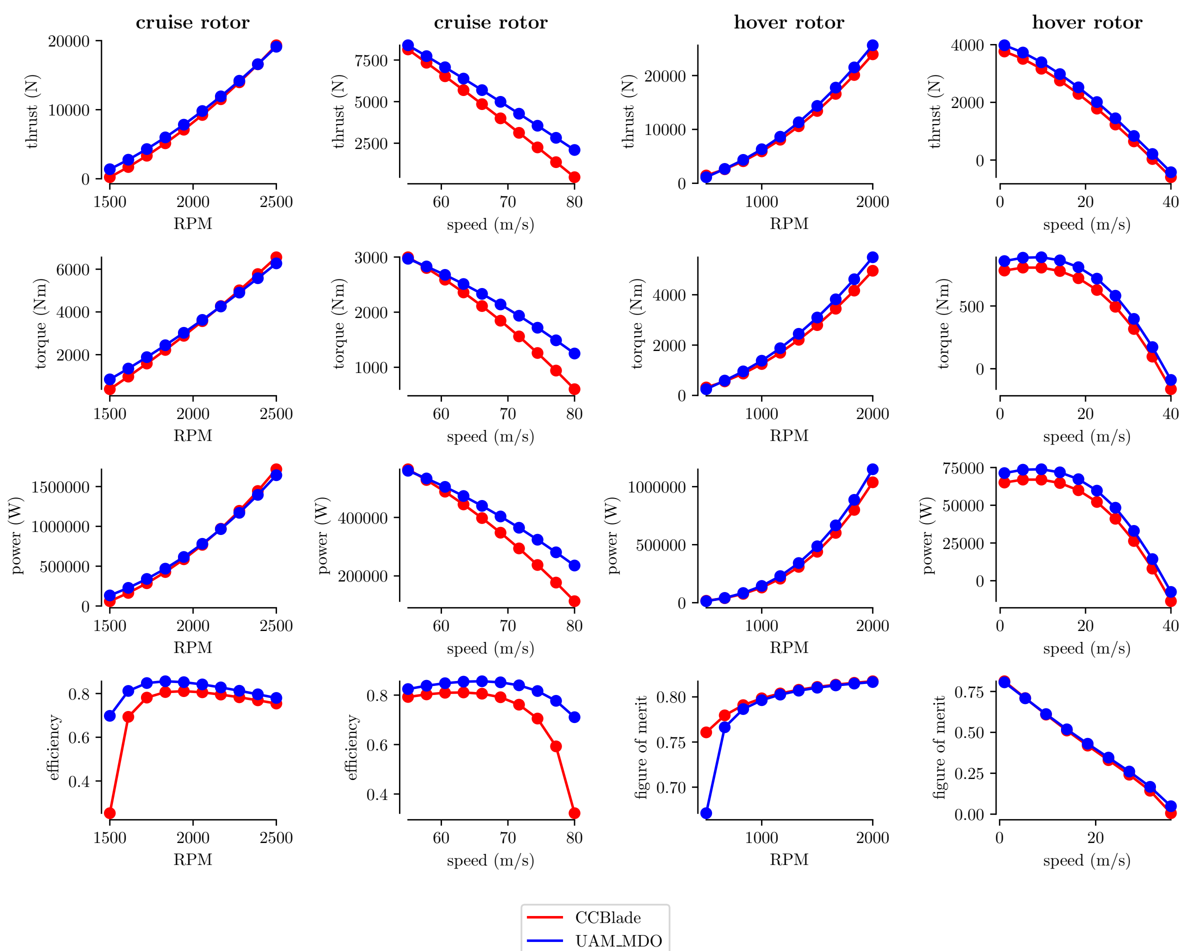

Figure 3.3. Thrust, torque, power, and either efficiency (for cruise) or figure of merit (for hover) measured at varying RPMs and speeds.

3.5.2 Glauert propeller model

The Glauert propeller model is a semi-analytic method for estimating the ideal efficiency of a propeller with arbitrary blade profile. Using diameter and solidity as the main geometric parameters and integrated design lift coefficient, the model takes in the variable inputs of advance ratio and power coefficient to predict the maximum performance of an assumed optimal blade profile.

Equations

The propeller airspeed is defined as

$$\eta = \frac{TV}{Q\omega} \tag{3.12}$$

where T is thrust, V is the vehicle airspeed, Q is torque, and ω is angular speed in radians per second. The definitions of coefficient of thrust and torque are defined as

$$C_T = \frac{T}{\rho n^2 D^4}, \tag{3.13}$$

$$C_P = \frac{P}{\rho n^3 D^5}, \tag{3.14}$$

where n is the rotational speed in revolutions per second and D is the propeller diameter.

The efficiency can then be written as

$$\eta = \frac{C_T J}{C_P} \tag{3.15}$$

where J is the advance ratio defined as

$$J = \frac{V}{nD}. \tag{3.16}$$

To estimate this efficiency, three terms are considered off of axial momentum theory, general momentum theory, and blade-element theory. The first term takes into account axial momentum losses, the second with wake rotation losses, and the third with airfoil profile drag losses. The three terms in order and their calculations can be seen below:

$$\eta_1 = 1 - \frac{2}{\pi} C_P \eta_2 \eta_3 \left(\frac{\eta_1}{J}\right)^3, \tag{3.17}$$

$$\eta_2 = 1 - \frac{4}{\pi^3} \frac{\eta_1}{J} C_P, \tag{3.18}$$

$$\eta_3 = 1 - \frac{\pi^4}{8} \frac{\eta_2^2}{C_P} \sigma \bar{C}_d f(\phi), \tag{3.19}$$

where σ is the propeller solidity, $\bar{C}_d$ is the blade-average two-dimensional drag coefficient, and $f(\phi)$ is defined as

$$f(\phi) = \frac{1}{8\cos\phi}(2 + 5\tan^2\phi) - \frac{3}{16}\tan^4\phi \log\frac{1-\cos\phi}{1+\cos\phi}, \tag{3.20}$$

where ϕ is the local inflow angle between the propeller disk plane and the resultant cross-sectional velocity. Together, the separate η_n terms can be combined as the ideal efficiency using

$$\eta = \eta_1 \eta_2 \eta_3. \tag{3.21}$$

These equations were originally developed by Glauert [24], and more recently used in a propeller sizing model by Gur [15]. By formulating this equation as a nonlinear equation in terms of a single unknown, it is possible to apply a bracketed root-finding algorithm that is probably convergent. Such an algorithm has been implemented in OpenMDAO and is used in the current thesis.

Validation

The Glauert propeller model is validated comparing results to either existing simulation data (from APC propellers, a propeller manufacturer) and experimental data (from the University

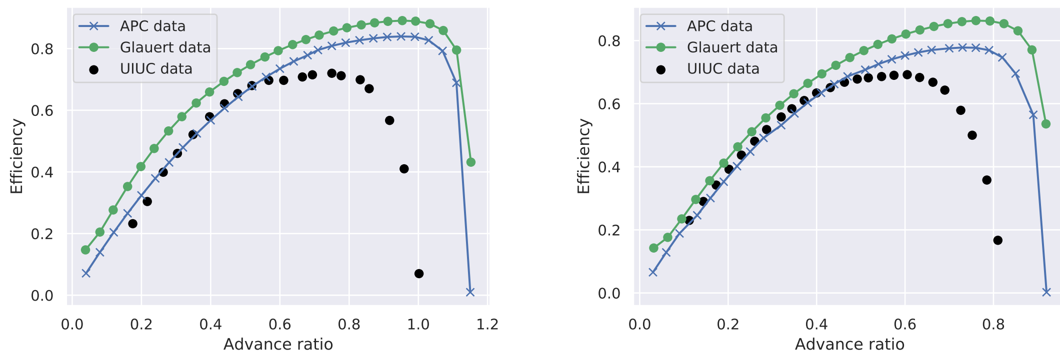

(a) 11in diameter, 10in pitch at 3000 RPM (b) 10in diameter, 7in pitch at 5000 RPM

Figure 3.4. Glauert propeller model validation versus simulation data from the propeller manufacturer (APC) and experimental results from UIUC.

of Illinois at Urbana-Champaign [6, 12]). The comparison can be seen in Fig. 3.4, and the efficiencies are predicted with less than 20% error.

This subsection, in full, is currently being prepared for submission for publication of the material. Ruh, Marius; Hwang, John T. The thesis author was not the primary investigator and author of this material.

3.6 Motor

The motor model developed provides a sizing-level predictive model that considers permanent-magnet synchronous motors (PMSMs) to provide available torque and efficiency given a mass, operating torque, and rotational speed.

Equations

In the model, the maximum continuous torque and maximum continuous power can be approximated using empirical relations. Using a smooth minimum function, the available torque is obtained as the minimum of the maximum torque and torque based on the maximum power, which can be represented as,

$$Q_{avail} = -\frac{1}{\rho} \log \left(e^{-\rho Q_{max}} + e^{-\rho P_{max}/\omega} \right), \tag{3.22}$$

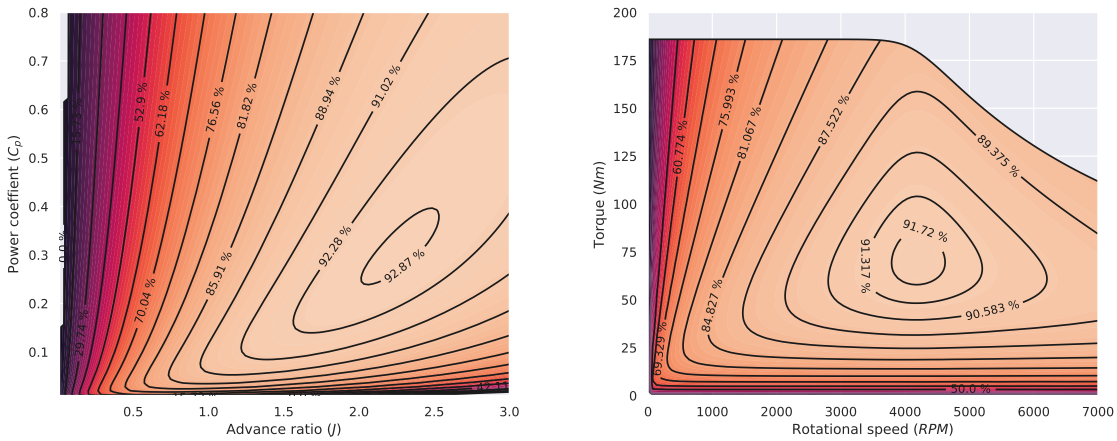

(a) Glauert propeller model (b) Semi-empirical motor model

Figure 3.5. Propeller (left) and motor (right) efficiency maps obtained using the Glauert propeller model and the semi-empirical motor model, respectively.

where ρ is a tuning parameter that controls the smoothness of this function, Q_{max} is the maximum torque, P_{max} is the maximum power, and ω is the rotational speed. A visualization of this can be seen on the right in Fig. 3.5.

Empirical equations are also used to model the geometry and mass breakdown of the motor—the mass of the stator, the mass of the rotor, the outer diameter motor, motor length, stator diameter, shaft diameter, and thickness of the stator.

The eddy loss is estimated via [17]

$$P_{eddy} = 1.1 * (\frac{1}{50})^{1.5} f_{supply}^{1.5} M_{stator}^{1} B_{mg}^{2}, \tag{3.23}$$

where f is the supply frequency and B_{mg} is the magnetic flux density. The hysteresis loss is estimated via [33]

$$P_{hyst} = f_{supply} M_{rotor} B_{mg}^{2} hyst_{coeff}, \tag{3.24}$$

where $hyst_{coeff}$ is a hysteresis coefficient with a default value of 1. The heat loss P_{heat} is computed using a simplified equation, and the loss terms are combined to compute the motor efficiency using

$$\eta = \frac{P_s}{P_s + P_{eddy} + P_{hyst} + P_{heat}}, \tag{3.25}$$

where η here is motor efficiency. An example of a motor efficiency map produced using the current model is shown in Fig. 3.5.

This section, in full, is currently being prepared for submission for publication of the material. Ivanov, Alex; Joshy, Anugrah J; Hwang, John T. The thesis author was not the primary investigator and author of this material.

3.7 Slipstream

3.7.1 Equations

The induced velocity field in the propellers' slipstream is modeled using analytical approximations. The slipstream contraction is approximated [36] using

$$R(x) = R\sqrt{\frac{1+a_x}{1+a_x\left(1+\frac{x}{\sqrt{R^2+x^2}}\right)}}, \tag{3.26}$$

which is derived assuming a uniform axial load distribution. As noted by Veldhuis, there are errors in this approximation due to nacelle effects [36], but we use it as a first-order model that is at least better than neglecting slipstream contraction entirely.

For the evolution of the axial and radial components of induced velocity, we use the analytical solution of Conway [8] for elliptically-loaded blades, following Alba [1]. These components are given by

$$V_r(r,x) = V_x(r,0)\left[\frac{|x|R(x)}{2r\sqrt{R(x)^2-r^2}}\left(\frac{1}{a}-a\right) - \frac{r}{2\sqrt{R(x)^2-r^2}}\arcsin\left(\frac{2R(x)}{b}\right)\right], \tag{3.27}$$

$$V_x(r,x) = V_x(r,0)\left[2 - \frac{aR(x)}{\sqrt{R(x)^2-r^2}} + \frac{x}{\sqrt{R(x)^2-r^2}}\arcsin\left(\frac{2R(x)}{b}\right)\right], \tag{3.28}$$

where

$$a = \sqrt{\frac{\sqrt{(R(x)^2 - x^2 - r^2)^2 + 4R(x)^2x^2} + (R(x)^2 - x^2 - r^2)}{2R(x)^2}}, \tag{3.29}$$

$$b = \sqrt{x^2 + (R(x) + r)^2} + \sqrt{x^2 + (R(x) - r)^2}. \tag{3.30}$$

The value of $V_x(r,0)$ is computed from $V_x(r,0) = V_{x_0}\sqrt{R(x)^2 - r^2}/R(x)$, where V_{x_0} is the axial induced velocity at the disk, averaged radially. The axial velocity component is considered zero for $r > R(x)$. Likewise, the tangential velocity is also considered zero for $r > R(x)$, and since modeling its evolution in x is more complicated, we use a swirl recovery factor (SRF) of 0.5, following Veldhuis [36]. Since we use a constant value of SRF, this model is not well-suited for use for investigating the stream-wise location of rotors relative to the wings to which they are attached. The SRF is a multiplier on the tangential induced velocity computed at the disk and it captures the influence of the wing on dampening the swirl in the slipstream.

3.7.2 Validation

Validation of the aero-propulsive model was completed by comparing RANS CFD predictions that use OVER-FLOW, STAR-CCM+, and FUN3D in Fig. 3.6. The geometry used is NASA's X-57 Maxwell, and was run at two different operating conditions: a cruise condition (unblown) and a high-lift condition (blown). At cruise, only the unpowered aerodynamics is considered to validate again the VLM model as well as the parasitic drag calculation at different angles of attack given a maximum C_l at a cruise speed of 77.2 m/s. For the high-lift setup, slipstream influence due to the propellers is included as well as a Fowler flap set at 30° deflection and 25% additional area modeled using equations for C_L and C_D from Raymer [30]. The unpowered aerodynamics for UAM MDO model match well and lie between the turbulent and transition models. For the high-lift configuration, the UAM MDO model follows a similar trend to the CFD data but underpredicts or overpredicts at certain angles of attack by a small margin. On average, the model shows an overall sufficient agreement. The CFD data was obtained from

Borer et al. [4] (for cruise) and Deere et al. [11].

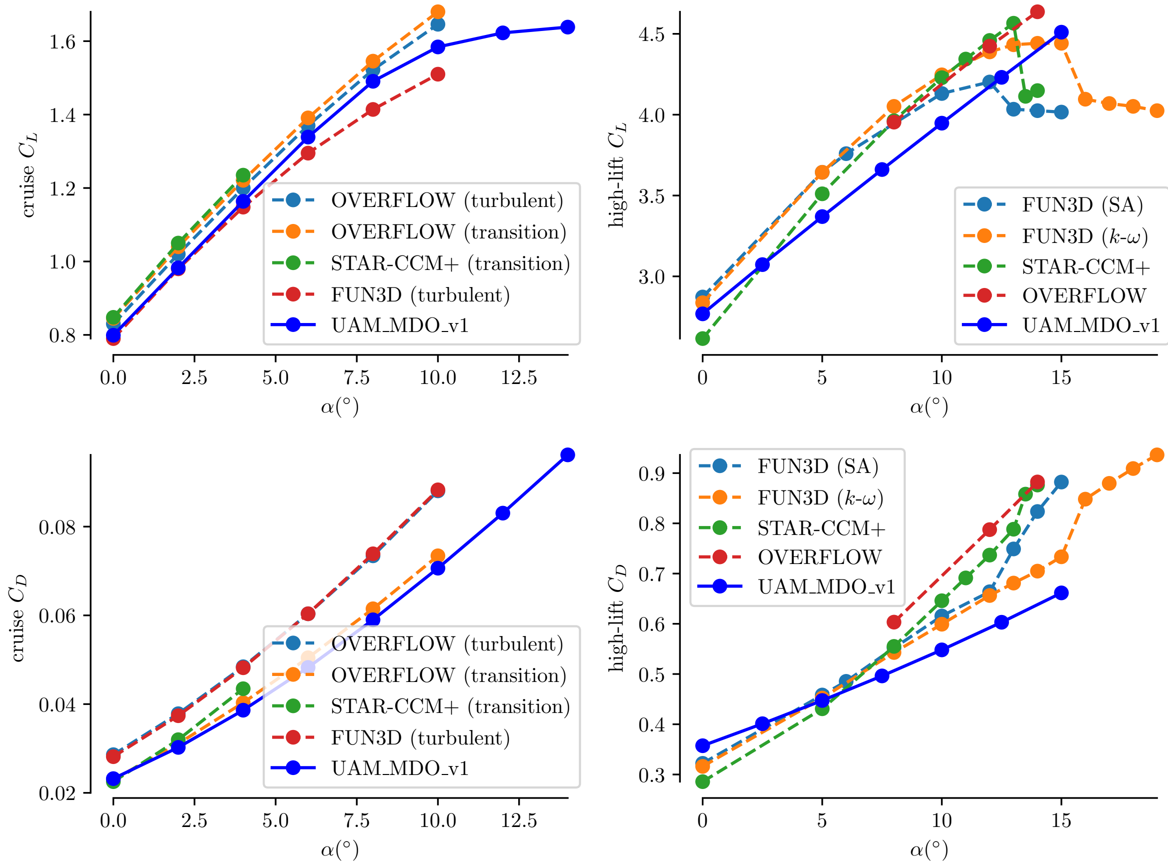

Figure 3.6. Unpowered (left) and powered (right) aerodynamics analysis comparing different RANS CFD solvers to our current UAM MDO model at varying angles of attack.

3.8 Weights and stability

The weights model is based off of several statistical equations obtained through regression analysis used for general aviation from Raymer [30]. A list of the equations used for the weight calculations of the different aircraft components are shown below:

$$W_{fuselage} = 0.052 * S_f^{1.086}(N_z W_{dg})^{0.177} L_t^{-0.051}(L/D)^{-0.072} q^{0.241} \quad (3.31)$$

$$W_{flightcontrols} = 0.053 * L^{1.536} * B_w^{0.371} (N_z W_{dg} * 10^{-4})^{0.80} \tag{3.32}$$

$$W_{horizontaltail} = 0.016 * (N_z W_{dg})^{0.414} q^{0.168} S_{ht}^{0.896} \left(\frac{100t/c}{\Lambda} \right)^{-0.12} \left(\frac{A}{\cos^2 \Lambda_{ht}} \right) \lambda_h^{-0.02} \tag{3.33}$$

$$W_{motor} = 9.80665 * \left(-2\mathrm{E}^{-5} P^2 + 0.1595P + 3.3081 \right) \tag{3.34}$$

$$W_{wing} = 0.036 S_w^{0.758} \left(\frac{A}{\cos^2 \Lambda} \right)^{0.6} q^{0.006} \lambda^{0.04} \left(\frac{100t/c}{\cos\Lambda}_{-0.3} \right) (N_z W_{dg})^{0.49} \tag{3.35}$$

All resulting weight calculations here are determined in pounds and are converted to SI units in the running model. Definitions of the terms in the equations can be seen below.

S_f = fuselage wetted area (ft^2)

N_z = ultimate load factor; = 1.5 X limit load factor

W_{dg} = flight design gross weight (lb)

L_t = tail length (ft)

L = fuselage structural length (ft)

D = fuselage structural depth (ft)

q = dynamic pressure at cruise (lb / ft^2)

B_w = wing span (ft)

S_{ht} = horizontal tail area (ft^2)

S_w = trapezoidal wing area (ft^2)

t/c = thickness-to-chord ratio

Λ = wing sweep at 25% of the mean aerodynamic chord (rad)

Λ^{ht}	=	tail sweep at 25% of the mean aerodynamic chord (rad)
A	=	aspect ratio
λ	=	wing taper ratio
λ^h	=	tail taper ratio
P	=	power input (kW)

The motor gear and propeller blade weights are calculated based off a percentage of the motor weight, while the weights of components such as the battery and payload are used as inputs for the model, allowing them to be set as design variables. Due to the coupling involved with some component requiring the design gross weight as an input, two solutions are set in place: The default is to use a nonlinear solver to converge the coupled weights model. The alternative is to rely on the use of an initial guess to be used as the design gross weight input. By setting this guess as a design variable, the optimizer is left in charge to ensure the gross weight guess and resulting calculated gross weight ultimately converge.

Stability

Once each component weight is calculated, a center of gravity (CG) location can be determined for the aircraft using a weighted sum involving the known CG positions of the individual components. The neutral point can then be determined using the known aerodynamic centers and moment coefficients for the lifting surfaces of the model. The total moment acting on the aircraft can be calculated by

$$C_M \frac{1}{2}\rho V^2 S c = \sum_i \left(C_{M_i} \tfrac{1}{2}\rho V^2 S_i c_i - C_{L_i} \tfrac{1}{2}\rho V^2 S_i \left(x_{ac_i} - x_{ref} \right) \right). \tag{3.36}$$

where ρ is the air density, V is the inflow velocity, S is the surface area, and c is the mean aerodynamic chord of the lifting surface. Taking the derivative with respect to α with the neutral point as the reference point, we obtain

$$\frac{\mathrm{d}C_M}{\mathrm{d}\alpha} = \sum_i \left(-\frac{\mathrm{d}C_{L_i}}{\mathrm{d}\alpha} \frac{S_i}{S} \right) \frac{x_{ac_i} - x_{np}}{c} = 0 \tag{3.37}$$

since $dC_{M_i} / d\alpha = 0$, and thus neutral point can be calculated by

$$x_{np} = \frac{\sum_i \frac{\mathrm{d}C_{L_i}}{\mathrm{d}\alpha} S_i x_{ac_i}}{\sum_i \frac{\mathrm{d}C_{L_i}}{\mathrm{d}\alpha} S_i}. \tag{3.38}$$

Using the neutral point and the aircraft CG, static margin can be calculated and used as a metric for longitudinal stability.

To ensure equilibrium is enforced properly, the forces from each discipline are rotated to a global frame and summed up. Each set of net forces for each mission is then set as constraints along their relevant axes.

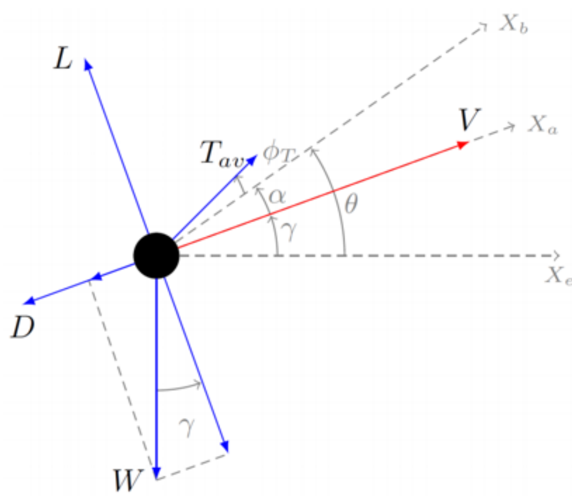

Figure 3.7. Aircraft references axes for equations of motion.

Chapter 4

Methodology and problem formulations

4.1 Methodology

The complexity of the multidisciplinary model motivates the use of a software framework to construct and optimize the model. The framework chosen needs to be able to handle hundreds of design variables efficiently, tackling the issue of dimensionality without suffering too greatly due to setbacks in computation power and time. The approach is to use NASA's OpenMDAO framework [14] to assemble, integrate, and differentiate the various disciplinary sub-models and solve the MDO problem. OpenMDAO is an open-source MDO framework written in Python, and it uses the modular analysis and unified derivatives (MAUD) architecture [20]. MAUD generalizes the adjoint method to compute derivatives efficiently given a complex, heterogenous model. To compute derivatives, given that

$$R(u) = \begin{pmatrix} x - x* \\ -\mathbf{R}(x,y) \\ f - F(x,y) \\ c - C(x,y) \end{pmatrix}, \tag{4.1}$$

where u denotes the vector of all the variables within the model (i.e. every output of every component), x is a vector of input variables, y is a vector of state variables, f is the objective variable while F is the objective function, c is the vector of constraint values with C being the constraint functions, and where $R(u) = 0$, MAUD solves the equation,

$$\left[\frac{\partial R}{\partial u}\right]\left[\frac{\mathrm{d}u}{\mathrm{d}r}\right] = \left[\mathbf{I}\right] = \left[\frac{\partial R}{\partial u}\right]^T\left[\frac{\mathrm{d}u}{\mathrm{d}r}\right]^T, \tag{4.2}$$

where the residuals R are formed from the various components of the model and $\partial R/\partial u$ contains the local derivatives of each component. With this, all analytic derivative computations from adjoint to chain rule are simplified and allow for simple and efficient processing. All optimization problems are solved using SNOPT [13], through the pyOPT interface [29]. SNOPT is an algorithm that solves sparse nonlinearly constrained optimization problems using a reduced-Hessian active-set approach.

4.2 Optimization formulations

Layout MDO

Two optimization formulations have been developed in order to explore and analyze eVTOL concept designs. We refer to the first as layout MDO, which is relatively inexpensive in computational cost—optimization problems are typically solved in less than one hour on a desktop workstation. Using general geometric design parameters as inputs, this formulation computes key geometric functionals, such as aerodynamic center and area, through various approximations. With no geometric mesh being used, the integrated discipline models are of similar fidelity. For the aerodynamics, a standard quadratic drag polar is computed with the wing and tail incidence angles used as inputs. For power, the motor draws from a battery that calculates power output based off of a chosen specific power and variable mass. The motor uses the semi-empirical motor model created to calculate generated shaft power for the rotors. Propulsion from the rotors is calculated through high-efficiency propeller estimation by Glauert. Parasitic drag and weight buildups are implemented with standard formulas, and net forces and moments are calculated and constrained to enforce equilibrium. Longitudinal stability is enforced by calculating the neutral point using estimations of the lifting surfaces lift curve slope and enforcing the aircraft center of gravity to be at an appropriate static margin. Performance can then be observed in a few different measures such as motor efficiency, range capabilities, or thrust margin minimization.

Due to the low computation time, the layout MDO is well-suited for comparing high-level design parameter changes, mainly focusing on the rotor layout design. The three concept design differences that we explore are tilt versus tractor, rotor number, and tilt rotor position. The design structure matrix visualizing the flowchart of inputs and outputs between the formulation's disciplines can be seen in Fig. 4.1.

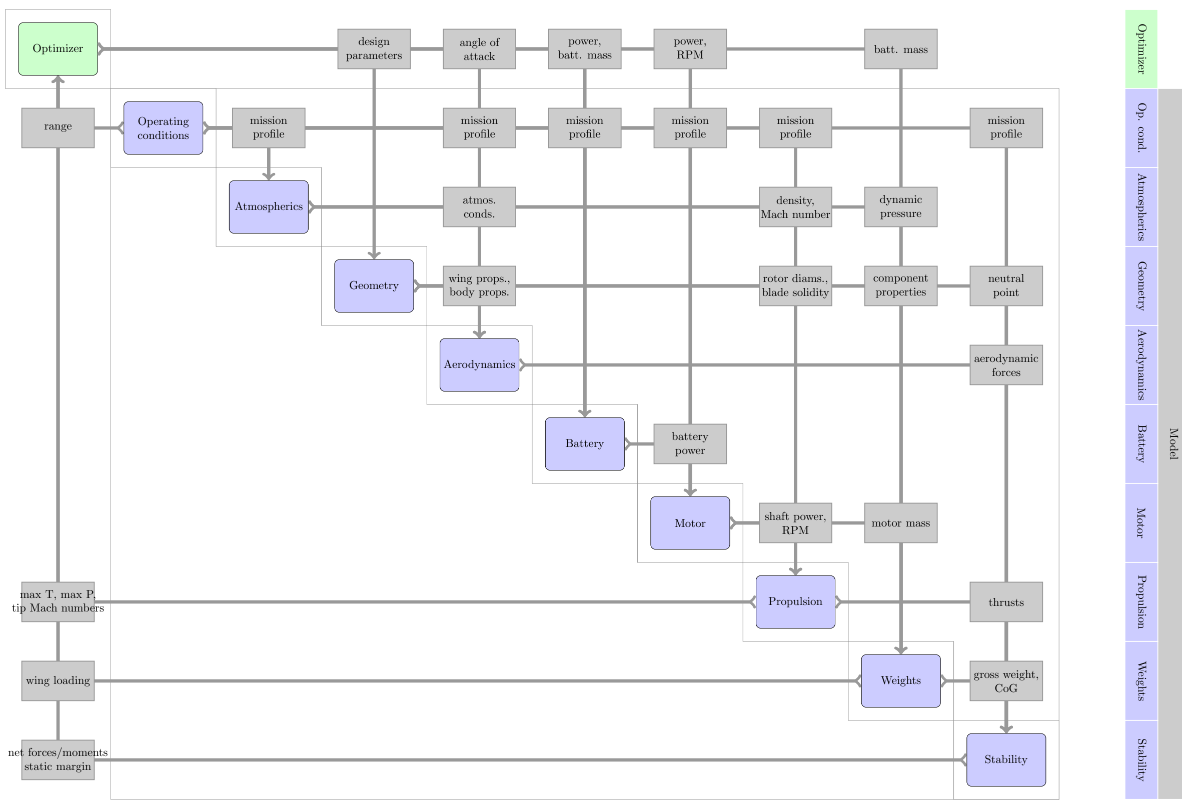

Figure 4.1. Design structure matrix for the layout MDO problem.

Refined MDO

The second optimization formulation is a slightly higher fidelity analysis which we refer to as the refined MDO, utilizing a CAD-free geometry modeler created within Python to generate discrete mesh representations of aircraft components. The lifting surfaces and rotor blades are generated identically using B-spline curves describing the twist, chord, and x/y/z positions.

The rotor mesh is then discretized radially for BEMT analysis, outputting the rotor's thrust, torque, power usage, and slipstream properties. The power usage is run through a simple empirical model to calculate a corresponding motor weight. Wireframe meshes are generated for the lifting surfaces, and along with the induced slipstream from the rotors, aerodynamics can be computed through VLM. Parasitic drag for the lifting surfaces is calculated by matching the section-wise lift coefficients obtained through VLM with drag coefficients using a standard quadratic drag polar. Parasitic drag for the body components and weight buildups are implemented with the same standard formulas as the layout MDO. The 3D forces obtained through the aerodynamics, weights, and propulsion are rotated to a consistent frame and used for net force and moment calculations for equilibrium constraints. Longitudinal stability is enforced with two possible ways of computing the aircraft neutral point, one using the lift curve slope of the lifting surfaces, and the other by observing the x location that satisfies $\frac{\mathrm{d}CL}{\alpha} = 0$ using a small perturbation in α passed to the VLM analysis.

The refined MDO takes considerably longer than the layout MDO, ranging from several hours to days on a standard desktop workstation. Due to this, we opt to use this formulation once a layout configuration is already decided so that further in-depth analysis and results can be explored. The design structure matrix visualizing the connections between each discipline can be seen in Fig. 4.2.

The two optimization formulations and their corresponding discipline models can be viewed in Tab. 4.1.

4.3 Layout configurations

For the model configuration, Uber's electric Common Reference Model (eCRM) model 002 was used, visualized in Fig. 4.3. This model is a four passenger + one pilot vehicle that

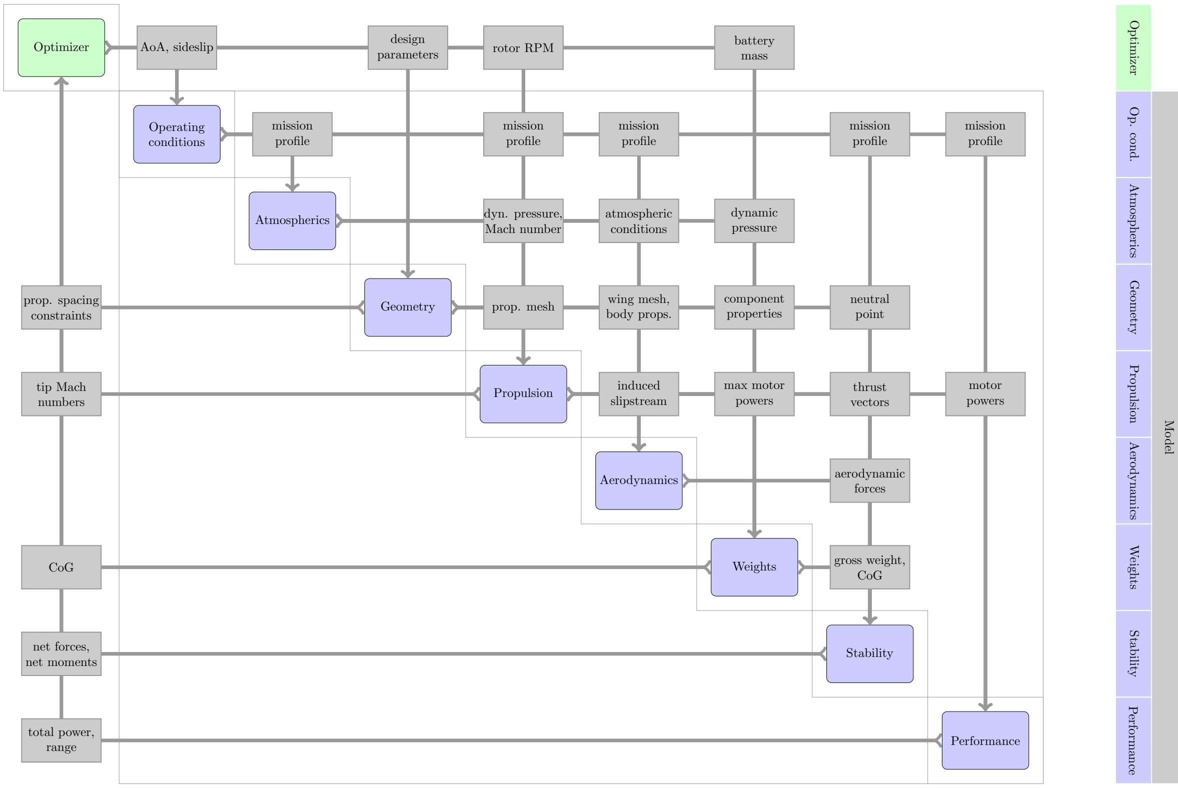

Figure 4.2. Design structure matrix for the refined MDO problem.

Table 4.1. Discipline model comparison overview.

Discipline model	Layout MDO	Refined MDO
Geometry	Parameter equations	3-D geometry
Aerodynamics	Quadratic drag polar	VLM
Motor	Semi-empirical	Empirical
Propulsion	Glauert	BEMT
Weights	Empirical	Empirical

consists of two symmetric sets of rotors located on the wings and a pair of rotors located on the rear fuselage near the tail all used solely for lift. These lift rotors sets feature double-stacked, co-rotating propellers each with a separate engine to increase efficiency and capitalize on the DEP benefits of redundancy. A symmetric pair of tractor rotors are located on the wing tips, classifying this configuration as a lift + cruise configuration, with rotors dedicated for each mission type. The design suits the needs of this thesis well as modifications to the rotor number and positions are simpler to apply and whose effects to performance can be measured more

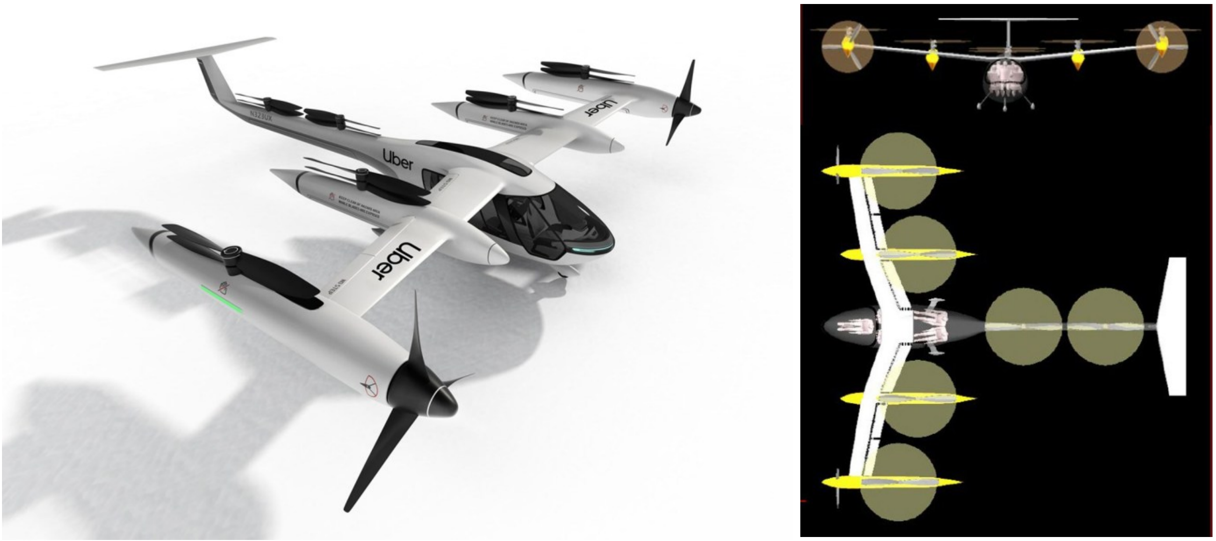

Figure 4.3. 3D rendering and layout visualization of the Uber eCRM-002 obtained online[1].

directly, as opposed to a more convoluted design where any small change could have underlying effects not captured.

General specifications of the geometry parameters such as CG positions and wing parameters were obtained Uber's available open-source model created in OpenVSP [18], a parametric aircraft geometry tool useable for engineering analysis, and recreated in our framework. The parameter values for the lifting surfaces can be seen in Tab. 4.2, while the CG positions of the aircraft components can be seen in the results chapter in Tab. 5.5.

Table 4.2. Lifting surface parameters obtained from open-source Uber eCRM-002 OpenVSP model.

Surface	Root chord (m)	Tip chord (m)	Taper ratio	Span (m)	Sweep (°)	Dihedral (°)	Twist (°)	Area (m^2)
Wing	1.147	0.819	0.714	10.67	-9.0	6.0	1.0	10.48
Tail	1.065	0.608	0.571	4.87	10.62	0.0	0.0	4.07

For the propeller blade geometry, single rotors were modeled and the blade and twist control points were set as design variables in a pre-optimization using the BEMT model involving a single operating condition. A tractor 5-blade propeller was optimized for a cruise condition

[1] https://evtol.news/aircraft/uber-elevate-ecrm-002/

while a lift 2-blade propeller was optimized for a hover condition, the parameters of which can be seen in Section 4.4. The tractor and lift propeller optimizations were set to maximize efficiency or figure of merit respectively, and the resulting blade twist and chord control point distribution can be seen in Fig. 4.4 and 4.5.

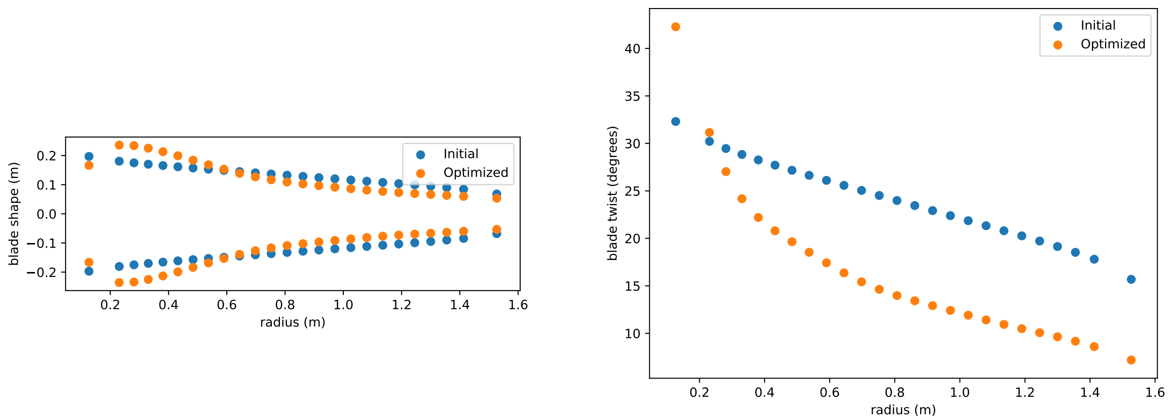

Figure 4.4. Optimized blade chord and twist distribution for a lift rotor (2 blades).

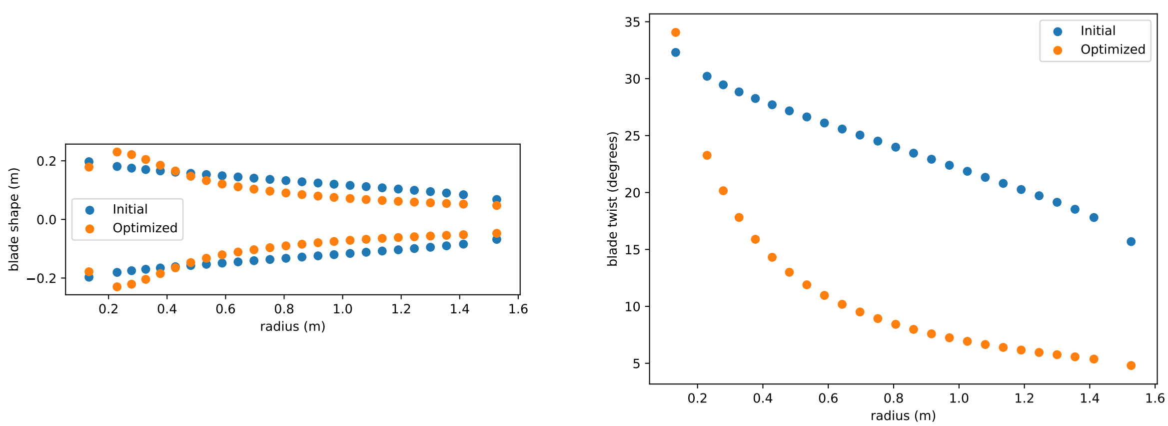

Figure 4.5. Optimized blade chord and twist distribution for a tractor rotor (5 blades).

Current models are insufficient to capture the effects of co-rotating propellers accurately without the use of CFD analysis, and so the stacked rotors are modeled using a simple stacked factor that is applied to the thrust and power, with the motor/rotor weights doubled for each set. The base configuration layout is modified with variations of both lift + cruise configurations with tractor propellers and vectored thrust configurations with tilt propellers are set up, with either 6 or 8 rotor sets used for lift and varying tilt rotor positions. The rotor diameters along the wing decrease from the 6 to 8 Lift rotor configurations to maintain some level of spacing along the wing. The layout naming shown in Fig. 4.6 will be the default used for the remainder of the thesis.

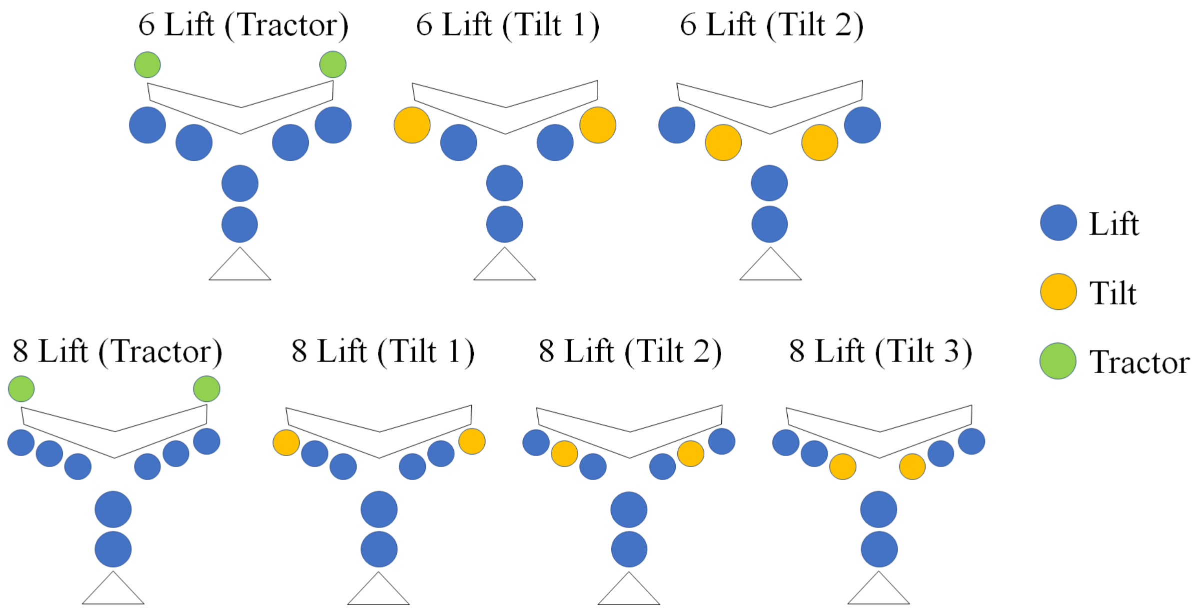

Figure 4.6. Visualizations of the layouts investigated using the layout MDO formulation.

4.4 Operating conditions and assumptions

Uber lists multiple specifications that will be considered its standard for urban air mobility, several of which assisted in formulating the mission parameters for this work. For both optimization formulations, four operating conditions are considered:

1. Nominal cruise
2. Reserve cruise
3. Nominal hover
4. Hover with one rotor inoperative

The nominal cruise point is set at 150 mph (241 km/h) while the reserve point is set at a lower speed for stall conditions. The nominal hover point is set at a low speed with a given time constraint, while a one-rotor-inoperable case (shortened as OEI for one-engine-inoperable in data tables) forces the motors/rotors to be sized appropriately for safety reasons. The one-rotor-inoperative case is duplicated for each lift rotor to ensure both safety and symmetry. For the lift rotors that are stacked, only one of the two engines is turned off as it is unlikely for both engines in a stacked rotor to fail simultaneously. These operating conditions follow in line with Uber's eCRM general specifications. Further details on each operating condition can be seen in Tab. 4.3

Table 4.3. An overview of the operating condition specifications.

Operating condition	Speed (m/s)	Altitude (km)	Thrust margin	Power margin	Distance/time constraint
Nominal cruise	66.7	2	1.3	1.4	
Reserve cruise	55.6	2	1.3	1.4	10 km
Nominal hover	5.0	0	1.0	1.4	2.5 min
OEI hover	2.0	0	1.0	1.4	

A general list of the assumptions surrounding the MDO setups can be seen in Tab. 4.4.

Table 4.4. An overview of the general problem assumptions. TR: tilt rotor. FR: fixed rotor.

Parameter	Value	Units
Battery energy density	200	Wh/kg
Battery power density	800	W/kg
Battery reserve	15	%
Parasitic drag margin	1.25	
Stacked factor	1.8	
TR solidity	0.15	
TR integrated lift coefficient	0.14	
TR max blade loading coefficient	1.5	
FR solidity	0.06	
FR integrated lift coefficient	0.16	
FR max blade loading coefficient	1.41	

4.5 Problem description

As a flat measure of performance, range was maximized to see which configurations performed the best while satisfying constraints. The layout MDO problem setup is shown in Fig. 4.5, optimizing both operational variables and some design parameter variables such as rotor diameter and battery location. We use the aforementioned operating conditions: one operating point each for nominal cruise, reserve cruise, nominal hover, and one engine-out hover case for each lift rotor in the configuration. Thus, for the ”6 Lift” configurations, there are 2 cruise + 1 hover + 6 hover inoperative conditions, or 9 total. Likewise, there are 11 missions for the ”8 Lift” configurations. Wing span and chord are combined together as a ”wing scale factor” that increases or decreases wing area while keeping its general parameters such as aspect ratio, sweep, and dihedral constant. Max diameters are scaled down for the 8 Lift rotor problem setup to maintain spacing between propellers. For the constraints, net force and moments are applied only on relevant axes. For the cruise missions, net forces along the x and y axes, pertaining to thrust, drag, lift, and weight, must be balanced, and pitching moment is constrained. For the hover missions, net force along the y axis, pertaining to thrust and weight, are balanced, and pitching and roll moments are constrained. Tip mach number acts as a surrogate for noise, and the maximum is set at 0.6 for each rotor across all operating conditions.

For the refined MDO, we have a similar set of design variables and constraints with some additions. Due to computational limitations, the number of operating conditions was reduced from each lift rotor having a separate engine-out operating condition to each pair of symmetric rotors sharing an OEI condition for one side. Since motor weights and design variables regarding the geometry are mirrored, theoretically an OEI condition on one side should account for the opposite side as well. Pitch angle is required for each rotor in each operating condition for BEMT analysis, but it is irrelevant in the Glauert model used by the layout MDO. An additional set of design variables describe the control points of the twist profile for each rotor pair. The center of gravity is constrained to ensure static margin is reasonable, and propeller spacing constraints

Table 4.5. Problem formulation for layout MDO.

Variable	Lower bound	Upper bound	6 Lift (Tractor)	6 Lift (Tilt)	8 Lift (Tractor)	8 Lift (Tilt)
maximize						
nominal cruise range						
with respect to						
incidence angles	-8°	8°	18	18	22	22
wing-mounted lift rotor diameters	2.0 m	3.1 m	2	2	0	0
	1.5 m	2.067 m	0	0	3	3
rear lift rotor diameters	2.0 m	2.738 m	2	2	2	2
tractor rotor diameters	1.5 m	2.0 m	1	0	1	0
normalized torque	0	1	72	54	110	88
motor speed	0 RPM	6000 RPM	72	54	110	88
battery position			1	1	1	1
battery mass	0 kg		1	1	1	1
wing scale factor	0.95	1.05	1	1	1	1
total design variables			170	133	251	206
subject to						
force equilibrium	0	0	11	11	13	13
moment equilibrium	0	0	18	18	22	22
tip mach number	0.0	0.6	8	6	10	8
CL max		1.7	18	18	22	22
blade loading coeff (lift rotor)		1.41	54	54	88	88
blade loading coeff (tractor rotor)		1.5	18	0	22	0
reserve range	10 km		1	1	1	1
hover time	2.5 min		1	1	1	1
total constraints			129	109	179	155

help minimize interactions between rotors, which are not currently modeled. A summary of all the design variables and constraints can be seen in Tab. 4.6.

This chapter, in full is currently being prepared for submission for publication of the material. Ha, Tae; Hwang, John T. The thesis author was the primary investigator and author of this material.

Table 4.6. Problem formulation for refined MDO.

Variable	Lower bound	Upper bound	Count	Notes
minimize				
total energy				
with respect to				
angle of attack	-3°	10°	2	cruise conditions only
tail trim angle	-8°	8°	7	all conditions
lift rotor blade pitch angle	-5°	30°	28	(2 rotor pairs + 2 individual) × 7 conditions
tractor rotor blade pitch angle	0°	55°	7	1 rotor pair × 7 conditions
blade twist profile control points	-10°	10°	50	(3 rotor pairs + 2 individual) × 10 control points
lift rotor radius	1.1 m	1.55 m	2	2 rotor pairs on wing
	1.1 m	1.369 m	2	2 individual rotors on rear
rotor speed	191 RPM	1910 RPM	56	8 rotors × 7 conditions
battery position	0	5	1	position along x-axis
battery weight	300 kg	800 kg	1	
wing area % change	-10.25	10.25	1	
total design variables			157	
subject to				
range	100 km		1	
CG	3.488	3.488	1	
force equilibrium	0	0	9	2 × (2 cruise) + 1 × (5 Hover)
moment equilibrium	0	0	12	1 × (2 cruise) + 2 × (5 Hover)
max tip mach number	0.0	0.6	8	
total constraints			31	

Chapter 5

Optimization results

5.1 Layout MDO

The layout MDO formulation converges in roughly hundreds to low thousands of function evaluations. Both optimality and feasibility decrease over 6 orders of magnitude to ensure constraints are fulfilled and a reasonable optimum is found. This was not guaranteed for each setup however as some layout configurations required tuning in terms of initial values for design variables to achieve convergence. All the following layout MDO results and data shown are of successful optimizations. An example of the SNOPT output history can be seen in Fig. 5.1 for the 6 Lift (Tractor) configuration optimization. The number of degrees of freedom indicate the number of design variables both not at a lower or upper bound and not used to satisfy a linear constraint. A more comprehensive list of data and results can be viewed in the tables in Appendix A and B. For reference, the abbreviated operating condition names in the data and the full names and description if required are shown below:

1. Cruise (The nominal cruise point)
2. Reserve (Cruise condition set at lower speed)
3. Hover (The nominal hover point)
4. Hover.OEI.LF1 (Hover point with the left outermost engine inoperable)

5. Hover.OEI.RF1 (Hover point with the right outermost engine inoperable)
6. Hover.OEI.LF2 (Hover point with the left second-to-outermost engine inoperable)
7. Hover.OEI.RF2 (Hover point with the right second-to-outermost engine inoperable)
8. Hover.OEI.RF (Hover point with the front of the two rear engines inoperable)
9. Hover.OEI.RR (Hover point with the rear of the two rear engines inoperable)

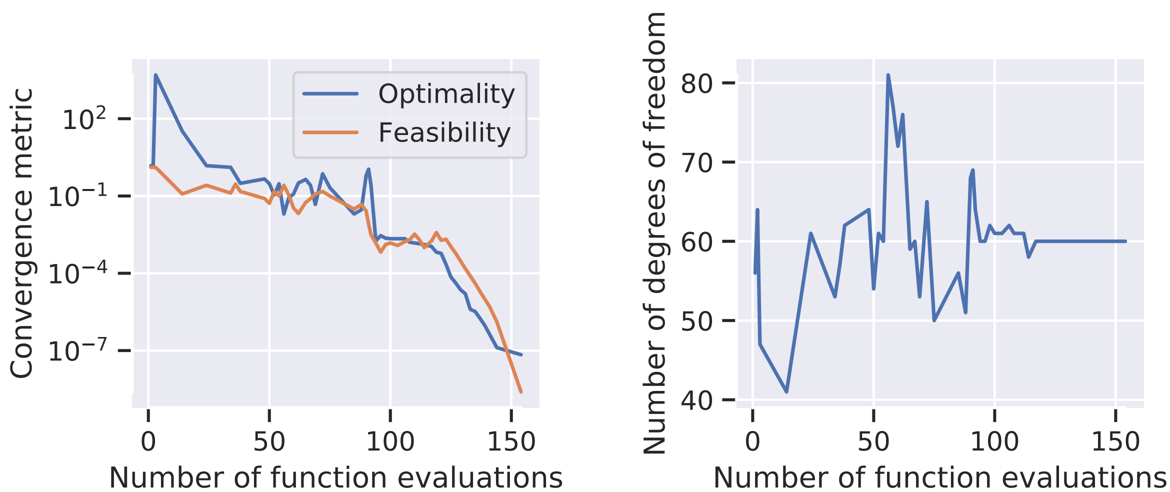

Figure 5.1. Optimization convergence history for the 6 Lift (Tractor) layout MDO.

A general set of performance metrics can be seen in Tab. 5.1.

Table 5.1. General overview of performance metrics comparing the various layout MDO configurations.

Layout	Cruise range (km)	Gross weight (lbs)	Battery weight (lbs)	Static margin
6 Lift (Tractor)	106.4	5724.5	2000.7	0.167
6 Lift (Tilt 1)	56.4	4102.2	986.9	0.038
6 Lift (Tilt 2)	116.0	5218.7	1941.7	0.1778
8 Lift (Tractor)	32.4	4843.8	854.3	0.001
8 Lift (Tilt 1)	13.5	4027.2	504.5	-0.137
8 Lift (Tilt 2)	31.8	4313.7	771.3	0.022
8 Lift (Tilt 3)	51.6	4656.7	1091.8	0.136

At first glance, the 6 Lift (Tractor) and 6 Lift (Tilt 2) layout configurations perform best all around. In terms of the prescribed objective function of range, these two configurations well outperform all other configurations by a significant factor. Gross weight and battery weight reflect similar information as the cruise range, showing a clear trend of higher cruise ranges associated with the capability to carry larger batteries and ultimately a larger gross weight. As for static margin, since there is no definitive 'ideal' value, this output was left as a 'soft' constraint, where the limits of the battery position CG (which was set as a design variable in the problem formulation) were manually controlled. A static margin value from 0.05 to 0.20 was considered reasonable, however if a value in that range was impossible to converge to, the constraint was relaxed and allowed to converge with only the main equilibrium constants in effect. This was the case in the configurations 6 Lift (Tilt 1), 8 Lift (Tractor), and 8 Lift (Tilt 1 and 2). While not impossible to utilize designs with low or negative static stability, such designs would require a computer-based autopilot to function normally. However, as eVTOL concepts are still in their primary stages in both development and community acceptance, many industries are currently looking towards manned vehicle development. In addition, the weight distributions for the layout MDO hold large margins of error, so calculated static margins are less trustworthy here and should not be used as a primary source of feasibility.

Looking at 6 vs 8 Lift rotor configurations, the 6 Lift rotor configurations perform better all around. The rotor data in tables A.2,A.3,A.4,A.5, for the 6 Lift (Tractor) configuration, and tables B.2, B.3, B.4, B.5, for the 8 Lift (Tractor) configuration, show both the 6 and 8 rotor layouts layouts have similar values in terms of motor and rotor efficiencies. Due to propeller spacing limiting the upper bounds of the rotor diameters, the total disc area for the 6 Lift rotor configurations is larger than that of the 8 Lift rotor configurations. With similar efficiencies being achieved, larger disc areas correlate to higher power and higher thrust output capabilities. Higher thrust outputs allow for feasible designs with larger gross weights as well as additional leniency on positioning for moment equilibrium constraint satisfaction. Due to the additional leniency on positioning, the aircraft CG location also can be altered slightly, assisting in achieving an acceptable static margin value.

For the tilt configurations, the engine out conditions strongly determines the best tilt rotor position. Due to the lack of current research regarding stacked rotors with tilt capability, the tilt rotors are modeled as a single rotating motor, where the entire propeller becomes a source of dead weight in the case of a failure scenario. This dead weight's position affects feasibility as satisfying moment constraints become more difficult as the moment arm lengths decrease for the functioning propellers. Wing area plays a factor as well, as rotor positions are tied parametrically to the wing. As a result, wing scaling can be used as a factor in satisfying moment constraints by moving the attached rotors. The final wing areas and L/D ratios can be seen in Tab. 5.2.

Table 5.2. Final wing area and L/D ratios for the optimized configurations.

Layout	Wing area (m^2)	L/D ratio
6 Lift (Tractor)	11.56	13.32
6 Lift (Tilt 1)	9.46	11.42
6 Lift (Tilt 2)	11.56	12.97
8 Lift (Tractor)	9.46	12.20
8 Lift (Tilt 1)	9.46	11.40
8 Lift (Tilt 2)	9.46	11.68
8 Lift (Tilt 3)	9.46	11.95

As a result, the two engine-out operating conditions for the tilt rotors (one each for both left and right sides) size the configuration design based off of worst-case scenario. As a reminder, the Tilt 1 configurations have the tilt rotor positioned on the tips of the wings, with each higher number correlating to the rotor position moving inwards towards the root of the wing. Looking at both 6 Lift and 8 Lift rotor configurations, as the tilt rotor position moves further in (and aft as well due to the wing having negative sweep), overall performance increases in both cruise range and static margin, highlighting the OEI operating condition as the main sizing factor and demonstrating its importance and role in the design process.

5.2 Refined MDO

Using the default 6 Lift (Tractor) configuration (identical to the Uber eCRM-002 base design), a refined MDO is run and iterates over hundreds of function evaluations, taking several days to process in total. During this time, feasibility decreases 5 orders of magnitude, showing constraints have been satisfied to an acceptable level. However, optimality struggles to decrease consistently and the optimization terminates due to numerical difficulties before convergence is reached, implying while a feasible design is produced, the resulting parameters have potential to improve. Several optimizations were run at various initial starting values, and the best performing optimization was chosen in terms of objective function value. The SNOPT output history of this run as well as the running number of degrees of freedom can be seen in Fig. 5.2. The abbreviated operating conditions follows the same naming convention as that of the layout MDO results.

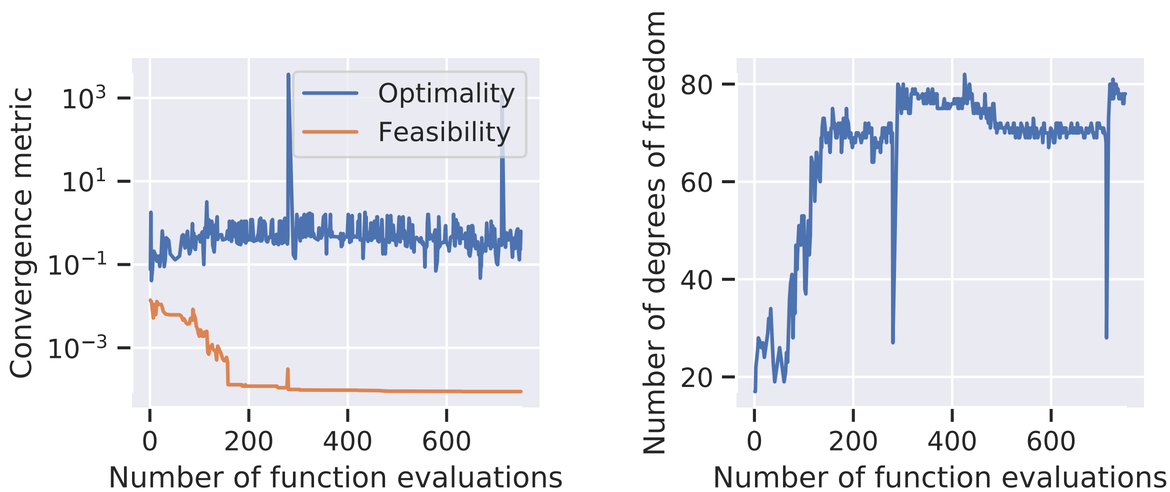

Figure 5.2. Optimization convergence history for the 6 Lift (Tractor) refined MDO.

The 3-D geometry produced with the inhouse Python framework can be seen in Fig. 5.3. Due to the symmetric nature of the optimization formulation and current focus, we exclude the vertical component of the tail that normally is sized for yaw moment and lateral stability.

Due to having results for one layout alone, as a reminder, the problem formulation is changed to minimize total power consumption knowing that the 100 km nominal cruise range

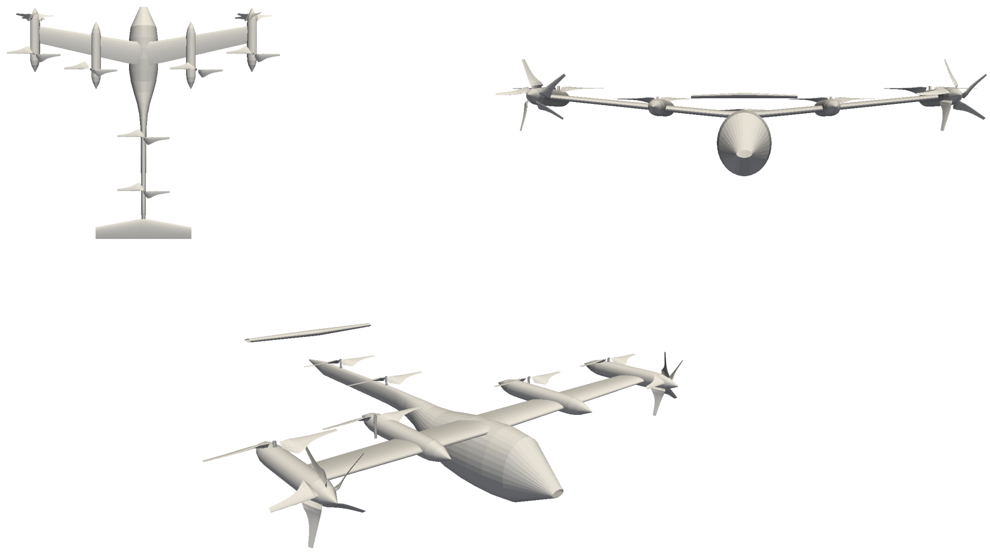

Figure 5.3. 3D visualization of the geometry used for the refined MDO.

requirement is already feasible. Due to its intended use, the configuration will likely not need to be able to fly for over this expected range, and instead adjusting the design to maximize efficiency is the next approach. A general overview of the performance metric data can be seen in Fig. 5.3. As a reminder, the right-side rotors do not have a engine-out operating condition due to the need to save on computational power; however, motor weights are mirrored and thus an engine-out condition on one side should theoretically size the other side appropriately for an identical but mirrored failure case.

Table 5.3. General performance overview for the 6 Lift (Tractor) configuration.

Condition	Alpha (deg)	Tail trim (deg)	Total power (kW)	L/D	Lift coeff	Drag coeff
Cruise	6.15	0.52	284.31	14.09	1.03	0.07
Reserve	10.0	3.17	313.58	12.43	1.49	0.12
Hover		-7.28	524.85			
Hover.OEI.LF1		-7.63	657.47			
Hover.OEI.LF2		-7.35	586.84			
Hover.OEI.RF		-8.0	545.18			
Hover.OEI.RR		-7.98	553.61			
	Payload weight (lb)	Battery weight (lb)	Battery weight fraction	Empty weight fraction	Gross weight (lb)	Wing area m^2
	770.8	1533.8	0.28	0.58	5483.4	11.21

The gross weight is slightly lower than that of the layout MDO results, with a few different possible factors. One is that by incorporating a 3-D geometry and a physics-based model for the aerodynamics along with slipstream influence being accounted for, lift and drag coefficients are able to be trusted more than those of the layout MDO formulation. The wing area increases slightly and lift-to-drag ratio appears high in the nominal cruise condition but lowers while total power usage increases in the reserve cruise operating condition. This trend contradicts the layout MDO results that claim the opposite, that for the airframe, lift-to-drag ratio should increase with total power usage decreasing at lower speeds. Using the refined MDO results, this shows the optimization is converging to some extent as the cruise operating condition is already operating near the maximum lift-to-drag ratio. One thing to note is that the lift coefficients for the cruise and reserve missions both seem fairly high. The relation between the cruise and reserve C_L can be explained using the standard equation that relates C_L to lift using the square of the inflow speed, and therefore the ratio of the inflow speeds squared is in proportion to the ratio of the lift coefficients, however the values of either condition would need further investigation. A detailed drag buildup along with the inputs used for the drag calculations can be seen in Tab. 5.4. This is still however a premature analysis as higher-fidelity tools are available in the form of computational fluid dynamics (CFD) simulations that can better predict both aerodynamic and drag analysis, but also identify interactions between components not captured in our model. For the fidelity and computational speed desired however, this level of analysis is sufficient for our formulation.

The other large factor in discrepancy regarding the difference between the refined and layout MDO gross weight lies in the weight breakdown, the buildup of which can be seen for the refined MDO in Tab. 5.5. The layout MDO's weight buildup is not included due to its lesser significance in terms of component locations aside from rotor positions as the purpose is mainly to identify rotor positioning benefits given an arbitrary configuration. While the refined MDO uses an empirical approach for the motor sizing, the layout MDO uses a semi-empirical model and thus the weights can quickly diverge as the central focus for both formulations lies in the

Table 5.4. Drag buildup for the 6 Lift (Tractor) refined MDO.

Component	Wetted area (m^2)	length (m)	FF	Re(1e-6)	Cf	Q	f	C_D
wing_C_D_i								0.014559
wing_C_D_p	23.305							0.011466
tail_C_D_i								0.026411
tail_C_D_p	8.505							0.011934
fuselage	32.555	12.168	1.242	53.5677	0.1104	1.05	6.426	0.004336
boom_left_1	4.426	3.3	1.314	14.5277	0.3075	1.3	5.849	0.001157
boom_right_1	4.426	3.3	1.314	14.5277	0.3075	1.3	5.849	0.001157
boom_left_2	4.687	3.5	1.267	15.4082	0.2907	1.3	6.204	0.001167
boom_right_2	4.687	3.5	1.267	15.4082	0.2907	1.3	6.204	0.001167

DEP-nature of the configurations.

Table 5.5. Weight buildup and component locations for the 6 Lift (Tractor) refined MDO.

Component	Weight (lbs)	CG (x)
wing	373.435	2.404
tail	136.564	11.735
fuselage	615.048	6.084
boom_left_1	41.975	1.988
boom_right_1	41.975	1.988
boom_left_2	44.346	2.75
boom_right_2	44.346	2.75
battery	1533.79	2.676
flight_ctrls	275.281	3.69
payload	770.786	3.3
wiring	127.07	3.5
landing_gear	189.393	3.69
left_front_1_rotor	162.671	2.738
right_front_1_rotor	162.671	2.738
left_front_2_rotor	144.252	3.5
right_front_2_rotor	144.252	3.5
left_pusher_rotor	142.695	0.589
right_pusher_rotor	142.695	0.589
rear_front_rotor	40.141	7.0
rear_rear_rotor	19.679	9.8
Gross weight	5483.4	3.488

The comparison of the total power consumption between the refined MDO results and the layout MDO of the same configuration can be seen in Fig. 5.4. While the total power consumed in the nominal cruise condition is nearly identical, the reserve cruise and hover conditions show some discrepancies. The reserve cruise discrepancy can be attributed to the aerodynamic performance. As mentioned before, the refined MDO results show the design operating at closer to the max lift-to-drag ratio, while the layout MDO shows by decreasing speed, lift-to-drag ratio can be increased. Thus, an increase or decrease in lift-to-drag ratio would affect the power required to operate, with the configuration requiring higher power as the lift-to-drag ratio decreases as speed decreases for the refined MDO, and the opposite for the layout MDO formulation. The hover condition total power discrepancies can be partially attributed to the difference in gross weight, of which the refined MDO results show a smaller value and thus a lower power output would be required to keep the configuration in force equilibrium. Through additional tuning to allow more identical configurations, a more proper comparison for the application of Glauert model and the BEMT model for a system-level analysis can be made.

Figure 5.4. Total power consumption comparison between the layout MDO and refined MDO formulations for the 6 Lift (Tractor) configuration.

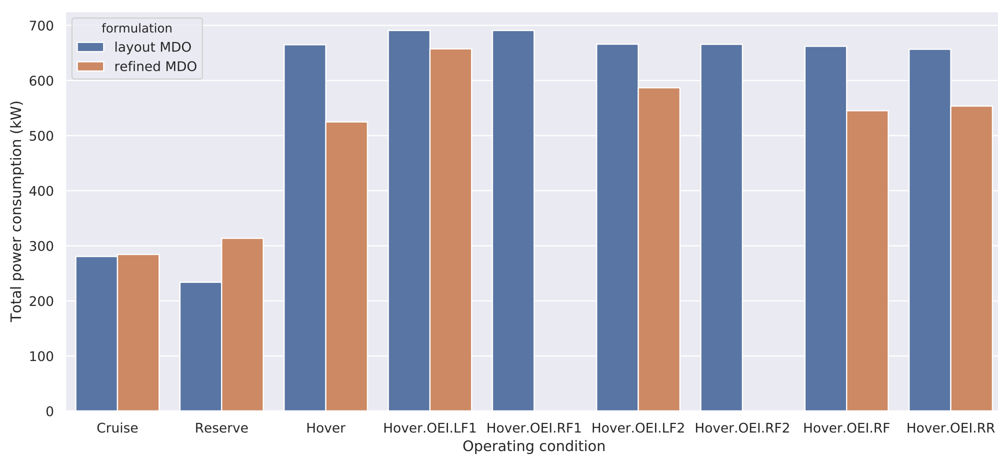

These two methods can be used together in the design process as a pseudo-multifidelity as results from the layout MDO can be compared with equivalent measures from the refined MDO, used back to adjust the parameters of the layout MDO setups. Through iterations of this process, a robust design that satisfies both the layout MDO and refined MDO formulations can be produced, capitalizing on DEP benefits from both rotor positioning and a unique 3-D geometry.

This chapter, in full is currently being prepared for submission for publication of the material. Ha, Tae; Hwang, John T. The thesis author was the primary investigator and author of this material.

Chapter 6

Conclusion and future work

Research objectives and procedure

This thesis aimed to accomplish three research objectives:

1. Develop a method for large-scale MDO of eVTOL concepts capable of exploring redundancy benefits through strict rotor *layout* comparisons that highlight design features

2. Develop a more *refined* method for large-scale MDO of eVTOL concepts using higher-fidelity models paired with a 3-D geometry to obtain designs based on results with increased validity

3. Explore the effects and determine which rotor layout design changes will potentially yield benefits for maximizing range capabilities

The first method utilizes parameter equations to build up a rudimentary geometry to be used alongside a sizing-level predictive motor model and a momentum-theory based rotor model. Due to its low computational cost, this method is well-suited for analyzing and comparing multiple high-level design parameter changes, focusing mainly on the rotor layout. The second refined method incorporates a 3-D geometry, created internally within the Python framework to provide clear parameters and exact derivative computation, with physics-based models for both aerodynamic and propulsion analysis. As a higher-fidelity model that takes considerably longer, this method is better suited as a further in-depth analysis to a single or low number of designs, either as a stand-alone set of results or for comparison with results obtained from the previously mentioned formulation.

The baseline configuration chosen to test these methods was Uber's eCRM-002 model due to its simplicity and relative ease to make changes such as rotor number and and positions that would show results with more direct correlation, as opposed to a more convoluted design where adding additional rotors could possibly add complications that would require finer testing beyond the scope of this thesis. The high-level changes that were made were increasing the number of rotors on the wing, changing the design from a lift + cruise configuration to a vectored thrust configuration, and finally changing the position of the tilt rotor for the vectored thrust variants. These designs were set to optimize under several operating conditions simultaneously, consisting of both cruise and hover missions. Among the hover conditions included failure scenarios where lift rotors would be inoperable, and the design would need to be sized appropriately so that in all conditions, force and moment equilibrium constraints would need to be satisfied using sets of operational and design parameter variables.

Optimization results

Looking at the optimization results for the first formulation that is labeled as the layout MDO, two configurations clearly performed the best in terms of range maximization and longitudinal stability measures, the 6 Lift (Tractor) and 6 Lift (Tilt 2) configurations. The change from 6 to 8 lift rotors only saw negative effects as overall rotor area decreased due to spacing limitations on the wing, and thus total power and thrust output were unable to sustain the extra mass of larger batteries and overall larger gross weight. For tilt rotor placement for the vectored cruise configurations, due to the engine failure operating condition, the design saw the largest benefit in moving tilt rotors closer to the aircraft CG due to the combination of using stacked lift rotors for redundancy and satisfying moment equilibrium constraints. The base configuration was tested again using the second formulation, labeled as the refined MDO, to provide more detailed analysis and saw similar general results, however notable discrepancies involving the aerodynamic and weight data and their possible explanations were discussed.

Future work

From here, there are many directions in which to either improve or expand on these results. For the layout MDO, to keep the scale and speed of the current working discipline models, any adjustments made would be either corrections or tuning, and likely the next approach would be to either integrate additional models such as a hybrid-system setup for increased design capability or more extensive use to test a larger and unexplored variety of design features for eVTOL concepts. For the refined MDO, with the 3-D geometry integrated into the analysis process, there are many areas to improve the model from a system-level standpoint. One feature would be the capability to integrate external geometries, allowing increased versatility and use as a tool. Another would be to add a controls module, which would directly influence the positioning of the rotors on aircraft, possibly contradicting suggested changes made from the layout MDO. While currently built for eVTOL analysis, it has potential for widespread analysis of any type of aircraft. Further tuning and adjustments of the current discipline models using high-fidelity analysis tools such as CFD simulations would help the validity of the results, and even the possibility of integrating such tools into the formulation could develop it into a multi-fidelity model. Ultimately, due to the large number of similarities in setup between the layout and refined MDO, being able to combine the two into one package capable of aircraft analysis would hold large potential as the proper infrastructure would be able to ease the implementation of additional discipline models and create one all-encompassing tool to perform aircraft analysis at any level.

Appendix A

Layout MDO data tables (for 6 Lift configurations)

Table A.1. General performance overview for the 6 Lift (Tractor) configuration.

Condition	Total power (kW)	Lift coeff	Drag coeff	L/D	Wing incidence angle (°)	Tail incidence angle (°)
Cruise	280595.5	0.9828	0.0738	13.3178	5.006	-0.414
Reserve	233845.5	1.4145	0.1044	13.5519	8.141	0.273
Hover	664933.1					
Hover.OEI.LF1	690786.3					
Hover.OEI.RF1	690785.9					
Hover.OEI.LF2	665973.3					
Hover.OEI.RF2	665695.1					
Hover.OEI.RF	662095.2					
Hover.OEI.RR	656706.5					

Payload weight (lb)	Battery weight (lb)	Battery weight fraction	Gross weight (lb)	Wing area (m^2)
784.8	2000.7	0.349	5724.5	11.56

Table A.2. Rotor metrics/outputs for the 6 Lift (Tractor) configuration (Part 1).

Condition	Rotor	Motor RPM	Thrust (N)	Thrust margin	Motor Torque (Nm)	Torque margin	Power (kW)	Power margin	Motor efficiency (%)
Cruise	LF1_rotor								
Cruise	RF1_rotor								
Cruise	LF2_rotor								
Cruise	RF2_rotor								
Cruise	LP1_rotor	4490.0	955.4	1.0	193.8	1.0	140.3	1.0	90.9
Cruise	RP1_rotor	4490.0	955.5	1.0	193.8	1.0	140.3	1.0	90.9
Cruise	RF_rotor								
Cruise	RR_rotor								
Reserve	LF1_rotor								
Reserve	RF1_rotor								
Reserve	LF2_rotor								
Reserve	RF2_rotor								
Reserve	LP1_rotor	4405.4	939.0	1.018	164.2	1.18	116.9	1.2	90.7
Reserve	RP1_rotor	4405.4	939.0	1.018	164.2	1.18	116.9	1.2	90.7
Reserve	RF_rotor								
Reserve	RR_rotor								
Condition	Rotor	Motor RPM	Thrust (N)	Thrust margin	Motor Torque (Nm)	Torque margin	Power (kW)	Power margin	Motor efficiency (%)
Hover	LF1_rotor	4220.1	5326.3	1.394	113.0	1.248	141.8	1.483	88.7
Hover	RF1_rotor	4220.1	5326.3	1.394	113.0	1.248	141.8	1.482	88.7
Hover	LF2_rotor	4213.1	5308.5	1.426	112.6	1.252	141.1	1.532	88.7
Hover	RF2_rotor	4213.1	5308.5	1.426	112.6	1.252	141.1	1.532	88.7
Hover	LP1_rotor								
Hover	RP1_rotor								
Hover	RF_rotor	4604.3	3857.2	1.0	72.7	1.034	99.2	1.0	89.1
Hover	RR_rotor	9.5	0.0	0.0	0.0	0.0	0.0	0.0	0.0
Hover.OEI.LF1	LF1_rotor	5031.7	3365.4	2.206	141.0	1.0	96.1	2.188	86.6
Hover.OEI.LF1	RF1_rotor	5000.9	3365.4	2.206	50.7	2.782	75.7	2.778	88.4
Hover.OEI.LF1	LF2_rotor	5031.7	7572.1	1.0	141.0	1.0	216.2	1.0	86.6
Hover.OEI.LF1	RF2_rotor	5031.7	7572.1	1.0	141.0	1.0	216.2	1.0	86.6
Hover.OEI.LF1	LP1_rotor								
Hover.OEI.LF1	RP1_rotor								
Hover.OEI.LF1	RF_rotor	4939.3	3572.5	1.08	56.1	1.34	82.5	1.203	88.7
Hover.OEI.LF1	RR_rotor	4999.7	0.0	0.0	0.0	0.0	4.3	6.805	0.1

Table A.3. Rotor metrics/outputs for the 6 Lift (Tractor) configuration (Part 2).

Condition	Rotor	Motor RPM	Thrust (N)	Thrust margin	Motor Torque (Nm)	Torque margin	Power (kW)	Power margin	Motor efficiency (%)
Hover.OEI.RF1	LF1_rotor	5000.9	3365.4	2.206	50.7	2.782	75.7	2.779	88.4
Hover.OEI.RF1	RF1_rotor	5031.7	3365.4	2.206	141.0	1.0	96.1	2.187	86.6
Hover.OEI.RF1	LF2_rotor	5031.7	7572.0	1.0	141.0	1.0	216.2	1.0	86.6
Hover.OEI.RF1	RF2_rotor	5031.7	7572.1	1.0	141.0	1.0	216.2	1.0	86.6
Hover.OEI.RF1	LP1_rotor								
Hover.OEI.RF1	RP1_rotor								
Hover.OEI.RF1	RF_rotor	4939.3	3572.5	1.08	56.1	1.34	82.5	1.202	88.7
Hover.OEI.RF1	RR_rotor	4999.8	0.0	0.0	0.0	0.0	4.3	6.805	0.1
Hover.OEI.LF2	LF1_rotor	4997.6	6711.3	1.106	121.2	1.164	182.7	1.15	87.4
Hover.OEI.LF2	RF1_rotor	5010.5	4731.5	1.569	77.2	1.826	115.1	1.825	88.7
Hover.OEI.LF2	LF2_rotor	4975.6	3290.7	2.301	138.1	1.021	92.9	2.328	86.8
Hover.OEI.LF2	RF2_rotor	4958.1	7352.2	1.03	137.3	1.027	206.7	1.046	86.9
Hover.OEI.LF2	LP1_rotor								
Hover.OEI.LF2	RP1_rotor								
Hover.OEI.LF2	RF_rotor	4934.5	2232.9	1.727	30.8	2.442	46.4	2.137	86.4
Hover.OEI.LF2	RR_rotor	5004.8	1111.4	1.151	13.0	3.36	22.1	1.317	77.5
Condition	Rotor	Motor RPM	Thrust (N)	Thrust margin	Motor Torque (Nm)	Torque margin	Power (kW)	Power margin	Motor efficiency (%)
Hover.OEI.RF2	LF1_rotor	5016.2	4711.7	1.576	76.7	1.838	114.6	1.835	88.7
Hover.OEI.RF2	RF1_rotor	5004.1	6694.3	1.109	120.7	1.169	182.2	1.153	87.5
Hover.OEI.RF2	LF2_rotor	4952.3	7334.8	1.032	137.0	1.03	206.0	1.049	86.9
Hover.OEI.RF2	RF2_rotor	4958.1	3267.6	2.317	137.3	1.027	91.9	2.353	86.9
Hover.OEI.RF2	LP1_rotor								
Hover.OEI.RF2	RP1_rotor								
Hover.OEI.RF2	RF_rotor	4936.0	2429.2	1.588	34.2	2.199	51.2	1.937	87.0
Hover.OEI.RF2	RR_rotor	5004.8	992.5	1.289	11.4	3.83	19.9	1.462	75.6
Hover.OEI.RF	LF1_rotor	5019.5	3880.5	1.913	60.2	2.343	89.9	2.338	88.7
Hover.OEI.RF	RF1_rotor	5017.9	3875.9	1.915	60.1	2.346	89.8	2.341	88.7
Hover.OEI.RF	LF2_rotor	4954.9	7342.6	1.031	137.1	1.029	206.3	1.048	86.9
Hover.OEI.RF	RF2_rotor	4958.1	7352.2	1.03	137.3	1.027	206.7	1.046	86.9
Hover.OEI.RF	LP1_rotor								
Hover.OEI.RF	RP1_rotor								
Hover.OEI.RF	RF_rotor	4957.2	1987.2	1.941	75.1	1.0	49.2	2.014	88.7
Hover.OEI.RF	RR_rotor	5004.8	1006.0	1.272	11.6	3.771	20.2	1.445	75.8
Condition	Rotor	Motor RPM	Thrust (N)	Thrust margin	Motor Torque (Nm)	Torque margin	Power (kW)	Power margin	Motor efficiency (%)
Hover.OEI.RR	LF1_rotor	5020.7	7424.3	1.0	137.7	1.024	210.2	1.0	86.8
Hover.OEI.RR	RF1_rotor	5020.1	7422.4	1.0	137.6	1.024	210.1	1.0	86.8
Hover.OEI.RR	LF2_rotor	4958.5	3486.8	2.172	53.1	2.653	78.5	2.753	88.6
Hover.OEI.RR	RF2_rotor	4959.8	3490.5	2.169	53.2	2.65	78.6	2.749	88.6
Hover.OEI.RR	LP1_rotor								
Hover.OEI.RR	RP1_rotor								
Hover.OEI.RR	RF_rotor	4942.9	2381.5	1.62	33.3	2.256	50.0	1.982	86.8
Hover.OEI.RR	RR_rotor	5008.0	1279.2	1.0	43.7	1.0	29.2	1.0	88.0

Table A.4. Rotor metrics/outputs for the 6 Lift (Tractor) configuration (Part 3).

Condition	Rotor	Rotor RPM	J	Thrust coeff	Power coeff	Disk loading (kg/m^2)	Tip Mach	Blade loading coeff	Rotor efficiency (%)
Cruise	LF1_rotor								
Cruise	RF1_rotor								
Cruise	LF2_rotor								
Cruise	RF2_rotor								
Cruise	LP1_rotor	1122.5	1.783	0.22	0.432	40.302	0.353	1.469	90.9
Cruise	RP1_rotor	1122.5	1.783	0.22	0.432	40.303	0.353	1.469	90.9
Cruise	RF_rotor								
Cruise	RR_rotor								
Reserve	LF1_rotor								
Reserve	RF1_rotor								
Reserve	LF2_rotor								
Reserve	RF2_rotor								
Reserve	LP1_rotor	1101.3	1.515	0.225	0.38	39.608	0.347	1.5	89.6
Reserve	RP1_rotor	1101.3	1.515	0.225	0.38	39.608	0.347	1.5	89.6
Reserve	RF_rotor								
Reserve	RR_rotor								

Condition	Rotor	Rotor RPM	J	Thrust coeff	Power coeff	Disk loading (kg/m^2)	Tip Mach	Blade loading coeff	Rotor efficiency (%)
Hover	LF1_rotor	1055.0	0.092	0.085	0.026	39.964	0.503	1.41	75.0
Hover	RF1_rotor	1055.0	0.092	0.085	0.026	39.964	0.503	1.41	75.0
Hover	LF2_rotor	1053.3	0.092	0.085	0.026	39.831	0.502	1.41	75.0
Hover	RF2_rotor	1053.3	0.092	0.085	0.026	39.831	0.502	1.41	75.0
Hover	LP1_rotor								
Hover	RP1_rotor								
Hover	RF_rotor	1151.1	0.095	0.085	0.026	37.106	0.485	1.41	74.5
Hover	RR_rotor	2.4	51.504	0.0	0.0	0.0	0.001	0.0	0.0
Hover.OEI.LF1	LF1_rotor	1257.9	0.031	0.085	0.023	56.814	0.6	1.41	85.4
Hover.OEI.LF1	RF1_rotor	1250.2	0.031	0.038	0.008	25.251	0.596	0.634	70.8
Hover.OEI.LF1	LF2_rotor	1257.9	0.031	0.085	0.023	56.814	0.6	1.41	85.4
Hover.OEI.LF1	RF2_rotor	1257.9	0.031	0.085	0.023	56.814	0.6	1.41	85.4
Hover.OEI.LF1	LP1_rotor								
Hover.OEI.LF1	RP1_rotor								
Hover.OEI.LF1	RF_rotor	1234.8	0.035	0.068	0.018	34.366	0.52	1.135	80.3
Hover.OEI.LF1	RR_rotor	1249.9	0.039	0.0	0.0	0.0	0.469	0.0	0.0

Table A.5. Rotor metrics/outputs for the 6 Lift (Tractor) configuration (Part 4).

Condition	Rotor	Rotor RPM	J	Thrust coeff	Power coeff	Disk loading (kg/m^2)	Tip Mach	Blade loading coeff	Rotor efficiency (%)
Hover.OEI.RF1	LF1_rotor	1250.2	0.031	0.038	0.008	25.251	0.596	0.634	70.8
Hover.OEI.RF1	RF1_rotor	1257.9	0.031	0.085	0.023	56.814	0.6	1.41	85.4
Hover.OEI.RF1	LF2_rotor	1257.9	0.031	0.085	0.023	56.814	0.6	1.41	85.4
Hover.OEI.RF1	RF2_rotor	1257.9	0.031	0.085	0.023	56.815	0.6	1.41	85.4
Hover.OEI.RF1	LP1_rotor								
Hover.OEI.RF1	RP1_rotor								
Hover.OEI.RF1	RF_rotor	1234.8	0.035	0.068	0.018	34.366	0.52	1.135	80.3
Hover.OEI.RF1	RR_rotor	1249.9	0.039	0.0	0.0	0.0	0.469	0.0	0.0
Hover.OEI.LF2	LF1_rotor	1249.4	0.031	0.076	0.02	50.356	0.596	1.267	83.5
Hover.OEI.LF2	RF1_rotor	1252.6	0.031	0.053	0.013	35.501	0.597	0.889	77.4
Hover.OEI.LF2	LF2_rotor	1243.9	0.031	0.085	0.023	55.555	0.593	1.41	85.2
Hover.OEI.LF2	RF2_rotor	1239.5	0.031	0.085	0.023	55.165	0.591	1.41	85.2
Hover.OEI.LF2	LP1_rotor								
Hover.OEI.LF2	RP1_rotor								
Hover.OEI.LF2	RF_rotor	1233.6	0.036	0.043	0.01	21.48	0.52	0.711	72.3
Hover.OEI.LF2	RR_rotor	1251.2	0.039	0.033	0.007	13.462	0.47	0.545	66.5
Condition	Rotor	Rotor RPM	J	Thrust coeff	Power coeff	Disk loading (kg/m^2)	Tip Mach	Blade loading coeff	Rotor efficiency (%)
Hover.OEI.RF2	LF1_rotor	1254.0	0.031	0.053	0.013	35.352	0.598	0.883	77.3
Hover.OEI.RF2	RF1_rotor	1251.0	0.031	0.076	0.02	50.228	0.597	1.26	83.4
Hover.OEI.RF2	LF2_rotor	1238.1	0.031	0.085	0.023	55.035	0.591	1.41	85.2
Hover.OEI.RF2	RF2_rotor	1239.5	0.031	0.085	0.023	55.164	0.591	1.41	85.2
Hover.OEI.RF2	LP1_rotor								
Hover.OEI.RF2	RP1_rotor								
Hover.OEI.RF2	RF_rotor	1234.0	0.036	0.046	0.011	23.368	0.52	0.773	73.9
Hover.OEI.RF2	RR_rotor	1251.2	0.039	0.029	0.006	12.021	0.47	0.487	64.0
Hover.OEI.RF	LF1_rotor	1254.9	0.031	0.044	0.01	29.116	0.599	0.726	73.6
Hover.OEI.RF	RF1_rotor	1254.5	0.031	0.044	0.01	29.081	0.598	0.726	73.6
Hover.OEI.RF	LF2_rotor	1238.7	0.031	0.085	0.023	55.093	0.591	1.41	85.2
Hover.OEI.RF	RF2_rotor	1239.5	0.031	0.085	0.023	55.165	0.591	1.41	85.2
Hover.OEI.RF	LP1_rotor								
Hover.OEI.RF	RP1_rotor								
Hover.OEI.RF	RF_rotor	1239.3	0.035	0.085	0.023	43.012	0.522	1.41	83.6
Hover.OEI.RF	RR_rotor	1251.2	0.039	0.03	0.006	12.186	0.47	0.493	64.3
Condition	Rotor	Rotor RPM	J	Thrust coeff	Power coeff	Disk loading (kg/m^2)	Tip Mach	Blade loading coeff	Rotor efficiency (%)
Hover.OEI.RR	LF1_rotor	1255.2	0.031	0.083	0.023	55.706	0.599	1.389	85.1
Hover.OEI.RR	RF1_rotor	1255.0	0.031	0.083	0.023	55.692	0.599	1.389	85.1
Hover.OEI.RR	LF2_rotor	1239.6	0.031	0.04	0.009	26.162	0.591	0.669	71.9
Hover.OEI.RR	RF2_rotor	1239.9	0.031	0.04	0.009	26.19	0.591	0.669	71.9
Hover.OEI.RR	LP1_rotor								
Hover.OEI.RR	RP1_rotor								
Hover.OEI.RR	RF_rotor	1235.7	0.035	0.045	0.01	22.91	0.521	0.755	73.5
Hover.OEI.RR	RR_rotor	1252.0	0.039	0.085	0.024	34.863	0.47	1.41	82.4

Table A.6. General performance overview for the 6 Lift (Tilt 1) configuration.

Condition	Total power (kW)	Lift coeff	Drag coeff	L/D	Wing incidence angle (°)	Tail incidence angle (°)
Cruise	229832.1	0.86	0.0753	11.424	3.947	-0.365
Reserve	172790.9	1.238	0.0977	12.6712	6.613	0.344
Hover	435839.1					
Hover.OEI.LF1	522633.0					
Hover.OEI.RF1	519117.1					
Hover.OEI.LF2	600975.3					
Hover.OEI.RF2	532698.7					
Hover.OEI.RF	529064.9					
Hover.OEI.RR	516041.3					
Payload weight (lb)	**Battery weight (lb)**	**Battery weight fraction**	**Gross weight (lb)**	**Wing area (m^2)**		
784.8	986.9	0.241	4102.2	9.46		

Table A.7. Rotor metrics/outputs for the 6 Lift (Tilt 1) configuration (Part 1).

Condition	Rotor	Motor RPM	Thrust (N)	Thrust margin	Motor Torque (Nm)	Torque margin	Power (kW)	Power margin	Motor efficiency (%)
Cruise	LF1_rotor	9.5	0.0	0.0	0.0	0.0	0.0	0.0	0.0
Cruise	RF1_rotor	2791.4	1595.7	4.284	513.4	1.0	229.8	1.0	91.4
Cruise	LF2_rotor								
Cruise	RF2_rotor								
Cruise	RF_rotor								
Cruise	RR_rotor								
Reserve	LF1_rotor	9.5	0.0	0.0	0.0	0.0	0.0	0.0	0.0
Reserve	RF1_rotor	2725.6	1439.0	4.75	398.0	1.29	172.8	1.33	92.0
Reserve	LF2_rotor								
Reserve	RF2_rotor								
Reserve	RF_rotor								
Reserve	RR_rotor								
Condition	**Rotor**	**Motor RPM**	**Thrust (N)**	**Thrust margin**	**Motor Torque (Nm)**	**Torque margin**	**Power (kW)**	**Power margin**	**Motor efficiency (%)**
Hover	LF1_rotor	2591.9	2968.6	2.302	186.1	1.585	77.1	3.119	91.8
Hover	RF1_rotor	2592.0	2968.9	2.302	186.1	2.759	77.1	2.982	91.8
Hover	LF2_rotor	3906.6	4564.4	1.659	98.0	1.438	113.9	1.898	88.7
Hover	RF2_rotor	3906.4	4563.9	1.659	98.0	1.439	113.9	1.898	88.7
Hover	RF_rotor	3257.0	1930.1	2.389	39.0	2.303	38.3	3.025	87.5
Hover	RR_rotor	2294.9	958.3	2.591	21.5	3.067	15.6	3.496	83.1
Hover.OEI.LF1	LF1_rotor	5000.0	0.0	0.0	0.1	0.0	0.0	0.0	1.6
Hover.OEI.LF1	RF1_rotor	4568.8	0.0	0.0	10.6	48.5	12.5	18.392	56.7
Hover.OEI.LF1	LF2_rotor	5031.7	7572.1	1.0	141.0	1.0	216.2	1.0	86.6
Hover.OEI.LF1	RF2_rotor	5031.7	7572.1	1.0	141.0	1.0	216.2	1.0	86.6
Hover.OEI.LF1	RF_rotor	5338.6	3088.7	1.493	44.1	2.036	70.7	1.639	87.9
Hover.OEI.LF1	RR_rotor	5616.4	0.0	0.0	1.5	44.336	7.1	7.708	31.0

Table A.8. Rotor metrics/outputs for the 6 Lift (Tilt 1) configuration (Part 2).

Condition	Rotor	Motor RPM	Thrust (N)	Thrust margin	Motor Torque (Nm)	Torque margin	Power (kW)	Power margin	Motor efficiency (%)
Hover.OEI.RF1	LF1_rotor	4704.8	0.0	0.0	10.7	27.452	13.0	18.507	57.1
Hover.OEI.RF1	RF1_rotor	5000.0	0.0	0.0	0.1	0.0	0.0	0.0	1.6
Hover.OEI.RF1	LF2_rotor	5031.7	7572.1	1.0	141.0	1.0	216.2	1.0	86.6
Hover.OEI.RF1	RF2_rotor	5031.7	7572.1	1.0	141.0	1.0	216.2	1.0	86.6
Hover.OEI.RF1	RF_rotor	4527.3	3088.7	1.493	49.4	1.818	66.6	1.741	88.6
Hover.OEI.RF1	RR_rotor	5615.1	0.0	0.0	1.6	41.449	7.3	7.542	32.5
Hover.OEI.LF2	LF1_rotor	5020.7	6835.1	1.0	295.0	1.0	240.3	1.0	90.3
Hover.OEI.LF2	RF1_rotor	4371.2	6835.1	1.0	324.6	1.581	229.3	1.002	90.7
Hover.OEI.LF2	LF2_rotor	4990.8	0.0	0.0	0.0	0.0	1.9	113.849	0.0
Hover.OEI.LF2	RF2_rotor	5019.7	0.0	0.0	0.0	0.0	4.3	50.301	0.0
Hover.OEI.LF2	RF_rotor	5034.5	4611.7	1.0	77.3	1.161	115.9	1.0	88.6
Hover.OEI.LF2	RR_rotor	5030.3	4.7	531.265	3.6	18.455	9.2	5.943	51.5

Condition	Rotor	Motor RPM	Thrust (N)	Thrust margin	Motor Torque (Nm)	Torque margin	Power (kW)	Power margin	Motor efficiency (%)
Hover.OEI.RF2	LF1_rotor	4755.6	5433.6	1.258	231.7	1.273	177.9	1.351	90.8
Hover.OEI.RF2	RF1_rotor	5009.8	4890.5	1.398	198.1	2.592	160.5	1.432	90.6
Hover.OEI.RF2	LF2_rotor	4535.7	2148.8	3.524	31.2	4.523	43.1	5.016	86.6
Hover.OEI.RF2	RF2_rotor	4954.6	3263.0	2.321	137.1	1.029	91.7	2.358	86.9
Hover.OEI.RF2	RF_rotor	5396.5	0.0	0.0	0.1	728.889	4.8	24.099	3.6
Hover.OEI.RF2	RR_rotor	5350.8	2483.1	1.0	33.6	1.96	54.7	1.0	86.7
Hover.OEI.RF	LF1_rotor	4898.7	2551.5	2.679	94.8	3.113	76.8	3.13	88.6
Hover.OEI.RF	RF1_rotor	4302.7	5773.7	1.184	266.7	1.925	184.8	1.244	91.0
Hover.OEI.RF	LF2_rotor	4701.3	6610.2	1.146	124.5	1.133	176.0	1.228	87.7
Hover.OEI.RF	RF2_rotor	5031.7	0.0	0.0	0.1	0.0	4.4	48.827	2.6
Hover.OEI.RF	RF_rotor	5458.7	2409.5	1.914	89.8	1.0	65.4	1.774	88.0
Hover.OEI.RF	RR_rotor	5317.0	922.0	2.693	11.7	5.612	21.7	2.523	75.9

Condition	Rotor	Motor RPM	Thrust (N)	Thrust margin	Motor Torque (Nm)	Torque margin	Power (kW)	Power margin	Motor efficiency (%)
Hover.OEI.RR	LF1_rotor	4619.3	3695.9	1.849	148.2	1.99	111.0	2.165	90.4
Hover.OEI.RR	RF1_rotor	4408.8	6282.2	1.088	290.9	1.765	206.9	1.111	90.9
Hover.OEI.RR	LF2_rotor	4211.9	5305.7	1.427	101.5	1.389	126.7	1.706	89.0
Hover.OEI.RR	RF2_rotor	4912.6	0.0	0.0	0.0	0.0	4.2	51.427	0.0
Hover.OEI.RR	RF_rotor	5162.3	1278.0	3.608	16.0	5.623	27.1	4.276	80.3
Hover.OEI.RR	RR_rotor	4618.5	1724.9	1.44	65.8	1.0	40.1	1.365	89.0

Table A.9. Rotor metrics/outputs for the 6 Lift (Tilt 1) configuration (Part 3).

Condition	Rotor	Rotor RPM	J	Thrust coeff	Power coeff	Disk loading (kg/m^2)	Tip Mach	Blade loading coeff	Rotor efficiency (%)
Cruise	LF1_rotor	2.4	540.758	0.0	0.0	0.0	0.001	0.0	0.0
Cruise	RF1_rotor	697.9	1.85	0.165	0.331	28.016	0.341	1.1	92.2
Cruise	LF2_rotor								
Cruise	RF2_rotor								
Cruise	RF_rotor								
Cruise	RR_rotor								
Reserve	LF1_rotor	2.4	450.767	0.0	0.0	0.0	0.001	0.0	0.0
Reserve	RF1_rotor	681.4	1.579	0.156	0.269	25.265	0.333	1.04	91.6
Reserve	LF2_rotor								
Reserve	RF2_rotor								
Reserve	RF_rotor								
Reserve	RR_rotor								
Condition	Rotor	Rotor RPM	J	Thrust coeff	Power coeff	Disk loading (kg/m^2)	Tip Mach	Blade loading coeff	Rotor efficiency (%)
Hover	LF1_rotor	648.0	0.149	0.225	0.114	40.093	0.309	1.5	74.5
Hover	RF1_rotor	648.0	0.149	0.225	0.114	40.097	0.309	1.5	74.5
Hover	LF2_rotor	976.7	0.099	0.085	0.027	34.248	0.466	1.41	74.0
Hover	RF2_rotor	976.6	0.099	0.085	0.027	34.244	0.466	1.41	74.0
Hover	RF_rotor	814.3	0.135	0.085	0.028	18.567	0.343	1.41	69.5
Hover	RR_rotor	573.7	0.191	0.085	0.031	9.218	0.242	1.41	62.7
Hover.OEI.LF1	LF1_rotor	1250.0	0.031	0.0	0.0	0.0	0.596	0.0	0.0
Hover.OEI.LF1	RF1_rotor	1142.2	0.034	0.0	0.002	0.0	0.545	0.0	0.0
Hover.OEI.LF1	LF2_rotor	1257.9	0.031	0.085	0.023	56.814	0.6	1.41	85.4
Hover.OEI.LF1	RF2_rotor	1257.9	0.031	0.085	0.023	56.814	0.6	1.41	85.4
Hover.OEI.LF1	RF_rotor	1334.6	0.033	0.05	0.012	29.713	0.562	0.84	75.9
Hover.OEI.LF1	RR_rotor	1404.1	0.031	0.0	0.0	0.0	0.591	0.0	0.0

Table A.10. Rotor metrics/outputs for the 6 Lift (Tilt 1) configuration (Part 4).

Condition	Rotor	Rotor RPM	J	Thrust coeff	Power coeff	Disk loading (kg/m^2)	Tip Mach	Blade loading coeff	Rotor efficiency (%)
Hover.OEI.RF1	LF1_rotor	1176.2	0.033	0.0	0.002	0.0	0.561	0.0	0.0
Hover.OEI.RF1	RF1_rotor	1250.0	0.031	0.0	0.0	0.0	0.596	0.0	0.0
Hover.OEI.RF1	LF2_rotor	1257.9	0.031	0.085	0.023	56.814	0.6	1.41	85.4
Hover.OEI.RF1	RF2_rotor	1257.9	0.031	0.085	0.023	56.814	0.6	1.41	85.4
Hover.OEI.RF1	RF_rotor	1131.8	0.039	0.07	0.019	29.713	0.477	1.168	79.9
Hover.OEI.RF1	RR_rotor	1403.8	0.031	0.0	0.0	0.0	0.591	0.0	0.0
Hover.OEI.LF2	LF1_rotor	1255.2	0.031	0.138	0.048	92.313	0.599	0.92	84.7
Hover.OEI.LF2	RF1_rotor	1092.8	0.035	0.182	0.07	92.313	0.521	1.214	88.4
Hover.OEI.LF2	LF2_rotor	1247.7	0.031	0.0	0.0	0.0	0.595	0.0	0.0
Hover.OEI.LF2	RF2_rotor	1254.9	0.031	0.0	0.0	0.0	0.599	0.0	0.0
Hover.OEI.LF2	RF_rotor	1258.6	0.035	0.085	0.023	44.363	0.53	1.41	83.7
Hover.OEI.LF2	RR_rotor	1257.6	0.035	0.0	0.001	0.045	0.53	0.001	0.1
Condition	Rotor	Rotor RPM	J	Thrust coeff	Power coeff	Disk loading (kg/m^2)	Tip Mach	Blade loading coeff	Rotor efficiency (%)
Hover.OEI.RF2	LF1_rotor	1188.9	0.033	0.122	0.042	73.384	0.567	0.816	80.7
Hover.OEI.RF2	RF1_rotor	1252.5	0.031	0.099	0.033	66.049	0.597	0.661	76.5
Hover.OEI.RF2	LF2_rotor	1133.9	0.034	0.03	0.006	16.123	0.541	0.492	64.8
Hover.OEI.RF2	RF2_rotor	1238.6	0.031	0.085	0.023	55.086	0.591	1.41	85.2
Hover.OEI.RF2	RF_rotor	1349.1	0.032	0.0	0.0	0.0	0.568	0.0	0.0
Hover.OEI.RF2	RR_rotor	1337.7	0.033	0.04	0.009	23.887	0.563	0.672	71.7
Hover.OEI.RF	LF1_rotor	1224.7	0.032	0.054	0.016	34.46	0.584	0.361	61.7
Hover.OEI.RF	RF1_rotor	1075.7	0.036	0.159	0.059	77.978	0.513	1.059	84.9
Hover.OEI.RF	LF2_rotor	1175.3	0.033	0.085	0.023	49.597	0.561	1.41	84.4
Hover.OEI.RF	RF2_rotor	1257.9	0.031	0.0	0.0	0.0	0.6	0.0	0.0
Hover.OEI.RF	RF_rotor	1364.7	0.032	0.085	0.023	52.153	0.575	1.41	84.8
Hover.OEI.RF	RR_rotor	1329.3	0.033	0.015	0.003	8.87	0.56	0.253	46.7
Condition	Rotor	Rotor RPM	J	Thrust coeff	Power coeff	Disk loading (kg/m^2)	Tip Mach	Blade loading coeff	Rotor efficiency (%)
Hover.OEI.RR	LF1_rotor	1154.8	0.034	0.088	0.029	49.916	0.551	0.588	72.9
Hover.OEI.RR	RF1_rotor	1102.2	0.035	0.165	0.062	84.846	0.526	1.097	86.2
Hover.OEI.RR	LF2_rotor	1053.0	0.037	0.085	0.024	39.81	0.502	1.41	83.1
Hover.OEI.RR	RF2_rotor	1228.1	0.032	0.0	0.0	0.0	0.586	0.0	0.0
Hover.OEI.RR	RF_rotor	1290.6	0.034	0.022	0.005	12.294	0.544	0.372	57.7
Hover.OEI.RR	RR_rotor	1154.6	0.038	0.085	0.024	37.335	0.486	1.41	82.8

Table A.11. General performance overview for the 6 Lift (Tilt 2) configuration.

Condition	Total power (kW)	Lift coeff	Drag coeff	L/D	Wing incidence angle (°)	Tail incidence angle (°)
Cruise	253796.2	0.8959	0.0691	12.9672	4.409	-0.628
Reserve	202181.6	1.2896	0.0946	13.6266	7.278	-0.035
Hover	626433.9					
Hover.OEI.LF1	718281.8					
Hover.OEI.RF1	720929.5					
Hover.OEI.LF2	678588.9					
Hover.OEI.RF2	679269.7					
Hover.OEI.RF	721269.6					
Hover.OEI.RR	619837.2					
Payload weight (lb)	Battery weight (lb)	Battery weight fraction	Gross weight (lb)	Wing area (m^2)		
784.8	1941.7	0.372	5218.7	11.56		

Table A.12. Rotor metrics/outputs for the 6 Lift (Tilt 2) configuration (Part 1).

Condition	Rotor	Motor RPM	Thrust (N)	Thrust margin	Motor Torque (Nm)	Torque margin	Power (kW)	Power margin	Motor efficiency (%)
Cruise	LF1_rotor								
Cruise	RF1_rotor								
Cruise	LF2_rotor	2698.8	894.5	9.561	295.9	1.436	126.9	2.401	92.2
Cruise	RF2_rotor	2698.7	894.5	9.561	295.9	1.436	126.9	2.401	92.2
Cruise	RF_rotor								
Cruise	RR_rotor								
Reserve	LF1_rotor								
Reserve	RF1_rotor								
Reserve	LF2_rotor	2470.2	851.6	10.042	257.0	1.653	101.1	3.013	92.0
Reserve	RF2_rotor	2469.0	851.0	10.049	256.9	1.654	101.1	3.015	92.0
Reserve	RF_rotor								
Reserve	RR_rotor								
Condition	Rotor	Motor RPM	Thrust (N)	Thrust margin	Motor Torque (Nm)	Torque margin	Power (kW)	Power margin	Motor efficiency (%)
Hover	LF1_rotor	4513.5	6092.7	1.243	127.9	1.102	173.4	1.246	87.9
Hover	RF1_rotor	4513.5	6092.7	1.243	127.9	1.102	173.4	1.246	87.9
Hover	LF2_rotor	2937.6	3813.3	2.243	234.8	1.81	109.9	2.773	92.0
Hover	RF2_rotor	2937.6	3813.3	2.243	234.8	1.81	109.9	2.773	92.0
Hover	RF_rotor	3520.6	2255.2	1.626	44.7	1.257	47.2	1.843	88.1
Hover	RR_rotor	2107.3	808.0	1.358	18.7	1.0	12.7	2.093	81.7
Hover.OEI.LF1	LF1_rotor	4000.1	2126.8	3.56	92.1	1.53	48.6	4.449	89.0
Hover.OEI.LF1	RF1_rotor	4761.1	2324.0	3.258	33.5	4.204	48.5	4.46	86.9
Hover.OEI.LF1	LF2_rotor	4352.1	8316.4	1.028	414.1	1.026	293.3	1.039	90.1
Hover.OEI.LF1	RF2_rotor	4242.0	7911.9	1.081	397.3	1.07	273.5	1.114	90.3
Hover.OEI.LF1	RF_rotor	3533.5	2128.3	1.723	36.3	1.548	38.8	2.241	87.3
Hover.OEI.LF1	RR_rotor	5524.0	425.7	2.578	7.3	2.572	15.7	1.693	67.4

Table A.13. Rotor metrics/outputs for the 6 Lift (Tilt 2) configuration (Part 2).

Condition	Rotor	Motor RPM	Thrust (N)	Thrust margin	Motor Torque (Nm)	Torque margin	Power (kW)	Power margin	Motor efficiency (%)
Hover.OEI.RF1	LF1_rotor	4061.7	2071.0	3.656	31.2	4.519	38.6	5.603	86.7
Hover.OEI.RF1	RF1_rotor	4000.1	2126.9	3.56	92.1	1.53	48.6	4.449	89.0
Hover.OEI.RF1	LF2_rotor	4383.0	8317.8	1.028	411.9	1.032	293.9	1.037	90.1
Hover.OEI.RF1	RF2_rotor	4319.6	8203.1	1.043	409.5	1.038	287.6	1.059	90.2
Hover.OEI.RF1	RF_rotor	3452.7	2022.7	1.813	34.5	1.628	36.2	2.404	87.0
Hover.OEI.RF1	RR_rotor	5516.5	460.6	2.382	7.5	2.481	16.1	1.652	68.1
Hover.OEI.LF2	LF1_rotor	5031.7	7572.1	1.0	141.0	1.0	216.2	1.0	86.6
Hover.OEI.LF2	RF1_rotor	3398.4	3403.1	2.225	66.4	2.124	67.2	3.218	88.6
Hover.OEI.LF2	LF2_rotor	4000.0	0.0	0.0	361.8	1.174	0.0	0.0	90.8
Hover.OEI.LF2	RF2_rotor	4399.3	8552.4	1.0	424.9	1.0	304.7	1.0	89.9
Hover.OEI.LF2	RF_rotor	5230.7	3668.0	1.0	55.7	1.009	86.9	1.0	88.5
Hover.OEI.LF2	RR_rotor	4146.4	0.0	0.0	0.1	227.544	3.6	7.336	2.5
Condition	Rotor	Motor RPM	Thrust (N)	Thrust margin	Motor Torque (Nm)	Torque margin	Power (kW)	Power margin	Motor efficiency (%)
Hover.OEI.RF2	LF1_rotor	3374.7	3403.1	2.225	66.7	2.113	67.1	3.222	88.6
Hover.OEI.RF2	RF1_rotor	5031.7	7572.1	1.0	141.0	1.0	216.2	1.0	86.6
Hover.OEI.RF2	LF2_rotor	4399.3	8552.4	1.0	424.9	1.0	304.7	1.0	89.9
Hover.OEI.RF2	RF2_rotor	4000.0	0.0	0.0	361.8	1.174	0.0	0.0	90.8
Hover.OEI.RF2	RF_rotor	5164.2	3668.0	1.0	56.2	1.0	86.6	1.004	88.5
Hover.OEI.RF2	RR_rotor	5526.5	0.0	0.0	0.0	0.0	4.8	5.583	0.4
Hover.OEI.RF	LF1_rotor	2933.6	2319.6	3.264	44.5	3.17	39.3	5.502	87.6
Hover.OEI.RF	RF1_rotor	4081.7	2191.8	3.455	33.3	4.231	41.2	5.244	87.1
Hover.OEI.RF	LF2_rotor	4872.4	8165.2	1.047	372.7	1.14	296.2	1.029	89.9
Hover.OEI.RF	RF2_rotor	4446.8	8427.4	1.015	414.0	1.026	299.9	1.016	90.0
Hover.OEI.RF	RF_rotor	3623.0	975.9	3.758	37.1	1.514	18.0	4.818	87.5
Hover.OEI.RF	RR_rotor	5694.8	1097.4	1.0	13.9	1.348	26.6	1.0	78.3
Condition	Rotor	Motor RPM	Thrust (N)	Thrust margin	Motor Torque (Nm)	Torque margin	Power (kW)	Power margin	Motor efficiency (%)
Hover.OEI.RR	LF1_rotor	3997.2	4778.5	1.585	92.0	1.532	109.1	1.982	89.0
Hover.OEI.RR	RF1_rotor	4377.8	3838.4	1.973	64.6	2.184	83.6	2.585	89.2
Hover.OEI.RR	LF2_rotor	4051.7	4771.6	1.792	219.5	1.936	142.9	2.132	91.3
Hover.OEI.RR	RF2_rotor	3893.8	6700.0	1.276	345.5	1.23	216.6	1.406	91.0
Hover.OEI.RR	RF_rotor	4154.4	2877.6	1.275	48.0	1.172	59.3	1.466	88.7
Hover.OEI.RR	RR_rotor	5502.0	295.2	3.717	9.3	2.013	8.3	3.199	72.0

Table A.14. Rotor metrics/outputs for the 6 Lift (Tilt 2) configuration (Part 3).

Condition	Rotor	Rotor RPM	J	Thrust coeff	Power coeff	Disk loading (kg/m^2)	Tip Mach	Blade loading coeff	Rotor efficiency (%)
Cruise	LF1_rotor								
Cruise	RF1_rotor								
Cruise	LF2_rotor	674.7	1.913	0.099	0.204	15.706	0.329	0.66	92.8
Cruise	RF2_rotor	674.7	1.913	0.099	0.204	15.705	0.329	0.66	92.8
Cruise	RF_rotor								
Cruise	RR_rotor								
Reserve	LF1_rotor								
Reserve	RF1_rotor								
Reserve	LF2_rotor	617.6	1.743	0.112	0.212	14.953	0.301	0.75	92.6
Reserve	RF2_rotor	617.2	1.743	0.112	0.212	14.942	0.301	0.75	92.6
Reserve	RF_rotor								
Reserve	RR_rotor								
Condition	Rotor	Rotor RPM	J	Thrust coeff	Power coeff	Disk loading (kg/m^2)	Tip Mach	Blade loading coeff	Rotor efficiency (%)
Hover	LF1_rotor	1128.4	0.086	0.085	0.026	45.714	0.538	1.41	75.7
Hover	RF1_rotor	1128.4	0.086	0.085	0.026	45.714	0.538	1.41	75.7
Hover	LF2_rotor	734.4	0.132	0.225	0.112	51.502	0.35	1.5	75.8
Hover	RF2_rotor	734.4	0.132	0.225	0.112	51.501	0.35	1.5	75.8
Hover	RF_rotor	880.2	0.124	0.085	0.028	21.694	0.371	1.41	70.8
Hover	RR_rotor	526.8	0.208	0.085	0.032	7.772	0.222	1.41	60.8
Hover.OEI.LF1	LF1_rotor	1000.0	0.039	0.085	0.024	35.906	0.477	1.41	82.6
Hover.OEI.LF1	RF1_rotor	1190.3	0.033	0.029	0.006	17.438	0.568	0.483	64.5
Hover.OEI.LF1	LF2_rotor	1088.0	0.036	0.224	0.09	112.319	0.519	1.49	93.5
Hover.OEI.LF1	RF2_rotor	1060.5	0.037	0.224	0.091	106.856	0.506	1.492	92.7
Hover.OEI.LF1	RF_rotor	883.4	0.05	0.079	0.022	20.474	0.372	1.321	79.7
Hover.OEI.LF1	RR_rotor	1381.0	0.032	0.006	0.002	4.095	0.582	0.108	22.8

Table A.15. Rotor metrics/outputs for the 6 Lift (Tilt 2) configuration (Part 4).

Condition	Rotor	Rotor RPM	J	Thrust coeff	Power coeff	Disk loading (kg/m^2)	Tip Mach	Blade loading coeff	Rotor efficiency (%)
Hover.OEI.RF1	LF1_rotor	1015.4	0.038	0.036	0.008	15.539	0.484	0.592	68.4
Hover.OEI.RF1	RF1_rotor	1000.0	0.039	0.085	0.024	35.906	0.477	1.41	82.6
Hover.OEI.RF1	LF2_rotor	1095.7	0.035	0.22	0.089	112.337	0.523	1.47	93.3
Hover.OEI.RF1	RF2_rotor	1079.9	0.036	0.224	0.091	110.789	0.515	1.492	93.3
Hover.OEI.RF1	RF_rotor	863.2	0.051	0.079	0.022	19.458	0.364	1.315	79.4
Hover.OEI.RF1	RR_rotor	1379.1	0.032	0.007	0.002	4.431	0.581	0.117	24.8
Hover.OEI.LF2	LF1_rotor	1257.9	0.031	0.085	0.023	56.814	0.6	1.41	85.4
Hover.OEI.LF2	RF1_rotor	849.6	0.046	0.083	0.024	25.534	0.405	1.389	80.9
Hover.OEI.LF2	LF2_rotor	1000.0	0.039	0.225	0.093	95.49	0.477	1.5	91.2
Hover.OEI.LF2	RF2_rotor	1099.8	0.035	0.225	0.091	115.507	0.525	1.5	94.0
Hover.OEI.LF2	RF_rotor	1307.7	0.034	0.062	0.016	35.285	0.551	1.039	79.4
Hover.OEI.LF2	RR_rotor	1036.6	0.042	0.0	0.0	0.0	0.437	0.0	0.0
Condition	Rotor	Rotor RPM	J	Thrust coeff	Power coeff	Disk loading (kg/m^2)	Tip Mach	Blade loading coeff	Rotor efficiency (%)
Hover.OEI.RF2	LF1_rotor	843.7	0.046	0.085	0.024	25.534	0.402	1.409	81.0
Hover.OEI.RF2	RF1_rotor	1257.9	0.031	0.085	0.023	56.814	0.6	1.41	85.4
Hover.OEI.RF2	LF2_rotor	1099.8	0.035	0.225	0.091	115.507	0.525	1.5	94.0
Hover.OEI.RF2	RF2_rotor	1000.0	0.039	0.225	0.093	95.49	0.477	1.5	91.2
Hover.OEI.RF2	RF_rotor	1291.1	0.034	0.064	0.016	35.285	0.544	1.066	79.7
Hover.OEI.RF2	RR_rotor	1381.6	0.032	0.0	0.0	0.0	0.582	0.0	0.0
Hover.OEI.RF	LF1_rotor	733.4	0.053	0.076	0.021	17.404	0.35	1.271	78.7
Hover.OEI.RF	RF1_rotor	1020.4	0.038	0.037	0.008	16.446	0.487	0.62	69.4
Hover.OEI.RF	LF2_rotor	1218.1	0.032	0.175	0.065	110.277	0.581	1.168	90.2
Hover.OEI.RF	RF2_rotor	1111.7	0.035	0.217	0.086	113.818	0.53	1.447	93.3
Hover.OEI.RF	RF_rotor	905.7	0.048	0.078	0.022	21.124	0.382	1.296	79.6
Hover.OEI.RF	RR_rotor	1423.7	0.031	0.016	0.003	10.557	0.6	0.262	48.0
Condition	Rotor	Rotor RPM	J	Thrust coeff	Power coeff	Disk loading (kg/m^2)	Tip Mach	Blade loading coeff	Rotor efficiency (%)
Hover.OEI.RR	LF1_rotor	999.3	0.039	0.085	0.024	35.854	0.477	1.41	82.6
Hover.OEI.RR	RF1_rotor	1094.4	0.035	0.057	0.014	28.8	0.522	0.944	77.4
Hover.OEI.RR	LF2_rotor	1012.9	0.038	0.148	0.055	64.443	0.483	0.987	82.3
Hover.OEI.RR	RF2_rotor	973.5	0.04	0.225	0.094	90.489	0.464	1.5	90.5
Hover.OEI.RR	RF_rotor	1038.6	0.042	0.078	0.021	27.682	0.438	1.292	80.6
Hover.OEI.RR	RR_rotor	1375.5	0.032	0.01	0.002	6.39	0.579	0.17	34.9

Appendix B

Layout MDO data tables (for 8 Lift configurations)

Table B.1. General performance overview for the 8 Lift (Tractor) configuration.

Condition	Total power (kW)	Lift coeff	Drag coeff	L/D	Wing incidence angle (°)	Tail incidence angle (°)
Cruise	258281.1	1.0157	0.0832	12.2008	4.967	0.086
Reserve	208367.6	1.4619	0.1142	12.8014	8.086	0.996
Hover	590268.7					
Hover.OEI.LF1	601929.3					
Hover.OEI.RF1	601515.0					
Hover.OEI.LF2	596086.7					
Hover.OEI.RF2	592534.6					
Hover.OEI.LF3	592813.5					
Hover.OEI.RF3	592813.5					
Hover.OEI.RF	562878.0					
Hover.OEI.RR	561248.0					
Payload weight (lb)	**Battery weight (lb)**	**Battery weight fraction**	**Gross weight (lb)**	**Wing area (m^2)**		
784.8	854.3	0.176	4843.8	9.46		

Table B.2. Rotor metrics/outputs for the 8 Lift (Tractor) configuration (Part 1).

Condition	Rotor	Motor RPM	Thrust (N)	Thrust margin	Motor Torque (Nm)	Torque margin	Power (kW)	Power margin	Motor efficiency (%)
Cruise	LF1_rotor								
Cruise	RF1_rotor								
Cruise	LF2_rotor								
Cruise	RF2_rotor								
Cruise	LF3_rotor								
Cruise	RF3_rotor								
Cruise	LP1_rotor	4304.2	882.3	1.0	186.2	1.0	129.1	1.0	91.0
Cruise	RP1_rotor	4304.2	882.3	1.0	186.2	1.0	129.1	1.0	91.0
Cruise	RF_rotor								
Cruise	RR_rotor								
Reserve	LF1_rotor								
Reserve	RF1_rotor								
Reserve	LF2_rotor								
Reserve	RF2_rotor								
Reserve	LF3_rotor								
Reserve	RF3_rotor								
Reserve	LP1_rotor	4169.1	841.0	1.049	154.6	1.204	104.2	1.24	90.7
Reserve	RP1_rotor	4169.2	841.0	1.049	154.6	1.204	104.2	1.24	90.7
Reserve	RF_rotor								
Reserve	RR_rotor								
Condition	Rotor	Motor RPM	Thrust (N)	Thrust margin	Motor Torque (Nm)	Torque margin	Power (kW)	Power margin	Motor efficiency (%)
Hover	LF1_rotor	7041.8	2931.3	1.148	40.8	1.024	87.4	1.099	86.8
Hover	RF1_rotor	7041.8	2931.3	1.128	40.8	1.024	87.4	1.075	86.8
Hover	LF2_rotor	6937.4	2845.0	1.183	39.7	1.053	83.7	1.147	86.8
Hover	RF2_rotor	6937.3	2845.0	1.183	39.7	1.053	83.7	1.147	86.8
Hover	LF3_rotor	6831.8	2759.1	1.22	38.6	1.083	80.2	1.198	86.7
Hover	RF3_rotor	6831.7	2759.0	1.22	38.6	1.083	80.2	1.198	86.7
Hover	LP1_rotor								
Hover	RP1_rotor								
Hover	RF_rotor	3879.3	2738.0	1.942	53.2	1.658	61.3	2.329	88.8
Hover	RR_rotor	2820.2	1447.1	1.434	30.4	2.071	26.3	1.571	86.0
Hover.OEI.LF1	LF1_rotor	7546.4	1496.2	2.25	41.8	1.0	42.7	2.25	86.6
Hover.OEI.LF1	RF1_rotor	6375.6	1496.2	2.209	16.5	2.536	34.5	2.722	80.4
Hover.OEI.LF1	LF2_rotor	7546.4	3366.4	1.0	41.8	1.0	96.1	1.0	86.6
Hover.OEI.LF1	RF2_rotor	7546.4	3366.4	1.0	41.8	1.0	96.1	1.0	86.6
Hover.OEI.LF1	LF3_rotor	7546.4	3366.4	1.0	41.8	1.0	96.1	1.0	86.6
Hover.OEI.LF1	RF3_rotor	7546.4	3366.4	1.0	41.8	1.0	96.1	1.0	86.6
Hover.OEI.LF1	LP1_rotor								
Hover.OEI.LF1	RP1_rotor								
Hover.OEI.LF1	RF_rotor	5592.3	5076.4	1.047	80.9	1.09	135.6	1.054	88.1
Hover.OEI.LF1	RR_rotor	4321.8	0.0	0.0	1.0	62.427	4.9	8.481	23.6
Condition	Rotor	Motor RPM	Thrust (N)	Thrust margin	Motor Torque (Nm)	Torque margin	Power (kW)	Power margin	Motor efficiency (%)
Hover.OEI.RF1	LF1_rotor	6382.4	1496.2	2.25	16.5	2.538	34.5	2.784	80.4
Hover.OEI.RF1	RF1_rotor	7546.4	1496.2	2.209	41.8	1.0	42.7	2.199	86.6
Hover.OEI.RF1	LF2_rotor	7546.4	3366.4	1.0	41.8	1.0	96.1	1.0	86.6
Hover.OEI.RF1	RF2_rotor	7546.4	3366.4	1.0	41.8	1.0	96.1	1.0	86.6
Hover.OEI.RF1	LF3_rotor	7546.4	3366.4	1.0	41.8	1.0	96.1	1.0	86.6
Hover.OEI.RF1	RF3_rotor	7546.4	3366.4	1.0	41.8	1.0	96.1	1.0	86.6
Hover.OEI.RF1	LP1_rotor								
Hover.OEI.RF1	RP1_rotor								
Hover.OEI.RF1	RF_rotor	5591.0	5076.4	1.047	80.9	1.09	135.6	1.054	88.1
Hover.OEI.RF1	RR_rotor	4095.1	0.0	0.0	0.9	72.952	4.4	9.286	20.9
Hover.OEI.LF2	LF1_rotor	7546.0	3366.1	1.0	41.8	1.0	96.1	1.0	86.6
Hover.OEI.LF2	RF1_rotor	6909.7	1894.6	1.745	21.2	1.976	46.5	2.018	82.9
Hover.OEI.LF2	LF2_rotor	6622.7	1128.3	2.984	32.0	1.308	28.9	3.327	86.0
Hover.OEI.LF2	RF2_rotor	7449.7	3280.7	1.026	40.8	1.024	92.7	1.037	86.6
Hover.OEI.LF2	LF3_rotor	7546.4	3366.4	1.0	41.8	1.0	96.1	1.0	86.6
Hover.OEI.LF2	RF3_rotor	7447.1	3278.5	1.027	40.8	1.024	92.6	1.038	86.6
Hover.OEI.LF2	LP1_rotor								
Hover.OEI.LF2	RP1_rotor								
Hover.OEI.LF2	RF_rotor	5462.1	5219.9	1.018	85.4	1.032	139.8	1.022	88.1
Hover.OEI.LF2	RR_rotor	3933.0	0.0	0.0	0.2	335.503	3.5	11.646	5.5

Table B.3. Rotor metrics/outputs for the 8 Lift (Tractor) configuration (Part 2).

Condition	Rotor	Motor RPM	Thrust (N)	Thrust margin	Motor Torque (Nm)	Torque margin	Power (kW)	Power margin	Motor efficiency (%)
Hover.OEI.RF2	LF1_rotor	6909.7	1994.5	1.688	22.6	1.849	49.4	1.946	83.5
Hover.OEI.RF2	RF1_rotor	7546.4	3305.7	1.0	40.8	1.024	93.9	1.0	86.6
Hover.OEI.RF2	LF2_rotor	7430.7	3264.0	1.031	40.6	1.029	92.0	1.044	86.6
Hover.OEI.RF2	RF2_rotor	7155.7	1345.3	2.502	37.9	1.102	36.8	2.612	86.5
Hover.OEI.RF2	LF3_rotor	7456.2	3286.4	1.024	40.9	1.022	92.9	1.034	86.6
Hover.OEI.RF2	RF3_rotor	7546.1	3366.2	1.0	41.8	1.0	96.1	1.0	86.6
Hover.OEI.RF2	LP1_rotor								
Hover.OEI.RF2	RP1_rotor								
Hover.OEI.RF2	RF_rotor	5555.7	4738.7	1.122	74.4	1.186	123.5	1.156	88.2
Hover.OEI.RF2	RR_rotor	3997.9	267.8	7.75	4.2	14.889	8.0	5.158	55.6
Hover.OEI.LF3	LF1_rotor	7523.3	3279.8	1.026	40.5	1.032	92.9	1.034	86.6
Hover.OEI.LF3	RF1_rotor	7189.4	2531.5	1.306	29.9	1.397	66.5	1.412	85.4
Hover.OEI.LF3	LF2_rotor	7520.1	3343.1	1.007	41.5	1.006	95.1	1.01	86.6
Hover.OEI.LF3	RF2_rotor	7228.8	3089.1	1.09	38.6	1.082	85.1	1.128	86.6
Hover.OEI.LF3	LF3_rotor	5512.3	798.3	4.217	23.3	1.795	17.9	5.368	84.1
Hover.OEI.LF3	RF3_rotor	7257.5	3113.7	1.081	38.9	1.074	86.1	1.116	86.6
Hover.OEI.LF3	LP1_rotor								
Hover.OEI.LF3	RP1_rotor								
Hover.OEI.LF3	RF_rotor	5405.4	5316.1	1.0	88.2	1.0	142.8	1.0	88.1
Hover.OEI.LF3	RR_rotor	3975.2	63.0	32.951	2.7	23.213	6.3	6.538	45.0
Condition	Rotor	Motor RPM	Thrust (N)	Thrust margin	Motor Torque (Nm)	Torque margin	Power (kW)	Power margin	Motor efficiency (%)
Hover.OEI.RF3	LF1_rotor	7189.4	2531.5	1.33	29.9	1.397	66.5	1.445	85.4
Hover.OEI.RF3	RF1_rotor	7523.3	3279.8	1.008	40.5	1.032	92.9	1.011	86.6
Hover.OEI.RF3	LF2_rotor	7228.8	3089.1	1.09	38.6	1.082	85.1	1.128	86.6
Hover.OEI.RF3	RF2_rotor	7520.1	3343.1	1.007	41.5	1.006	95.1	1.01	86.6
Hover.OEI.RF3	LF3_rotor	7257.5	3113.7	1.081	38.9	1.074	86.1	1.116	86.6
Hover.OEI.RF3	RF3_rotor	5512.3	798.3	4.217	23.3	1.795	17.9	5.368	84.1
Hover.OEI.RF3	LP1_rotor								
Hover.OEI.RF3	RP1_rotor								
Hover.OEI.RF3	RF_rotor	5405.4	5316.1	1.0	88.2	1.0	142.8	1.0	88.1
Hover.OEI.RF3	RR_rotor	3975.2	63.0	32.951	2.7	23.213	6.3	6.538	45.0
Hover.OEI.RF	LF1_rotor	7206.1	3031.1	1.111	37.8	1.106	83.1	1.156	86.5
Hover.OEI.RF	RF1_rotor	7206.1	3031.1	1.091	37.8	1.106	83.1	1.13	86.5
Hover.OEI.RF	LF2_rotor	7064.8	2950.5	1.141	37.0	1.129	79.9	1.203	86.5
Hover.OEI.RF	RF2_rotor	7064.8	2950.5	1.141	37.0	1.129	79.9	1.203	86.5
Hover.OEI.RF	LF3_rotor	6919.9	2830.7	1.189	35.6	1.173	75.4	1.275	86.4
Hover.OEI.RF	RF3_rotor	6919.9	2830.7	1.189	35.6	1.173	75.4	1.275	86.4
Hover.OEI.RF	LP1_rotor								
Hover.OEI.RF	RP1_rotor								
Hover.OEI.RF	RF_rotor	4806.6	1868.2	2.846	70.9	1.243	45.0	3.175	88.9
Hover.OEI.RF	RR_rotor	4626.5	2075.7	1.0	29.1	2.158	41.3	1.0	86.1
Condition	Rotor	Motor RPM	Thrust (N)	Thrust margin	Motor Torque (Nm)	Torque margin	Power (kW)	Power margin	Motor efficiency (%)
Hover.OEI.RR	LF1_rotor	7149.6	3021.7	1.114	37.9	1.104	82.6	1.164	86.5
Hover.OEI.RR	RF1_rotor	7149.6	3021.7	1.094	37.9	1.104	82.6	1.137	86.5
Hover.OEI.RR	LF2_rotor	6997.4	2894.5	1.163	36.4	1.149	77.7	1.236	86.4
Hover.OEI.RR	RF2_rotor	6997.4	2894.5	1.163	36.4	1.149	77.7	1.236	86.4
Hover.OEI.RR	LF3_rotor	6807.0	2739.1	1.229	34.6	1.209	72.0	1.335	86.3
Hover.OEI.RR	RF3_rotor	6807.0	2739.1	1.229	34.6	1.209	72.0	1.335	86.3
Hover.OEI.RR	LP1_rotor								
Hover.OEI.RR	RP1_rotor								
Hover.OEI.RR	RF_rotor	5487.8	2635.1	2.017	35.6	2.475	59.4	2.407	87.0
Hover.OEI.RR	RR_rotor	4507.3	1642.8	1.264	62.9	1.0	37.3	1.107	89.1

Table B.4. Rotor metrics/outputs for the 8 Lift (Tractor) configuration (Part 3).

Condition	Rotor	Rotor RPM	J	Thrust coeff	Power coeff	Disk loading (kg/m^2)	Tip Mach	Blade loading coeff	Rotor efficiency (%)
Cruise	LF1_rotor								
Cruise	RF1_rotor								
Cruise	LF2_rotor								
Cruise	RF2_rotor								
Cruise	LF3_rotor								
Cruise	RF3_rotor								
Cruise	LP1_rotor	1076.0	1.86	0.221	0.452	37.215	0.339	1.476	91.2
Cruise	RP1_rotor	1076.0	1.86	0.221	0.452	37.215	0.339	1.476	91.2
Cruise	RF_rotor								
Cruise	RR_rotor								
Reserve	LF1_rotor								
Reserve	RF1_rotor								
Reserve	LF2_rotor								
Reserve	RF2_rotor								
Reserve	LF3_rotor								
Reserve	RF3_rotor								
Reserve	LP1_rotor	1042.3	1.6	0.225	0.4	35.473	0.328	1.5	90.0
Reserve	RP1_rotor	1042.3	1.6	0.225	0.4	35.475	0.328	1.5	90.0
Reserve	RF_rotor								
Reserve	RR_rotor								

Condition	Rotor	Rotor RPM	J	Thrust coeff	Power coeff	Disk loading (kg/m^2)	Tip Mach	Blade loading coeff	Rotor efficiency (%)
Hover	LF1_rotor	1760.4	0.082	0.085	0.026	49.471	0.56	1.41	76.2
Hover	RF1_rotor	1760.5	0.082	0.085	0.026	49.471	0.56	1.41	76.2
Hover	LF2_rotor	1734.3	0.084	0.085	0.026	48.015	0.552	1.41	76.0
Hover	RF2_rotor	1734.3	0.084	0.085	0.026	48.014	0.552	1.41	76.0
Hover	LF3_rotor	1707.9	0.085	0.085	0.026	46.564	0.543	1.41	75.8
Hover	RF3_rotor	1707.9	0.085	0.085	0.026	46.564	0.543	1.41	75.8
Hover	LP1_rotor								
Hover	RP1_rotor								
Hover	RF_rotor	969.8	0.113	0.085	0.027	26.339	0.409	1.41	72.3
Hover	RR_rotor	705.1	0.155	0.085	0.029	13.921	0.297	1.41	66.9
Hover.OEI.LF1	LF1_rotor	1886.6	0.031	0.085	0.023	56.814	0.6	1.41	85.4
Hover.OEI.LF1	RF1_rotor	1593.9	0.036	0.053	0.013	25.251	0.507	0.878	76.0
Hover.OEI.LF1	LF2_rotor	1886.6	0.031	0.085	0.023	56.814	0.6	1.41	85.4
Hover.OEI.LF1	RF2_rotor	1886.6	0.031	0.085	0.023	56.814	0.6	1.41	85.4
Hover.OEI.LF1	LF3_rotor	1886.6	0.031	0.085	0.023	56.814	0.6	1.41	85.4
Hover.OEI.LF1	RF3_rotor	1886.6	0.031	0.085	0.023	56.814	0.6	1.41	85.4
Hover.OEI.LF1	LP1_rotor								
Hover.OEI.LF1	RP1_rotor								
Hover.OEI.LF1	RF_rotor	1398.1	0.031	0.075	0.02	48.834	0.589	1.258	83.2
Hover.OEI.LF1	RR_rotor	1080.5	0.041	0.0	0.0	0.0	0.455	0.0	0.0

Condition	Rotor	Rotor RPM	J	Thrust coeff	Power coeff	Disk loading (kg/m^2)	Tip Mach	Blade loading coeff	Rotor efficiency (%)
Hover.OEI.RF1	LF1_rotor	1595.6	0.036	0.053	0.013	25.251	0.507	0.876	75.9
Hover.OEI.RF1	RF1_rotor	1886.6	0.031	0.085	0.023	56.814	0.6	1.41	85.4
Hover.OEI.RF1	LF2_rotor	1886.6	0.031	0.085	0.023	56.814	0.6	1.41	85.4
Hover.OEI.RF1	RF2_rotor	1886.6	0.031	0.085	0.023	56.814	0.6	1.41	85.4
Hover.OEI.RF1	LF3_rotor	1886.6	0.031	0.085	0.023	56.814	0.6	1.41	85.4
Hover.OEI.RF1	RF3_rotor	1886.6	0.031	0.085	0.023	56.814	0.6	1.41	85.4
Hover.OEI.RF1	LP1_rotor								
Hover.OEI.RF1	RP1_rotor								
Hover.OEI.RF1	RF_rotor	1397.7	0.031	0.076	0.02	48.834	0.589	1.259	83.2
Hover.OEI.RF1	RR_rotor	1023.8	0.043	0.0	0.0	0.0	0.431	0.0	0.0
Hover.OEI.LF2	LF1_rotor	1886.5	0.031	0.085	0.023	56.809	0.6	1.41	85.4
Hover.OEI.LF2	RF1_rotor	1727.4	0.034	0.057	0.014	31.975	0.549	0.947	77.8
Hover.OEI.LF2	LF2_rotor	1655.7	0.035	0.083	0.023	42.844	0.527	1.381	83.3
Hover.OEI.LF2	RF2_rotor	1862.4	0.031	0.085	0.023	55.368	0.592	1.41	85.2
Hover.OEI.LF2	LF3_rotor	1886.6	0.031	0.085	0.023	56.814	0.6	1.41	85.4
Hover.OEI.LF2	RF3_rotor	1861.8	0.031	0.085	0.023	55.33	0.592	1.41	85.2
Hover.OEI.LF2	LP1_rotor								
Hover.OEI.LF2	RP1_rotor								
Hover.OEI.LF2	RF_rotor	1365.5	0.032	0.081	0.022	50.214	0.575	1.356	84.2
Hover.OEI.LF2	RR_rotor	983.2	0.045	0.0	0.0	0.0	0.414	0.0	0.0

Table B.5. Rotor metrics/outputs for the 8 Lift (Tractor) configuration (Part 4).

Condition	Rotor	Rotor RPM	J	Thrust coeff	Power coeff	Disk loading (kg/m^2)	Tip Mach	Blade loading coeff	Rotor efficiency (%)
Hover.OEI.RF2	LF1_rotor	1727.4	0.034	0.06	0.015	33.66	0.549	0.996	78.7
Hover.OEI.RF2	RF1_rotor	1886.6	0.031	0.083	0.022	55.789	0.6	1.385	85.1
Hover.OEI.RF2	LF2_rotor	1857.7	0.031	0.085	0.023	55.086	0.591	1.41	85.2
Hover.OEI.RF2	RF2_rotor	1788.9	0.032	0.085	0.023	51.084	0.569	1.41	84.6
Hover.OEI.RF2	LF3_rotor	1864.0	0.031	0.085	0.023	55.464	0.593	1.41	85.2
Hover.OEI.RF2	RF3_rotor	1886.5	0.031	0.085	0.023	56.81	0.6	1.41	85.4
Hover.OEI.RF2	LP1_rotor								
Hover.OEI.RF2	RP1_rotor								
Hover.OEI.RF2	RF_rotor	1388.9	0.032	0.071	0.019	45.585	0.585	1.19	82.2
Hover.OEI.RF2	RR_rotor	999.5	0.044	0.008	0.002	2.577	0.421	0.13	27.0
Hover.OEI.LF3	LF1_rotor	1880.8	0.031	0.083	0.022	55.353	0.598	1.382	85.0
Hover.OEI.LF3	RF1_rotor	1797.3	0.032	0.07	0.018	42.723	0.572	1.168	81.7
Hover.OEI.LF3	LF2_rotor	1880.0	0.031	0.085	0.023	56.42	0.598	1.41	85.3
Hover.OEI.LF3	RF2_rotor	1807.2	0.032	0.085	0.023	52.133	0.575	1.41	84.8
Hover.OEI.LF3	LF3_rotor	1378.1	0.042	0.085	0.024	30.314	0.438	1.41	81.8
Hover.OEI.LF3	RF3_rotor	1814.4	0.032	0.085	0.023	52.548	0.577	1.41	84.8
Hover.OEI.LF3	LP1_rotor								
Hover.OEI.LF3	RP1_rotor								
Hover.OEI.LF3	RF_rotor	1351.3	0.032	0.085	0.023	51.14	0.569	1.41	84.7
Hover.OEI.LF3	RR_rotor	993.8	0.044	0.002	0.001	0.606	0.419	0.031	4.8
Condition	Rotor	Rotor RPM	J	Thrust coeff	Power coeff	Disk loading (kg/m^2)	Tip Mach	Blade loading coeff	Rotor efficiency (%)
Hover.OEI.RF3	LF1_rotor	1797.3	0.032	0.07	0.018	42.723	0.572	1.168	81.7
Hover.OEI.RF3	RF1_rotor	1880.8	0.031	0.083	0.022	55.353	0.598	1.382	85.0
Hover.OEI.RF3	LF2_rotor	1807.2	0.032	0.085	0.023	52.133	0.575	1.41	84.8
Hover.OEI.RF3	RF2_rotor	1880.0	0.031	0.085	0.023	56.42	0.598	1.41	85.3
Hover.OEI.RF3	LF3_rotor	1814.4	0.032	0.085	0.023	52.548	0.577	1.41	84.8
Hover.OEI.RF3	RF3_rotor	1378.1	0.042	0.085	0.024	30.314	0.438	1.41	81.8
Hover.OEI.RF3	LP1_rotor								
Hover.OEI.RF3	RP1_rotor								
Hover.OEI.RF3	RF_rotor	1351.3	0.032	0.085	0.023	51.14	0.569	1.41	84.7
Hover.OEI.RF3	RR_rotor	993.8	0.044	0.002	0.001	0.606	0.419	0.031	4.8
Hover.OEI.RF	LF1_rotor	1801.5	0.032	0.084	0.023	51.155	0.573	1.392	84.5
Hover.OEI.RF	RF1_rotor	1801.5	0.032	0.084	0.023	51.155	0.573	1.392	84.5
Hover.OEI.RF	LF2_rotor	1766.2	0.033	0.085	0.023	49.795	0.562	1.41	84.5
Hover.OEI.RF	RF2_rotor	1766.2	0.033	0.085	0.023	49.795	0.562	1.41	84.5
Hover.OEI.RF	LF3_rotor	1730.0	0.034	0.085	0.023	47.773	0.55	1.41	84.2
Hover.OEI.RF	RF3_rotor	1730.0	0.034	0.085	0.023	47.773	0.55	1.41	84.2
Hover.OEI.RF	LP1_rotor								
Hover.OEI.RF	RP1_rotor								
Hover.OEI.RF	RF_rotor	1201.6	0.036	0.085	0.024	40.437	0.506	1.41	83.2
Hover.OEI.RF	RR_rotor	1156.6	0.038	0.045	0.01	19.968	0.487	0.752	73.0
Condition	Rotor	Rotor RPM	J	Thrust coeff	Power coeff	Disk loading (kg/m^2)	Tip Mach	Blade loading coeff	Rotor efficiency (%)
Hover.OEI.RR	LF1_rotor	1787.4	0.032	0.085	0.023	50.997	0.568	1.41	84.6
Hover.OEI.RR	RF1_rotor	1787.4	0.032	0.085	0.023	50.997	0.568	1.41	84.6
Hover.OEI.RR	LF2_rotor	1749.4	0.033	0.085	0.023	48.849	0.556	1.41	84.3
Hover.OEI.RR	RF2_rotor	1749.4	0.033	0.085	0.023	48.849	0.556	1.41	84.3
Hover.OEI.RR	LF3_rotor	1701.7	0.034	0.085	0.023	46.227	0.541	1.41	84.0
Hover.OEI.RR	RF3_rotor	1701.7	0.034	0.085	0.023	46.227	0.541	1.41	84.0
Hover.OEI.RR	LP1_rotor								
Hover.OEI.RR	RP1_rotor								
Hover.OEI.RR	RF_rotor	1372.0	0.032	0.041	0.009	25.349	0.578	0.678	72.0
Hover.OEI.RR	RR_rotor	1126.8	0.039	0.085	0.024	35.558	0.475	1.41	82.5

Table B.6. General performance overview for the 8 Lift (Tilt 1) configuration.

Condition	Total power (kW)	Lift coeff	Drag coeff	L/D	Wing incidence angle (°)	Tail incidence angle (°)
Cruise	227941.5	0.8443	0.0741	11.4003	3.717	-0.065
Reserve	171603.3	1.2154	0.0952	12.7717	6.28	0.778
Hover	478201.4					
Hover.OEI.LF1	509638.5					
Hover.OEI.RF1	508409.9					
Hover.OEI.LF2	534251.5					
Hover.OEI.RF2	518433.3					
Hover.OEI.LF3	531274.0					
Hover.OEI.RF3	485225.6					
Hover.OEI.RF	472069.1					
Hover.OEI.RR	478808.1					
Payload weight (lb)	**Battery weight (lb)**	**Battery weight fraction**	**Gross weight (lb)**	**Wing area (m^2)**		
784.8	504.5	0.125	4027.2	9.46		

Table B.7. Rotor metrics/outputs for the 8 Lift (Tilt 1) configuration (Part 1).

Condition	Rotor	Motor RPM	Thrust (N)	Thrust margin	Motor Torque (Nm)	Torque margin	Power (kW)	Power margin	Motor efficiency (%)
Cruise	LF1_rotor	3840.5	784.9	5.74	184.6	1.0	114.0	1.499	91.2
Cruise	RF1_rotor	3839.9	784.8	5.071	184.6	1.0	114.0	1.276	91.2
Cruise	LF2_rotor								
Cruise	RF2_rotor								
Cruise	LF3_rotor								
Cruise	RF3_rotor								
Cruise	RF_rotor								
Cruise	RR_rotor								
Reserve	LF1_rotor	3563.2	700.8	6.429	149.3	1.237	85.8	1.992	90.9
Reserve	RF1_rotor	3563.2	700.8	5.679	149.3	1.237	85.8	1.695	90.9
Reserve	LF2_rotor								
Reserve	RF2_rotor								
Reserve	LF3_rotor								
Reserve	RF3_rotor								
Reserve	RF_rotor								
Reserve	RR_rotor								
Condition	Rotor	Motor RPM	Thrust (N)	Thrust margin	Motor Torque (Nm)	Torque margin	Power (kW)	Power margin	Motor efficiency (%)
Hover	LF1_rotor	4358.0	1658.9	2.716	68.2	2.708	50.3	3.399	86.7
Hover	RF1_rotor	4358.0	1658.8	2.399	68.2	2.708	50.3	2.892	86.7
Hover	LF2_rotor	6743.5	2688.2	1.252	37.7	1.11	77.3	1.243	86.7
Hover	RF2_rotor	6743.5	2688.3	1.252	37.7	1.11	77.3	1.243	86.7
Hover	LF3_rotor	6635.1	2602.5	1.294	36.5	1.144	73.9	1.3	86.6
Hover	RF3_rotor	6635.1	2602.5	1.294	36.5	1.144	73.9	1.3	86.6
Hover	RF_rotor	3691.7	2479.7	1.788	48.7	1.784	53.6	2.112	88.5
Hover	RR_rotor	2612.3	1241.7	2.533	26.7	2.873	21.6	3.344	85.0
Hover.OEI.LF1	LF1_rotor	5000.0	0.0	0.0	78.1	2.364	0.0	0.0	87.5
Hover.OEI.LF1	RF1_rotor	3471.1	0.0	0.0	0.1	0.0	3.9	36.824	1.0
Hover.OEI.LF1	LF2_rotor	7546.4	3366.4	1.0	41.8	1.0	96.1	1.0	86.6
Hover.OEI.LF1	RF2_rotor	7546.4	3366.4	1.0	41.8	1.0	96.1	1.0	86.6
Hover.OEI.LF1	LF3_rotor	7546.4	3366.4	1.0	41.8	1.0	96.1	1.0	86.6
Hover.OEI.LF1	RF3_rotor	7546.4	3366.4	1.0	41.8	1.0	96.1	1.0	86.6
Hover.OEI.LF1	RF_rotor	5554.3	4433.3	1.0	68.2	1.273	113.2	1.0	88.3
Hover.OEI.LF1	RR_rotor	5679.2	0.0	0.0	2.1	36.157	8.2	8.863	38.9
Condition	Rotor	Motor RPM	Thrust (N)	Thrust margin	Motor Torque (Nm)	Torque margin	Power (kW)	Power margin	Motor efficiency (%)
Hover.OEI.RF1	LF1_rotor	4904.7	0.0	0.0	1.3	137.27	6.6	26.041	14.7
Hover.OEI.RF1	RF1_rotor	5000.0	0.0	0.0	78.1	2.364	0.0	0.0	87.5
Hover.OEI.RF1	LF2_rotor	7546.4	3366.4	1.0	41.8	1.0	96.1	1.0	86.6
Hover.OEI.RF1	RF2_rotor	7546.4	3366.4	1.0	41.8	1.0	96.1	1.0	86.6
Hover.OEI.RF1	LF3_rotor	7546.4	3366.4	1.0	41.8	1.0	96.1	1.0	86.6
Hover.OEI.RF1	RF3_rotor	7546.4	3366.4	1.0	41.8	1.0	96.1	1.0	86.6
Hover.OEI.RF1	RF_rotor	5294.9	4433.3	1.0	70.7	1.23	111.6	1.015	88.5
Hover.OEI.RF1	RR_rotor	4857.5	0.0	0.0	1.4	55.068	6.0	12.059	29.7
Hover.OEI.LF2	LF1_rotor	7179.6	4502.3	1.001	144.8	1.275	170.7	1.001	89.3
Hover.OEI.LF2	RF1_rotor	6400.8	3289.2	1.21	108.0	1.71	114.1	1.274	88.8
Hover.OEI.LF2	LF2_rotor	5235.7	720.2	4.674	21.1	1.979	15.6	6.17	83.3
Hover.OEI.LF2	RF2_rotor	7130.0	3005.2	1.12	37.7	1.11	81.9	1.173	86.5
Hover.OEI.LF2	LF3_rotor	6647.3	2129.8	1.581	25.3	1.652	52.5	1.828	84.5
Hover.OEI.LF2	RF3_rotor	4437.1	1163.9	2.892	15.4	2.711	22.6	4.255	80.0
Hover.OEI.LF2	RF_rotor	5039.6	0.0	0.0	0.1	647.301	4.5	25.171	4.0
Hover.OEI.LF2	RR_rotor	5514.1	3107.8	1.012	43.6	1.757	72.3	1.0	87.7

Table B.8. Rotor metrics/outputs for the 8 Lift (Tilt 1) configuration (Part 2).

Condition	Rotor	Motor RPM	Thrust (N)	Thrust margin	Motor Torque (Nm)	Torque margin	Power (kW)	Power margin	Motor efficiency (%)
Hover.OEI.RF2	LF1_rotor	5893.1	3016.3	1.494	103.3	1.787	100.6	1.699	88.8
Hover.OEI.RF2	RF1_rotor	6846.5	3930.4	1.013	127.5	1.448	143.5	1.013	89.2
Hover.OEI.RF2	LF2_rotor	6927.5	2837.0	1.187	35.7	1.17	75.6	1.271	86.4
Hover.OEI.RF2	RF2_rotor	5551.0	809.6	4.158	23.6	1.771	18.2	5.267	84.2
Hover.OEI.RF2	LF3_rotor	5057.2	1511.9	2.227	19.8	2.113	31.9	3.01	82.7
Hover.OEI.RF2	RF3_rotor	6850.9	2774.5	1.213	35.0	1.195	73.3	1.311	86.3
Hover.OEI.RF2	RF_rotor	5040.3	0.0	0.0	0.7	116.441	5.3	21.209	18.6
Hover.OEI.RF2	RR_rotor	5442.2	3039.9	1.035	42.7	1.792	70.0	1.033	87.7
Hover.OEI.LF3	LF1_rotor	7182.1	4505.5	1.0	144.9	1.274	170.9	1.0	89.3
Hover.OEI.LF3	RF1_rotor	6807.2	3979.8	1.0	130.0	1.42	145.4	1.0	89.2
Hover.OEI.LF3	LF2_rotor	5631.9	1797.2	1.873	22.9	1.824	40.6	2.368	83.9
Hover.OEI.LF3	RF2_rotor	5794.0	1984.5	1.696	25.6	1.634	46.1	2.083	84.8
Hover.OEI.LF3	LF3_rotor	5405.8	767.8	4.385	22.4	1.862	17.0	5.659	83.8
Hover.OEI.LF3	RF3_rotor	5447.5	1754.2	1.919	22.8	1.835	39.0	2.463	83.9
Hover.OEI.LF3	RF_rotor	3151.7	0.0	0.0	0.0	0.0	2.7	42.432	0.0
Hover.OEI.LF3	RR_rotor	4843.7	3144.8	1.0	48.2	1.59	69.6	1.038	88.4
Hover.OEI.RF3	LF1_rotor	5859.4	2330.2	1.933	75.1	2.458	74.2	2.304	87.0
Hover.OEI.RF3	RF1_rotor	6322.4	2847.5	1.398	91.2	2.024	96.0	1.514	88.0
Hover.OEI.RF3	LF2_rotor	5996.1	2125.4	1.584	27.3	1.532	50.7	1.896	85.2
Hover.OEI.RF3	RF2_rotor	6751.5	2694.6	1.249	34.1	1.227	70.4	1.365	86.2
Hover.OEI.RF3	LF3_rotor	7027.1	2919.1	1.153	36.7	1.14	78.7	1.221	86.4
Hover.OEI.RF3	RF3_rotor	6658.1	629.8	5.345	15.0	2.79	14.8	6.501	79.2
Hover.OEI.RF3	RF_rotor	5302.3	3483.6	1.273	51.6	1.682	81.9	1.383	88.3
Hover.OEI.RF3	RR_rotor	4850.9	869.2	3.618	11.0	6.992	18.7	3.863	74.9
Hover.OEI.RF	LF1_rotor	5522.2	1484.2	3.036	44.3	4.168	43.6	3.924	82.3
Hover.OEI.RF	RF1_rotor	4896.9	1409.2	2.824	45.0	4.099	39.1	3.715	82.6
Hover.OEI.RF	LF2_rotor	7099.8	2979.8	1.13	37.4	1.118	81.0	1.187	86.5
Hover.OEI.RF	RF2_rotor	6986.0	2885.1	1.167	36.3	1.152	77.4	1.241	86.4
Hover.OEI.RF	LF3_rotor	6534.1	2523.8	1.334	32.0	1.304	64.2	1.495	86.0
Hover.OEI.RF	RF3_rotor	6976.6	2877.3	1.17	36.2	1.155	77.1	1.246	86.4
Hover.OEI.RF	RF_rotor	5361.1	2324.2	1.907	86.9	1.0	62.0	1.827	88.2
Hover.OEI.RF	RR_rotor	4678.1	1425.0	2.207	18.4	4.157	27.7	2.608	82.0
Hover.OEI.RR	LF1_rotor	5897.9	2547.8	1.768	83.6	2.208	82.5	2.073	87.7
Hover.OEI.RR	RF1_rotor	5825.6	2088.1	1.906	65.7	2.81	65.2	2.229	86.1
Hover.OEI.RR	LF2_rotor	5836.2	2013.5	1.672	25.9	1.612	47.1	2.042	84.9
Hover.OEI.RR	RF2_rotor	6268.0	2322.5	1.45	29.7	1.41	57.3	1.678	85.7
Hover.OEI.RR	LF3_rotor	6439.4	2451.2	1.373	31.2	1.34	61.7	1.557	85.9
Hover.OEI.RR	RF3_rotor	7194.3	3059.7	1.1	38.3	1.091	84.0	1.144	86.5
Hover.OEI.RR	RF_rotor	5326.7	1407.4	3.15	17.6	4.941	30.4	3.728	81.4
Hover.OEI.RR	RR_rotor	5008.2	2028.2	1.551	76.6	1.0	50.7	1.425	88.7

Table B.9. Rotor metrics/outputs for the 8 Lift (Tilt 1) configuration (Part 3).

Condition	Rotor	Rotor RPM	J	Thrust coeff	Power coeff	Disk loading (kg/m^2)	Tip Mach	Blade loading coeff	Rotor efficiency (%)
Cruise	LF1_rotor	960.1	2.017	0.217	0.477	30.998	0.312	1.446	91.7
Cruise	RF1_rotor	960.0	2.017	0.217	0.477	30.994	0.312	1.446	91.7
Cruise	LF2_rotor								
Cruise	RF2_rotor								
Cruise	LF3_rotor								
Cruise	RF3_rotor								
Cruise	RF_rotor								
Cruise	RR_rotor								
Reserve	LF1_rotor	890.8	1.812	0.225	0.448	27.676	0.29	1.5	90.9
Reserve	RF1_rotor	890.8	1.812	0.225	0.448	27.676	0.29	1.5	90.9
Reserve	LF2_rotor								
Reserve	RF2_rotor								
Reserve	LF3_rotor								
Reserve	RF3_rotor								
Reserve	RF_rotor								
Reserve	RR_rotor								
Condition	Rotor	Rotor RPM	J	Thrust coeff	Power coeff	Disk loading (kg/m^2)	Tip Mach	Blade loading coeff	Rotor efficiency (%)
Hover	LF1_rotor	1089.5	0.133	0.225	0.112	50.393	0.346	1.5	75.7
Hover	RF1_rotor	1089.5	0.133	0.225	0.112	50.392	0.346	1.5	75.7
Hover	LF2_rotor	1685.9	0.086	0.085	0.026	45.369	0.536	1.41	75.7
Hover	RF2_rotor	1685.9	0.086	0.085	0.026	45.369	0.536	1.41	75.7
Hover	LF3_rotor	1658.8	0.087	0.085	0.026	43.921	0.528	1.41	75.5
Hover	RF3_rotor	1658.8	0.087	0.085	0.026	43.921	0.528	1.41	75.5
Hover	RF_rotor	922.9	0.119	0.085	0.027	23.854	0.389	1.41	71.5
Hover	RR_rotor	653.1	0.168	0.085	0.03	11.944	0.275	1.41	65.4
Hover.OEI.LF1	LF1_rotor	1250.0	0.046	0.225	0.098	66.334	0.398	1.5	87.0
Hover.OEI.LF1	RF1_rotor	867.8	0.067	0.0	0.0	0.0	0.276	0.0	0.0
Hover.OEI.LF1	LF2_rotor	1886.6	0.031	0.085	0.023	56.814	0.6	1.41	85.4
Hover.OEI.LF1	RF2_rotor	1886.6	0.031	0.085	0.023	56.815	0.6	1.41	85.4
Hover.OEI.LF1	LF3_rotor	1886.6	0.031	0.085	0.023	56.814	0.6	1.41	85.4
Hover.OEI.LF1	RF3_rotor	1886.6	0.031	0.085	0.023	56.814	0.6	1.41	85.4
Hover.OEI.LF1	RF_rotor	1388.6	0.032	0.067	0.017	42.647	0.585	1.114	81.1
Hover.OEI.LF1	RR_rotor	1419.8	0.031	0.0	0.001	0.0	0.598	0.0	0.0
Condition	Rotor	Rotor RPM	J	Thrust coeff	Power coeff	Disk loading (kg/m^2)	Tip Mach	Blade loading coeff	Rotor efficiency (%)
Hover.OEI.RF1	LF1_rotor	1226.2	0.047	0.0	0.002	0.0	0.39	0.0	0.0
Hover.OEI.RF1	RF1_rotor	1250.0	0.046	0.225	0.098	66.334	0.398	1.5	87.0
Hover.OEI.RF1	LF2_rotor	1886.6	0.031	0.085	0.023	56.814	0.6	1.41	85.4
Hover.OEI.RF1	RF2_rotor	1886.6	0.031	0.085	0.023	56.814	0.6	1.41	85.4
Hover.OEI.RF1	LF3_rotor	1886.6	0.031	0.085	0.023	56.814	0.6	1.41	85.4
Hover.OEI.RF1	RF3_rotor	1886.6	0.031	0.085	0.023	56.814	0.6	1.41	85.4
Hover.OEI.RF1	RF_rotor	1323.7	0.033	0.074	0.019	42.647	0.558	1.225	82.2
Hover.OEI.RF1	RR_rotor	1214.4	0.036	0.0	0.0	0.0	0.512	0.0	0.0
Hover.OEI.LF2	LF1_rotor	1794.9	0.032	0.225	0.088	136.771	0.571	1.5	96.8
Hover.OEI.LF2	RF1_rotor	1600.2	0.036	0.207	0.083	99.92	0.509	1.379	90.9
Hover.OEI.LF2	LF2_rotor	1308.9	0.044	0.085	0.024	27.349	0.416	1.41	81.3
Hover.OEI.LF2	RF2_rotor	1782.5	0.033	0.085	0.023	50.717	0.567	1.41	84.6
Hover.OEI.LF2	LF3_rotor	1661.8	0.035	0.069	0.018	35.944	0.529	1.15	80.6
Hover.OEI.LF2	RF3_rotor	1109.3	0.052	0.085	0.025	19.642	0.353	1.41	80.0
Hover.OEI.LF2	RF_rotor	1259.9	0.035	0.0	0.0	0.0	0.531	0.0	0.0
Hover.OEI.LF2	RR_rotor	1378.5	0.032	0.048	0.011	29.896	0.581	0.792	75.0

Table B.10. Rotor metrics/outputs for the 8 Lift (Tilt 1) configuration (Part 4).

Condition	Rotor	Rotor RPM	J	Thrust coeff	Power coeff	Disk loading (kg/m^2)	Tip Mach	Blade loading coeff	Rotor efficiency (%)
Hover.OEI.RF2	LF1_rotor	1473.3	0.039	0.224	0.093	91.63	0.469	1.492	90.6
Hover.OEI.RF2	RF1_rotor	1711.6	0.034	0.216	0.085	119.399	0.544	1.44	94.0
Hover.OEI.RF2	LF2_rotor	1731.9	0.034	0.085	0.023	47.879	0.551	1.41	84.2
Hover.OEI.RF2	RF2_rotor	1387.7	0.042	0.085	0.024	30.741	0.441	1.41	81.9
Hover.OEI.RF2	LF3_rotor	1264.3	0.046	0.085	0.024	25.516	0.402	1.41	81.1
Hover.OEI.RF2	RF3_rotor	1712.7	0.034	0.085	0.023	46.825	0.545	1.41	84.1
Hover.OEI.RF2	RF_rotor	1260.1	0.035	0.0	0.0	0.0	0.531	0.0	0.0
Hover.OEI.RF2	RR_rotor	1360.6	0.032	0.048	0.011	29.243	0.573	0.795	75.0
Hover.OEI.LF3	LF1_rotor	1795.5	0.032	0.225	0.088	136.868	0.571	1.5	96.8
Hover.OEI.LF3	RF1_rotor	1701.8	0.034	0.221	0.088	120.898	0.541	1.475	94.5
Hover.OEI.LF3	LF2_rotor	1408.0	0.041	0.081	0.023	30.331	0.448	1.351	81.4
Hover.OEI.LF3	RF2_rotor	1448.5	0.04	0.085	0.024	33.492	0.461	1.41	82.2
Hover.OEI.LF3	LF3_rotor	1351.5	0.043	0.085	0.024	29.155	0.43	1.41	81.6
Hover.OEI.LF3	RF3_rotor	1361.9	0.043	0.085	0.024	29.606	0.433	1.41	81.7
Hover.OEI.LF3	RF_rotor	787.9	0.056	0.0	0.0	0.0	0.332	0.0	0.0
Hover.OEI.LF3	RR_rotor	1210.9	0.036	0.062	0.016	30.253	0.51	1.039	78.7
Condition	Rotor	Rotor RPM	J	Thrust coeff	Power coeff	Disk loading (kg/m^2)	Tip Mach	Blade loading coeff	Rotor efficiency (%)
Hover.OEI.RF3	LF1_rotor	1464.9	0.04	0.175	0.069	70.788	0.466	1.166	85.1
Hover.OEI.RF3	RF1_rotor	1580.6	0.037	0.184	0.071	86.501	0.503	1.223	87.8
Hover.OEI.RF3	LF2_rotor	1499.0	0.039	0.085	0.024	35.869	0.477	1.41	82.6
Hover.OEI.RF3	RF2_rotor	1687.9	0.034	0.085	0.023	45.476	0.537	1.41	83.9
Hover.OEI.RF3	LF3_rotor	1756.8	0.033	0.085	0.023	49.264	0.559	1.41	84.4
Hover.OEI.RF3	RF3_rotor	1664.5	0.035	0.046	0.011	23.915	0.529	0.762	73.8
Hover.OEI.RF3	RF_rotor	1325.6	0.033	0.058	0.014	33.512	0.558	0.96	78.2
Hover.OEI.RF3	RR_rotor	1212.7	0.036	0.017	0.004	8.361	0.511	0.286	50.2
Hover.OEI.RF	LF1_rotor	1380.6	0.042	0.125	0.045	45.088	0.439	0.836	77.9
Hover.OEI.RF	RF1_rotor	1224.2	0.047	0.151	0.059	42.808	0.389	1.009	79.9
Hover.OEI.RF	LF2_rotor	1775.0	0.033	0.085	0.023	50.29	0.564	1.41	84.5
Hover.OEI.RF	RF2_rotor	1746.5	0.033	0.085	0.023	48.691	0.555	1.41	84.3
Hover.OEI.RF	LF3_rotor	1633.5	0.036	0.085	0.024	42.594	0.52	1.41	83.5
Hover.OEI.RF	RF3_rotor	1744.1	0.033	0.085	0.023	48.559	0.555	1.41	84.3
Hover.OEI.RF	RF_rotor	1340.3	0.033	0.085	0.023	50.305	0.565	1.41	84.5
Hover.OEI.RF	RR_rotor	1169.5	0.037	0.03	0.006	13.708	0.493	0.505	65.0
Condition	Rotor	Rotor RPM	J	Thrust coeff	Power coeff	Disk loading (kg/m^2)	Tip Mach	Blade loading coeff	Rotor efficiency (%)
Hover.OEI.RR	LF1_rotor	1474.5	0.039	0.189	0.075	77.396	0.469	1.258	86.9
Hover.OEI.RR	RF1_rotor	1456.4	0.04	0.158	0.061	63.433	0.463	1.057	83.0
Hover.OEI.RR	LF2_rotor	1459.1	0.04	0.085	0.024	33.982	0.464	1.41	82.3
Hover.OEI.RR	RF2_rotor	1567.0	0.037	0.085	0.024	39.196	0.498	1.41	83.0
Hover.OEI.RR	LF3_rotor	1609.8	0.036	0.085	0.024	41.369	0.512	1.41	83.3
Hover.OEI.RR	RF3_rotor	1798.6	0.032	0.085	0.023	51.637	0.572	1.41	84.7
Hover.OEI.RR	RF_rotor	1331.7	0.033	0.023	0.005	13.538	0.561	0.384	58.7
Hover.OEI.RR	RR_rotor	1252.0	0.035	0.085	0.023	43.9	0.527	1.41	83.7

Table B.11. General performance overview for the 8 Lift (Tilt 2) configuration.

Condition	Total power (kW)	Lift coeff	Drag coeff	L/D	Wing incidence angle (°)	Tail incidence angle (°)
Cruise	238664.5	0.9044	0.0774	11.678	4.244	-0.252
Reserve	184640.7	1.3019	0.1022	12.7402	7.041	0.508
Hover	533771.9					
Hover.OEI.LF1	564078.4					
Hover.OEI.RF1	566932.9					
Hover.OEI.LF2	592872.7					
Hover.OEI.RF2	591934.0					
Hover.OEI.LF3	556988.7					
Hover.OEI.RF3	557027.4					
Hover.OEI.RF	549207.1					
Hover.OEI.RR	542462.9					
Payload weight (lb)	**Battery weight (lb)**	**Battery weight fraction**	**Gross weight (lb)**	**Wing area (m^2)**		
784.8	771.3	0.179	4313.7	9.46		

Table B.12. Rotor metrics/outputs for the 8 Lift (Tilt 2) configuration (Part 1).

Condition	Rotor	Motor RPM	Thrust (N)	Thrust margin	Motor Torque (Nm)	Torque margin	Power (kW)	Power margin	Motor efficiency (%)
Cruise	LF1_rotor								
Cruise	RF1_rotor								
Cruise	LF2_rotor	3932.2	820.8	5.859	188.8	1.0	119.3	1.567	91.2
Cruise	RF2_rotor	3932.2	820.8	5.859	188.8	1.0	119.3	1.567	91.2
Cruise	LF3_rotor								
Cruise	RF3_rotor								
Cruise	RF_rotor								
Cruise	RR_rotor								
Reserve	LF1_rotor								
Reserve	RF1_rotor								
Reserve	LF2_rotor	3692.3	752.5	6.391	155.1	1.217	92.3	2.026	90.9
Reserve	RF2_rotor	3692.3	752.5	6.391	155.1	1.217	92.3	2.026	90.9
Reserve	LF3_rotor								
Reserve	RF3_rotor								
Reserve	RF_rotor								
Reserve	RR_rotor								
Hover	LF1_rotor	7171.7	3040.5	1.107	42.2	1.0	92.0	1.044	86.8
Hover	RF1_rotor	7171.7	3040.5	1.107	42.2	1.0	92.0	1.044	86.8
Hover	LF2_rotor	4508.2	1775.2	2.709	72.6	2.598	55.1	3.392	87.1
Hover	RF2_rotor	4508.2	1775.2	2.709	72.6	2.598	55.1	3.392	87.1
Hover	LF3_rotor	6928.4	2837.7	1.186	39.6	1.056	83.4	1.151	86.8
Hover	RF3_rotor	6928.4	2837.7	1.186	39.6	1.056	83.4	1.151	86.8
Hover	RF_rotor	3708.9	2502.9	1.804	49.1	1.953	54.3	2.071	88.5
Hover	RR_rotor	2443.3	1086.1	1.804	23.8	3.114	18.3	2.64	84.1
Hover.OEI.LF1	LF1_rotor	5417.9	771.2	4.365	22.5	1.874	17.1	5.625	83.9
Hover.OEI.LF1	RF1_rotor	5793.1	1983.9	1.697	25.6	1.651	46.1	2.084	84.8
Hover.OEI.LF1	LF2_rotor	7522.8	4476.0	1.074	138.9	1.359	172.0	1.087	89.1
Hover.OEI.LF1	RF2_rotor	6432.9	2980.5	1.614	95.3	1.981	101.8	1.836	88.2
Hover.OEI.LF1	LF3_rotor	6521.4	2514.1	1.339	31.9	1.309	63.9	1.504	86.0
Hover.OEI.LF1	RF3_rotor	5959.5	2099.5	1.603	27.0	1.549	49.8	1.928	85.1
Hover.OEI.LF1	RF_rotor	4884.9	4341.6	1.04	73.1	1.311	106.1	1.059	88.8
Hover.OEI.LF1	RR_rotor	4511.2	1.3	0.0	2.7	27.202	7.2	6.695	45.1
Hover.OEI.RF1	LF1_rotor	5793.2	1984.0	1.697	25.6	1.651	46.1	2.083	84.8
Hover.OEI.RF1	RF1_rotor	5417.8	771.2	4.365	22.5	1.874	17.1	5.626	83.9
Hover.OEI.RF1	LF2_rotor	6434.7	2994.8	1.606	95.8	1.97	102.4	1.826	88.3
Hover.OEI.RF1	RF2_rotor	7526.1	4481.7	1.073	139.1	1.357	172.3	1.086	89.1
Hover.OEI.RF1	LF3_rotor	5985.1	2117.6	1.59	27.2	1.537	50.4	1.905	85.2
Hover.OEI.RF1	RF3_rotor	6564.5	2547.4	1.322	32.3	1.293	65.1	1.476	86.0
Hover.OEI.RF1	RF_rotor	5105.7	4310.7	1.048	70.0	1.37	106.4	1.057	88.7
Hover.OEI.RF1	RR_rotor	4511.2	1.0	0.0	2.7	27.51	7.2	6.731	44.8
Hover.OEI.LF2	LF1_rotor	7546.4	3366.4	1.0	41.8	1.01	96.1	1.0	86.6
Hover.OEI.LF2	RF1_rotor	6297.0	0.0	0.0	0.8	50.695	6.9	14.019	20.2
Hover.OEI.LF2	LF2_rotor	4500.0	0.0	0.0	64.7	2.919	0.0	0.0	86.2
Hover.OEI.LF2	RF2_rotor	7520.1	4809.2	1.0	151.3	1.247	187.0	1.0	89.2
Hover.OEI.LF2	LF3_rotor	7546.4	3366.4	1.0	41.8	1.0	96.1	1.0	86.6
Hover.OEI.LF2	RF3_rotor	7546.4	3366.4	1.0	41.8	1.0	96.1	1.0	86.6
Hover.OEI.LF2	RF_rotor	5277.1	4265.8	1.059	67.4	1.423	106.0	1.061	88.5
Hover.OEI.LF2	RR_rotor	5615.4	0.0	0.0	0.0	0.0	4.8	10.002	0.0

Table B.13. Rotor metrics/outputs for the 8 Lift (Tilt 2) configuration (Part 2).

Condition	Rotor	Motor RPM	Thrust (N)	Thrust margin	Motor Torque (Nm)	Torque margin	Power (kW)	Power margin	Motor efficiency (%)
Hover.OEI.RF2	LF1_rotor	5449.4	0.0	0.0	0.1	699.31	4.8	20.162	1.8
Hover.OEI.RF2	RF1_rotor	7546.4	3366.4	1.0	41.8	1.01	96.1	1.0	86.6
Hover.OEI.RF2	LF2_rotor	7522.7	4809.2	1.0	151.3	1.248	187.0	1.0	89.2
Hover.OEI.RF2	RF2_rotor	4500.0	0.0	0.0	64.7	2.919	0.0	0.0	86.2
Hover.OEI.RF2	LF3_rotor	7546.4	3366.4	1.0	41.8	1.0	96.1	1.0	86.6
Hover.OEI.RF2	RF3_rotor	7546.4	3366.4	1.0	41.8	1.0	96.1	1.0	86.6
Hover.OEI.RF2	RF_rotor	5525.9	4265.8	1.059	65.2	1.472	107.5	1.045	88.3
Hover.OEI.RF2	RR_rotor	4536.8	0.0	0.0	0.4	185.12	4.4	11.04	11.0
Hover.OEI.LF3	LF1_rotor	6479.5	2481.8	1.356	31.5	1.339	62.8	1.531	86.0
Hover.OEI.LF3	RF1_rotor	6109.9	2206.8	1.525	28.3	1.494	53.4	1.8	85.4
Hover.OEI.LF3	LF2_rotor	6965.0	3781.4	1.272	120.1	1.571	137.9	1.356	89.0
Hover.OEI.LF3	RF2_rotor	6637.6	3349.0	1.436	107.4	1.757	117.9	1.587	88.7
Hover.OEI.LF3	LF3_rotor	5080.6	678.2	4.964	20.0	2.095	14.4	6.69	82.8
Hover.OEI.LF3	RF3_rotor	5992.0	2122.4	1.586	27.3	1.534	50.6	1.899	85.2
Hover.OEI.LF3	RF_rotor	4982.1	4516.1	1.0	75.8	1.264	112.4	1.0	88.7
Hover.OEI.LF3	RR_rotor	4511.0	27.7	70.835	3.2	23.378	7.8	6.221	48.7
Condition	Rotor	Motor RPM	Thrust (N)	Thrust margin	Motor Torque (Nm)	Torque margin	Power (kW)	Power margin	Motor efficiency (%)
Hover.OEI.RF3	LF1_rotor	6109.9	2206.8	1.526	28.3	1.494	53.4	1.8	85.4
Hover.OEI.RF3	RF1_rotor	6479.4	2481.8	1.356	31.5	1.339	62.8	1.531	86.0
Hover.OEI.RF3	LF2_rotor	6637.5	3348.9	1.436	107.4	1.757	117.9	1.587	88.7
Hover.OEI.RF3	RF2_rotor	6964.9	3781.4	1.272	120.1	1.571	137.9	1.356	89.0
Hover.OEI.RF3	LF3_rotor	5991.9	2122.4	1.586	27.3	1.534	50.6	1.899	85.2
Hover.OEI.RF3	RF3_rotor	5080.5	678.2	4.964	20.0	2.095	14.4	6.69	82.8
Hover.OEI.RF3	RF_rotor	4982.2	4516.3	1.0	75.9	1.264	112.4	1.0	88.7
Hover.OEI.RF3	RR_rotor	4521.4	28.1	69.737	3.2	23.254	7.8	6.19	48.8
Hover.OEI.RF	LF1_rotor	6056.0	2168.0	1.553	27.8	1.519	52.1	1.845	85.3
Hover.OEI.RF	RF1_rotor	6056.0	2168.0	1.553	27.8	1.519	52.1	1.845	85.3
Hover.OEI.RF	LF2_rotor	6910.9	3207.2	1.499	99.0	1.907	113.6	1.647	88.3
Hover.OEI.RF	RF2_rotor	6910.9	3207.2	1.499	99.0	1.907	113.6	1.647	88.3
Hover.OEI.RF	LF3_rotor	6345.8	2380.5	1.414	30.3	1.377	59.2	1.622	85.8
Hover.OEI.RF	RF3_rotor	6345.8	2380.5	1.414	30.3	1.377	59.2	1.622	85.8
Hover.OEI.RF	RF_rotor	5657.0	2587.8	1.745	95.9	1.0	72.6	1.548	87.6
Hover.OEI.RF	RR_rotor	5624.5	1128.8	1.736	14.2	5.231	26.8	1.802	78.6
Condition	Rotor	Motor RPM	Thrust (N)	Thrust margin	Motor Torque (Nm)	Torque margin	Power (kW)	Power margin	Motor efficiency (%)
Hover.OEI.RR	LF1_rotor	6148.0	2234.4	1.507	28.6	1.477	54.3	1.77	85.5
Hover.OEI.RR	RF1_rotor	6148.0	2234.4	1.507	28.6	1.477	54.3	1.77	85.5
Hover.OEI.RR	LF2_rotor	6602.8	3691.1	1.303	121.4	1.555	131.9	1.418	89.1
Hover.OEI.RR	RF2_rotor	6602.8	3691.1	1.303	121.4	1.555	131.9	1.418	89.1
Hover.OEI.RR	LF3_rotor	5905.1	2061.3	1.633	26.5	1.576	48.6	1.977	85.0
Hover.OEI.RR	RF3_rotor	5905.1	2061.3	1.633	26.5	1.576	48.6	1.977	85.0
Hover.OEI.RR	RF_rotor	4861.9	1221.3	3.698	15.4	6.239	24.7	4.553	79.8
Hover.OEI.RR	RR_rotor	4922.3	1959.3	1.0	74.2	1.0	48.2	1.0	88.8

Table B.14. Rotor metrics/outputs for the 8 Lift (Tilt 2) configuration (Part 3).

Condition	Rotor	Rotor RPM	J	Thrust coeff	Power coeff	Disk loading (kg/m^2)	Tip Mach	Blade loading coeff	Rotor efficiency (%)
Cruise	LF1_rotor								
Cruise	RF1_rotor								
Cruise	LF2_rotor	983.1	1.97	0.216	0.465	32.414	0.32	1.442	91.6
Cruise	RF2_rotor	983.0	1.97	0.216	0.465	32.413	0.32	1.442	91.6
Cruise	LF3_rotor								
Cruise	RF3_rotor								
Cruise	RF_rotor								
Cruise	RR_rotor								
Reserve	LF1_rotor								
Reserve	RF1_rotor								
Reserve	LF2_rotor	923.1	1.748	0.225	0.434	29.718	0.3	1.5	90.7
Reserve	RF2_rotor	923.1	1.748	0.225	0.434	29.718	0.3	1.5	90.7
Reserve	LF3_rotor								
Reserve	RF3_rotor								
Reserve	RF_rotor								
Reserve	RR_rotor								

Condition	Rotor	Rotor RPM	J	Thrust coeff	Power coeff	Disk loading (kg/m^2)	Tip Mach	Blade loading coeff	Rotor efficiency (%)
Hover	LF1_rotor	1792.9	0.081	0.085	0.026	51.314	0.57	1.41	76.3
Hover	RF1_rotor	1792.9	0.081	0.085	0.026	51.314	0.57	1.41	76.3
Hover	LF2_rotor	1127.0	0.129	0.225	0.112	53.926	0.358	1.5	76.1
Hover	RF2_rotor	1127.0	0.129	0.225	0.112	53.926	0.358	1.5	76.1
Hover	LF3_rotor	1732.1	0.084	0.085	0.026	47.89	0.551	1.41	76.0
Hover	RF3_rotor	1732.1	0.084	0.085	0.026	47.89	0.551	1.41	76.0
Hover	RF_rotor	927.2	0.118	0.085	0.027	24.077	0.391	1.41	71.6
Hover	RR_rotor	610.8	0.179	0.085	0.031	10.448	0.257	1.41	64.0
Hover.OEI.LF1	LF1_rotor	1354.5	0.043	0.085	0.024	29.285	0.431	1.41	81.6
Hover.OEI.LF1	RF1_rotor	1448.3	0.04	0.085	0.024	33.481	0.461	1.41	82.2
Hover.OEI.LF1	LF2_rotor	1880.7	0.031	0.204	0.077	135.972	0.598	1.358	95.4
Hover.OEI.LF1	RF2_rotor	1608.2	0.036	0.186	0.072	90.543	0.511	1.237	88.4
Hover.OEI.LF1	LF3_rotor	1630.4	0.036	0.085	0.024	42.429	0.519	1.41	83.5
Hover.OEI.LF1	RF3_rotor	1489.9	0.039	0.085	0.024	35.432	0.474	1.41	82.5
Hover.OEI.LF1	RF_rotor	1221.2	0.036	0.085	0.024	41.765	0.514	1.41	83.4
Hover.OEI.LF1	RR_rotor	1127.8	0.039	0.0	0.001	0.012	0.475	0.0	0.0

Condition	Rotor	Rotor RPM	J	Thrust coeff	Power coeff	Disk loading (kg/m^2)	Tip Mach	Blade loading coeff	Rotor efficiency (%)
Hover.OEI.RF1	LF1_rotor	1448.3	0.04	0.085	0.024	33.483	0.461	1.41	82.2
Hover.OEI.RF1	RF1_rotor	1354.5	0.043	0.085	0.024	29.284	0.431	1.41	81.6
Hover.OEI.RF1	LF2_rotor	1608.7	0.036	0.186	0.072	90.975	0.512	1.242	88.5
Hover.OEI.RF1	RF2_rotor	1881.5	0.031	0.204	0.077	136.145	0.598	1.359	95.4
Hover.OEI.RF1	LF3_rotor	1496.3	0.039	0.085	0.024	35.738	0.476	1.41	82.6
Hover.OEI.RF1	RF3_rotor	1641.1	0.035	0.085	0.023	42.992	0.522	1.41	83.6
Hover.OEI.RF1	RF_rotor	1276.4	0.034	0.077	0.021	41.468	0.538	1.282	82.5
Hover.OEI.RF1	RR_rotor	1127.8	0.039	0.0	0.001	0.01	0.475	0.0	0.0
Hover.OEI.LF2	LF1_rotor	1886.6	0.031	0.085	0.023	56.814	0.6	1.41	85.4
Hover.OEI.LF2	RF1_rotor	1574.3	0.037	0.0	0.001	0.0	0.501	0.0	0.0
Hover.OEI.LF2	LF2_rotor	1125.0	0.052	0.225	0.1	53.73	0.358	1.5	85.1
Hover.OEI.LF2	RF2_rotor	1880.0	0.031	0.219	0.084	146.094	0.598	1.46	97.6
Hover.OEI.LF2	LF3_rotor	1886.6	0.031	0.085	0.023	56.814	0.6	1.41	85.4
Hover.OEI.LF2	RF3_rotor	1886.6	0.031	0.085	0.023	56.814	0.6	1.41	85.4
Hover.OEI.LF2	RF_rotor	1319.3	0.033	0.071	0.019	41.036	0.556	1.187	81.6
Hover.OEI.LF2	RR_rotor	1403.8	0.031	0.0	0.0	0.0	0.591	0.0	0.0

Table B.15. Rotor metrics/outputs for the 8 Lift (Tilt 2) configuration (Part 4).

Condition	Rotor	Rotor RPM	J	Thrust coeff	Power coeff	Disk loading (kg/m^2)	Tip Mach	Blade loading coeff	Rotor efficiency (%)
Hover.OEI.RF2	LF1_rotor	1362.4	0.043	0.0	0.0	0.0	0.433	0.0	0.0
Hover.OEI.RF2	RF1_rotor	1886.6	0.031	0.085	0.023	56.814	0.6	1.41	85.4
Hover.OEI.RF2	LF2_rotor	1880.7	0.031	0.219	0.084	146.094	0.598	1.459	97.6
Hover.OEI.RF2	RF2_rotor	1125.0	0.052	0.225	0.1	53.73	0.358	1.5	85.1
Hover.OEI.RF2	LF3_rotor	1886.6	0.031	0.085	0.023	56.814	0.6	1.41	85.4
Hover.OEI.RF2	RF3_rotor	1886.6	0.031	0.085	0.023	56.814	0.6	1.41	85.4
Hover.OEI.RF2	RF_rotor	1381.5	0.032	0.065	0.016	41.036	0.582	1.083	80.6
Hover.OEI.RF2	RR_rotor	1134.2	0.039	0.0	0.0	0.0	0.478	0.0	0.0
Hover.OEI.LF3	LF1_rotor	1619.9	0.036	0.085	0.024	41.885	0.515	1.41	83.4
Hover.OEI.LF3	RF1_rotor	1527.5	0.038	0.085	0.024	37.244	0.486	1.41	82.8
Hover.OEI.LF3	LF2_rotor	1741.3	0.033	0.201	0.078	114.872	0.554	1.339	92.6
Hover.OEI.LF3	RF2_rotor	1659.4	0.035	0.196	0.076	101.736	0.528	1.305	90.5
Hover.OEI.LF3	LF3_rotor	1270.1	0.046	0.085	0.024	25.752	0.404	1.41	81.1
Hover.OEI.LF3	RF3_rotor	1498.0	0.039	0.085	0.024	35.82	0.476	1.41	82.6
Hover.OEI.LF3	RF_rotor	1245.5	0.035	0.085	0.023	43.443	0.525	1.41	83.6
Hover.OEI.LF3	RR_rotor	1127.7	0.039	0.001	0.001	0.266	0.475	0.011	1.1
Condition	Rotor	Rotor RPM	J	Thrust coeff	Power coeff	Disk loading (kg/m^2)	Tip Mach	Blade loading coeff	Rotor efficiency (%)
Hover.OEI.RF3	LF1_rotor	1527.5	0.038	0.085	0.024	37.243	0.486	1.41	82.8
Hover.OEI.RF3	RF1_rotor	1619.8	0.036	0.085	0.024	41.884	0.515	1.41	83.4
Hover.OEI.RF3	LF2_rotor	1659.4	0.035	0.196	0.076	101.734	0.528	1.305	90.5
Hover.OEI.RF3	RF2_rotor	1741.2	0.033	0.201	0.078	114.871	0.554	1.339	92.6
Hover.OEI.RF3	LF3_rotor	1498.0	0.039	0.085	0.024	35.819	0.476	1.41	82.6
Hover.OEI.RF3	RF3_rotor	1270.1	0.046	0.085	0.024	25.752	0.404	1.41	81.1
Hover.OEI.RF3	RF_rotor	1245.6	0.035	0.085	0.023	43.446	0.525	1.41	83.6
Hover.OEI.RF3	RR_rotor	1130.4	0.039	0.001	0.001	0.27	0.476	0.011	1.1
Hover.OEI.RF	LF1_rotor	1514.0	0.038	0.085	0.024	36.589	0.482	1.41	82.7
Hover.OEI.RF	RF1_rotor	1514.0	0.038	0.085	0.024	36.589	0.482	1.41	82.7
Hover.OEI.RF	LF2_rotor	1727.7	0.034	0.173	0.065	97.43	0.549	1.153	88.5
Hover.OEI.RF	RF2_rotor	1727.7	0.034	0.173	0.065	97.43	0.549	1.153	88.5
Hover.OEI.RF	LF3_rotor	1586.5	0.037	0.085	0.024	40.175	0.505	1.41	83.2
Hover.OEI.RF	RF3_rotor	1586.5	0.037	0.085	0.024	40.175	0.505	1.41	83.2
Hover.OEI.RF	RF_rotor	1414.2	0.031	0.085	0.023	56.012	0.596	1.41	85.3
Hover.OEI.RF	RR_rotor	1406.1	0.031	0.017	0.003	10.859	0.592	0.277	49.5
Condition	Rotor	Rotor RPM	J	Thrust coeff	Power coeff	Disk loading (kg/m^2)	Tip Mach	Blade loading coeff	Rotor efficiency (%)
Hover.OEI.RR	LF1_rotor	1537.0	0.038	0.085	0.024	37.71	0.489	1.41	82.8
Hover.OEI.RR	RF1_rotor	1537.0	0.038	0.085	0.024	37.71	0.489	1.41	82.8
Hover.OEI.RR	LF2_rotor	1650.7	0.035	0.218	0.087	112.13	0.525	1.454	93.2
Hover.OEI.RR	RF2_rotor	1650.7	0.035	0.218	0.087	112.13	0.525	1.454	93.2
Hover.OEI.RR	LF3_rotor	1476.3	0.039	0.085	0.024	34.788	0.47	1.41	82.4
Hover.OEI.RR	RF3_rotor	1476.3	0.039	0.085	0.024	34.788	0.47	1.41	82.4
Hover.OEI.RR	RF_rotor	1215.5	0.036	0.024	0.005	11.749	0.512	0.4	59.5
Hover.OEI.RR	RR_rotor	1230.6	0.036	0.085	0.024	42.408	0.518	1.41	83.5

Table B.16. General performance overview for the 8 Lift (Tilt 3) configuration.

Condition	Total power (kW)	Lift coeff	Drag coeff	L/D	Wing incidence angle (°)	Tail incidence angle (°)
Cruise	252293.9	0.9764	0.0817	11.9466	4.834	-0.368
Reserve	201256.2	1.4054	0.1111	12.6541	7.895	0.341
Hover	600876.0					
Hover.OEI.LF1	644547.2					
Hover.OEI.RF1	661504.9					
Hover.OEI.LF2	635106.5					
Hover.OEI.RF2	628723.4					
Hover.OEI.LF3	627920.0					
Hover.OEI.RF3	625230.1					
Hover.OEI.RF	578859.6					
Hover.OEI.RR	571374.2					

Payload weight (lb)	Battery weight (lb)	Battery weight fraction	Gross weight (lb)	Wing area (m^2)
784.8	1091.8	0.234	4656.7	9.46

Table B.17. Rotor metrics/outputs for the 8 Lift (Tilt 3) configuration (Part 1).

Condition	Rotor	Motor RPM	Thrust (N)	Thrust margin	Motor Torque (Nm)	Torque margin	Power (kW)	Power margin	Motor efficiency (%)
Cruise	LF1_rotor								
Cruise	RF1_rotor								
Cruise	LF2_rotor								
Cruise	RF2_rotor								
Cruise	LF3_rotor	4045.6	866.2	5.743	193.9	1.0	126.1	1.544	91.2
Cruise	RF3_rotor	4045.6	866.2	5.743	193.9	1.0	126.1	1.544	91.2
Cruise	RF_rotor								
Cruise	RR_rotor								
Reserve	LF1_rotor								
Reserve	RF1_rotor								
Reserve	LF2_rotor								
Reserve	RF2_rotor								
Reserve	LF3_rotor	3849.3	817.9	6.082	162.2	1.195	100.6	1.935	91.0
Reserve	RF3_rotor	3849.3	817.9	6.082	162.2	1.195	100.6	1.935	91.0
Reserve	RF_rotor								
Reserve	RR_rotor								
Condition	Rotor	Motor RPM	Thrust (N)	Thrust margin	Motor Torque (Nm)	Torque margin	Power (kW)	Power margin	Motor efficiency (%)
Hover	LF1_rotor	7497.7	3323.2	1.013	45.9	1.0	104.5	1.0	86.9
Hover	RF1_rotor	7497.7	3323.2	1.013	45.9	1.0	104.5	1.0	86.9
Hover	LF2_rotor	7366.2	3207.7	1.05	44.4	1.0	99.4	1.0	86.9
Hover	RF2_rotor	7366.2	3207.7	1.05	44.4	1.0	99.4	1.0	86.9
Hover	LF3_rotor	4646.4	1885.7	2.638	76.9	2.522	59.9	3.252	87.5
Hover	RF3_rotor	4646.4	1885.7	2.638	76.9	2.522	59.9	3.252	87.5
Hover	RF_rotor	3772.9	2589.9	1.641	50.6	1.676	56.9	1.838	88.6
Hover	RR_rotor	2344.1	999.8	2.323	22.2	1.403	16.5	3.051	83.5
Hover.OEI.LF1	LF1_rotor	5872.8	906.2	3.715	26.2	1.749	21.3	4.914	85.0
Hover.OEI.LF1	RF1_rotor	7000.3	2743.2	1.227	33.9	1.354	72.7	1.437	86.1
Hover.OEI.LF1	LF2_rotor	7303.5	3153.2	1.068	39.4	1.128	87.6	1.134	86.6
Hover.OEI.LF1	RF2_rotor	5398.8	830.1	4.056	8.7	5.126	17.4	5.699	70.8
Hover.OEI.LF1	LF3_rotor	7460.6	4861.6	1.023	154.2	1.257	189.0	1.031	89.3
Hover.OEI.LF1	RF3_rotor	7044.5	4334.5	1.148	140.4	1.381	162.4	1.199	89.3
Hover.OEI.LF1	RF_rotor	4715.5	3884.6	1.094	64.9	1.308	90.7	1.152	89.0
Hover.OEI.LF1	RR_rotor	3622.7	0.0	0.0	0.3	92.186	3.4	14.742	9.5
Condition	Rotor	Motor RPM	Thrust (N)	Thrust margin	Motor Torque (Nm)	Torque margin	Power (kW)	Power margin	Motor efficiency (%)
Hover.OEI.RF1	LF1_rotor	5343.6	1604.0	2.099	20.5	2.238	34.8	3.001	83.0
Hover.OEI.RF1	RF1_rotor	6237.6	1022.2	3.293	29.4	1.562	25.1	4.163	85.6
Hover.OEI.RF1	LF2_rotor	6556.8	2541.4	1.325	32.3	1.376	64.9	1.532	86.0
Hover.OEI.RF1	RF2_rotor	7545.4	3365.6	1.0	41.8	1.062	96.0	1.034	86.6
Hover.OEI.RF1	LF3_rotor	7504.7	4919.3	1.011	155.7	1.245	191.9	1.015	89.2
Hover.OEI.RF1	RF3_rotor	7514.0	4931.5	1.009	156.0	1.243	192.5	1.011	89.2
Hover.OEI.RF1	RF_rotor	5029.9	0.0	0.0	1.2	72.471	5.9	17.683	26.3
Hover.OEI.RF1	RR_rotor	5271.4	2323.0	1.0	31.2	1.0	50.3	1.0	86.3
Hover.OEI.LF2	LF1_rotor	7396.3	3231.7	1.042	40.3	1.14	90.7	1.152	86.6
Hover.OEI.LF2	RF1_rotor	5433.5	1745.2	1.929	22.7	2.025	38.7	2.699	83.9
Hover.OEI.LF2	LF2_rotor	4711.5	583.2	5.772	17.3	2.568	11.7	8.457	81.3
Hover.OEI.LF2	RF2_rotor	7010.7	2905.5	1.159	36.5	1.216	78.2	1.271	86.4
Hover.OEI.LF2	LF3_rotor	7438.1	4832.4	1.029	153.4	1.264	187.5	1.039	89.3
Hover.OEI.LF2	RF3_rotor	7165.5	4484.7	1.109	144.4	1.343	169.9	1.147	89.3
Hover.OEI.LF2	RF_rotor	5640.0	1245.3	3.414	15.5	5.462	29.0	3.608	79.8
Hover.OEI.LF2	RR_rotor	3782.1	1673.4	1.388	25.1	1.242	29.5	1.705	85.0

Table B.18. Rotor metrics/outputs for the 8 Lift (Tilt 3) configuration (Part 2).

Condition	Rotor	Motor RPM	Thrust (N)	Thrust margin	Motor Torque (Nm)	Torque margin	Power (kW)	Power margin	Motor efficiency (%)
Hover.OEI.RF2	LF1_rotor	5971.7	2108.1	1.597	27.1	1.695	50.1	2.086	85.2
Hover.OEI.RF2	RF1_rotor	6884.8	2802.1	1.201	35.3	1.3	74.3	1.407	86.3
Hover.OEI.RF2	LF2_rotor	6412.8	2431.1	1.385	30.9	1.435	61.0	1.629	85.9
Hover.OEI.RF2	RF2_rotor	6537.6	1122.9	2.998	32.1	1.384	28.6	3.474	86.0
Hover.OEI.RF2	LF3_rotor	7069.6	4365.5	1.139	141.2	1.373	163.9	1.188	89.3
Hover.OEI.RF2	RF3_rotor	7505.0	4919.7	1.011	155.7	1.245	191.9	1.015	89.2
Hover.OEI.RF2	RF_rotor	5656.6	1333.6	3.188	16.6	5.114	30.7	3.402	80.6
Hover.OEI.RF2	RR_rotor	3713.2	1618.4	1.435	24.4	1.281	28.2	1.786	84.8
Hover.OEI.LF3	LF1_rotor	7546.4	3366.4	1.0	41.8	1.098	96.1	1.088	86.6
Hover.OEI.LF3	RF1_rotor	7361.5	1376.8	2.445	13.7	3.345	34.2	3.054	77.9
Hover.OEI.LF3	LF2_rotor	7546.4	3366.4	1.0	41.8	1.062	96.1	1.034	86.6
Hover.OEI.LF3	RF2_rotor	7546.4	3366.4	1.0	41.8	1.062	96.1	1.034	86.6
Hover.OEI.LF3	LF3_rotor	5000.0	0.0	0.0	78.1	2.483	0.0	0.0	87.5
Hover.OEI.LF3	RF3_rotor	7546.4	4974.1	1.0	157.1	1.234	194.7	1.0	89.2
Hover.OEI.LF3	RF_rotor	5111.7	4251.2	1.0	68.7	1.235	104.5	1.0	88.7
Hover.OEI.LF3	RR_rotor	5504.1	0.0	0.0	1.0	31.042	6.2	8.07	23.4
Condition	Rotor	Motor RPM	Thrust (N)	Thrust margin	Motor Torque (Nm)	Torque margin	Power (kW)	Power margin	Motor efficiency (%)
Hover.OEI.RF3	LF1_rotor	7253.6	1376.8	2.445	13.8	3.322	33.9	3.082	78.0
Hover.OEI.RF3	RF1_rotor	7546.4	3366.4	1.0	41.8	1.098	96.1	1.088	86.6
Hover.OEI.RF3	LF2_rotor	7546.4	3366.4	1.0	41.8	1.062	96.1	1.034	86.6
Hover.OEI.RF3	RF2_rotor	7546.4	3366.4	1.0	41.8	1.062	96.1	1.034	86.6
Hover.OEI.RF3	LF3_rotor	7546.4	4974.1	1.0	157.1	1.234	194.7	1.0	89.2
Hover.OEI.RF3	RF3_rotor	5000.0	0.0	0.0	78.1	2.483	0.0	0.0	87.5
Hover.OEI.RF3	RF_rotor	5086.8	4251.2	1.0	68.9	1.23	104.3	1.001	88.7
Hover.OEI.RF3	RR_rotor	4426.0	0.0	0.0	0.2	165.73	4.0	12.558	5.5
Hover.OEI.RF	LF1_rotor	6926.1	2834.1	1.188	35.7	1.286	75.5	1.385	86.4
Hover.OEI.RF	RF1_rotor	6947.6	2853.4	1.18	35.9	1.278	76.2	1.372	86.4
Hover.OEI.RF	LF2_rotor	6897.3	2812.2	1.197	35.4	1.253	74.7	1.33	86.4
Hover.OEI.RF	RF2_rotor	6904.1	2817.8	1.195	35.5	1.251	74.9	1.327	86.4
Hover.OEI.RF	LF3_rotor	5848.0	2987.1	1.665	102.7	1.888	99.2	1.963	88.7
Hover.OEI.RF	RF3_rotor	5790.9	2929.1	1.698	101.0	1.92	96.6	2.015	88.7
Hover.OEI.RF	RF_rotor	5291.7	2264.4	1.877	84.8	1.0	59.6	1.752	88.3
Hover.OEI.RF	RR_rotor	4284.7	1206.6	1.925	15.7	1.986	22.1	2.272	80.2
Condition	Rotor	Motor RPM	Thrust (N)	Thrust margin	Motor Torque (Nm)	Torque margin	Power (kW)	Power margin	Motor efficiency (%)
Hover.OEI.RR	LF1_rotor	6861.1	2779.4	1.211	35.0	1.31	73.5	1.423	86.3
Hover.OEI.RR	RF1_rotor	6274.2	2327.1	1.447	29.7	1.545	57.4	1.821	85.7
Hover.OEI.RR	LF2_rotor	6696.9	2651.2	1.27	33.5	1.323	68.8	1.444	86.2
Hover.OEI.RR	RF2_rotor	7073.1	2957.5	1.138	37.1	1.196	80.1	1.24	86.5
Hover.OEI.RR	LF3_rotor	5605.7	2744.7	1.812	95.4	2.031	88.7	2.197	88.5
Hover.OEI.RR	RF3_rotor	6183.3	3339.5	1.489	112.9	1.717	115.0	1.694	89.0
Hover.OEI.RR	RF_rotor	4969.4	3549.0	1.198	55.4	1.532	81.9	1.275	88.6
Hover.OEI.RR	RR_rotor	3037.3	399.8	5.811	13.1	2.384	6.0	8.38	77.7

Table B.19. Rotor metrics/outputs for the 8 Lift (Tilt 3) configuration (Part 3).

Condition	Rotor	Rotor RPM	J	Thrust coeff	Power coeff	Disk loading (kg/m^2)	Tip Mach	Blade loading coeff	Rotor efficiency (%)
Cruise	LF1_rotor								
Cruise	RF1_rotor								
Cruise	LF2_rotor								
Cruise	RF2_rotor								
Cruise	LF3_rotor	1011.4	1.914	0.216	0.452	34.206	0.329	1.438	91.4
Cruise	RF3_rotor	1011.4	1.914	0.216	0.452	34.206	0.329	1.438	91.4
Cruise	RF_rotor								
Cruise	RR_rotor								
Reserve	LF1_rotor								
Reserve	RF1_rotor								
Reserve	LF2_rotor								
Reserve	RF2_rotor								
Reserve	LF3_rotor	962.3	1.677	0.225	0.417	32.299	0.313	1.5	90.4
Reserve	RF3_rotor	962.3	1.677	0.225	0.417	32.299	0.313	1.5	90.4
Reserve	RF_rotor								
Reserve	RR_rotor								
Condition	Rotor	Rotor RPM	J	Thrust coeff	Power coeff	Disk loading (kg/m^2)	Tip Mach	Blade loading coeff	Rotor efficiency (%)
Hover	LF1_rotor	1874.4	0.077	0.085	0.026	56.085	0.596	1.41	76.8
Hover	RF1_rotor	1874.4	0.077	0.085	0.026	56.085	0.596	1.41	76.8
Hover	LF2_rotor	1841.6	0.079	0.085	0.026	54.135	0.586	1.41	76.6
Hover	RF2_rotor	1841.6	0.079	0.085	0.026	54.135	0.586	1.41	76.6
Hover	LF3_rotor	1161.6	0.125	0.225	0.112	57.283	0.369	1.5	76.4
Hover	RF3_rotor	1161.6	0.125	0.225	0.112	57.283	0.369	1.5	76.4
Hover	RF_rotor	943.2	0.116	0.085	0.027	24.914	0.397	1.41	71.9
Hover	RR_rotor	586.0	0.187	0.085	0.031	9.618	0.247	1.41	63.2
Hover.OEI.LF1	LF1_rotor	1468.2	0.04	0.085	0.024	34.409	0.467	1.41	82.4
Hover.OEI.LF1	RF1_rotor	1750.1	0.033	0.08	0.022	46.296	0.557	1.335	83.5
Hover.OEI.LF1	LF2_rotor	1825.9	0.032	0.085	0.023	53.216	0.581	1.41	84.9
Hover.OEI.LF1	RF2_rotor	1349.7	0.043	0.041	0.009	14.009	0.429	0.679	70.5
Hover.OEI.LF1	LF3_rotor	1865.1	0.031	0.225	0.087	147.686	0.593	1.5	98.1
Hover.OEI.LF1	RF3_rotor	1761.1	0.033	0.225	0.089	131.674	0.56	1.5	96.1
Hover.OEI.LF1	RF_rotor	1178.9	0.037	0.081	0.022	37.369	0.497	1.354	82.4
Hover.OEI.LF1	RR_rotor	905.7	0.048	0.0	0.0	0.0	0.382	0.0	0.0
Condition	Rotor	Rotor RPM	J	Thrust coeff	Power coeff	Disk loading (kg/m^2)	Tip Mach	Blade loading coeff	Rotor efficiency (%)
Hover.OEI.RF1	LF1_rotor	1335.9	0.043	0.08	0.022	27.071	0.425	1.34	80.9
Hover.OEI.RF1	RF1_rotor	1559.4	0.037	0.085	0.024	38.817	0.496	1.41	83.0
Hover.OEI.RF1	LF2_rotor	1639.2	0.035	0.085	0.023	42.891	0.521	1.41	83.5
Hover.OEI.RF1	RF2_rotor	1886.3	0.031	0.085	0.023	56.8	0.6	1.41	85.4
Hover.OEI.RF1	LF3_rotor	1876.2	0.031	0.225	0.087	149.438	0.597	1.5	98.4
Hover.OEI.RF1	RF3_rotor	1878.5	0.031	0.225	0.087	149.809	0.597	1.5	98.4
Hover.OEI.RF1	RF_rotor	1257.5	0.035	0.0	0.0	0.0	0.53	0.0	0.0
Hover.OEI.RF1	RR_rotor	1317.8	0.033	0.039	0.009	22.347	0.555	0.648	70.9
Hover.OEI.LF2	LF1_rotor	1849.1	0.031	0.085	0.023	54.541	0.588	1.409	85.1
Hover.OEI.LF2	RF1_rotor	1358.4	0.043	0.085	0.024	29.454	0.432	1.41	81.7
Hover.OEI.LF2	LF2_rotor	1177.9	0.049	0.085	0.024	22.146	0.375	1.41	80.5
Hover.OEI.LF2	RF2_rotor	1752.7	0.033	0.085	0.023	49.035	0.557	1.41	84.4
Hover.OEI.LF2	LF3_rotor	1859.5	0.031	0.225	0.087	146.798	0.591	1.5	98.0
Hover.OEI.LF2	RF3_rotor	1791.4	0.032	0.225	0.088	136.236	0.57	1.5	96.7
Hover.OEI.LF2	RF_rotor	1410.0	0.031	0.018	0.004	11.98	0.594	0.303	52.2
Hover.OEI.LF2	RR_rotor	945.5	0.046	0.054	0.013	16.097	0.398	0.907	75.0

Table B.20. Rotor metrics/outputs for the 8 Lift (Tilt 3) configuration (Part 4).

Condition	Rotor	Rotor RPM	J	Thrust coeff	Power coeff	Disk loading (kg/m^2)	Tip Mach	Blade loading coeff	Rotor efficiency (%)
Hover.OEI.RF2	LF1_rotor	1492.9	0.039	0.085	0.024	35.577	0.475	1.41	82.5
Hover.OEI.RF2	RF1_rotor	1721.2	0.034	0.085	0.023	47.29	0.547	1.41	84.1
Hover.OEI.RF2	LF2_rotor	1603.2	0.036	0.085	0.024	41.028	0.51	1.41	83.3
Hover.OEI.RF2	RF2_rotor	1634.4	0.036	0.085	0.024	42.641	0.52	1.41	83.5
Hover.OEI.RF2	LF3_rotor	1767.4	0.033	0.225	0.089	132.614	0.562	1.5	96.2
Hover.OEI.RF2	RF3_rotor	1876.3	0.031	0.225	0.087	149.452	0.597	1.5	98.4
Hover.OEI.RF2	RF_rotor	1414.2	0.031	0.019	0.004	12.829	0.596	0.323	54.1
Hover.OEI.RF2	RR_rotor	928.3	0.047	0.055	0.014	15.569	0.391	0.91	74.9
Hover.OEI.LF3	LF1_rotor	1886.6	0.031	0.085	0.023	56.814	0.6	1.41	85.4
Hover.OEI.LF3	RF1_rotor	1840.4	0.032	0.036	0.008	23.236	0.585	0.606	69.8
Hover.OEI.LF3	LF2_rotor	1886.6	0.031	0.085	0.023	56.814	0.6	1.41	85.4
Hover.OEI.LF3	RF2_rotor	1886.6	0.031	0.085	0.023	56.814	0.6	1.41	85.4
Hover.OEI.LF3	LF3_rotor	1250.0	0.046	0.225	0.098	66.334	0.398	1.5	87.0
Hover.OEI.LF3	RF3_rotor	1886.6	0.031	0.225	0.086	151.102	0.6	1.5	98.6
Hover.OEI.LF3	RF_rotor	1277.9	0.034	0.076	0.02	40.895	0.538	1.261	82.2
Hover.OEI.LF3	RR_rotor	1376.0	0.032	0.0	0.0	0.0	0.58	0.0	0.0
Condition	Rotor	Rotor RPM	J	Thrust coeff	Power coeff	Disk loading (kg/m^2)	Tip Mach	Blade loading coeff	Rotor efficiency (%)
Hover.OEI.RF3	LF1_rotor	1813.4	0.032	0.037	0.008	23.236	0.577	0.624	70.3
Hover.OEI.RF3	RF1_rotor	1886.6	0.031	0.085	0.023	56.814	0.6	1.41	85.4
Hover.OEI.RF3	LF2_rotor	1886.6	0.031	0.085	0.023	56.814	0.6	1.41	85.4
Hover.OEI.RF3	RF2_rotor	1886.6	0.031	0.085	0.023	56.814	0.6	1.41	85.4
Hover.OEI.RF3	LF3_rotor	1886.6	0.031	0.225	0.086	151.102	0.6	1.5	98.6
Hover.OEI.RF3	RF3_rotor	1250.0	0.046	0.225	0.098	66.334	0.398	1.5	87.0
Hover.OEI.RF3	RF_rotor	1271.7	0.034	0.076	0.02	40.895	0.536	1.273	82.3
Hover.OEI.RF3	RR_rotor	1106.5	0.04	0.0	0.0	0.0	0.466	0.0	0.0
Hover.OEI.RF	LF1_rotor	1731.5	0.034	0.085	0.023	47.83	0.551	1.409	84.2
Hover.OEI.RF	RF1_rotor	1736.9	0.033	0.085	0.023	48.156	0.552	1.41	84.3
Hover.OEI.RF	LF2_rotor	1724.3	0.034	0.085	0.023	47.461	0.548	1.41	84.2
Hover.OEI.RF	RF2_rotor	1726.0	0.034	0.085	0.023	47.556	0.549	1.41	84.2
Hover.OEI.RF	LF3_rotor	1462.0	0.04	0.225	0.094	90.742	0.465	1.5	90.6
Hover.OEI.RF	RF3_rotor	1447.7	0.04	0.225	0.094	88.98	0.46	1.5	90.3
Hover.OEI.RF	RF_rotor	1322.9	0.033	0.085	0.023	49.012	0.557	1.41	84.4
Hover.OEI.RF	RR_rotor	1071.2	0.041	0.031	0.007	11.607	0.451	0.509	64.8
Condition	Rotor	Rotor RPM	J	Thrust coeff	Power coeff	Disk loading (kg/m^2)	Tip Mach	Blade loading coeff	Rotor efficiency (%)
Hover.OEI.RR	LF1_rotor	1715.3	0.034	0.084	0.023	46.907	0.546	1.408	84.1
Hover.OEI.RR	RF1_rotor	1568.6	0.037	0.085	0.024	39.274	0.499	1.41	83.1
Hover.OEI.RR	LF2_rotor	1674.2	0.035	0.085	0.023	44.743	0.532	1.41	83.8
Hover.OEI.RR	RF2_rotor	1768.3	0.033	0.085	0.023	49.912	0.562	1.41	84.5
Hover.OEI.RR	LF3_rotor	1401.4	0.041	0.225	0.095	83.379	0.446	1.5	89.5
Hover.OEI.RR	RF3_rotor	1545.8	0.038	0.225	0.093	101.447	0.492	1.5	92.1
Hover.OEI.RR	RF_rotor	1242.4	0.035	0.067	0.017	34.14	0.523	1.114	80.0
Hover.OEI.RR	RR_rotor	759.3	0.058	0.045	0.011	8.653	0.32	0.756	70.6

Appendix C

Refined MDO data tables

Table C.1. Rotor metrics/outputs for the 6 Lift (Tractor) configuration (Part 1).

Condition	Rotor	Rotor RPM	Pitch (°)	Diameter (m)	Thrust (N)	Thrust margin
Cruise	LF1_rotor					
Cruise	RF1_rotor					
Cruise	LF2_rotor					
Cruise	RF2_rotor					
Cruise	LP_rotor	1909.9	25.5	2.0	939.8	1.258
Cruise	RP_rotor	1909.9	25.5	2.0	939.8	1.258
Cruise	RF_rotor					
Cruise	RR_rotor					
Reserve	LF1_rotor					
Reserve	RF1_rotor					
Reserve	LF2_rotor					
Reserve	RF2_rotor					
Reserve	LP_rotor	1528.0	31.0	2.0	1182.3	1.0
Reserve	RP_rotor	1528.0	31.0	2.0	1182.3	1.0
Reserve	RF_rotor					
Reserve	RR_rotor					
Condition	Rotor	Rotor RPM	Pitch (°)	Diameter (m)	Thrust (N)	Thrust margin
Hover	LF1_rotor	1380.4	-5.0	3.1	5657.0	1.228
Hover	RF1_rotor	1375.3	-5.0	3.1	5614.2	1.0
Hover	LF2_rotor	1364.3	-5.0	3.1	5451.1	1.174
Hover	RF2_rotor	1375.2	-5.0	3.1	5539.0	1.156
Hover	LP_rotor					
Hover	RP_rotor					
Hover	RF_rotor	1334.8	-3.3	2.738	1986.6	1.002
Hover	RR_rotor	424.9	1.9	2.738	209.3	1.669
Hover.OEI.LF1	LF1_rotor	1394.1	3.9	3.1	4826.6	1.439
Hover.OEI.LF1	RF1_rotor	986.9	3.9	3.1	4826.6	1.163
Hover.OEI.LF1	LF2_rotor	1374.8	-2.1	3.1	6401.1	1.0
Hover.OEI.LF1	RF2_rotor	1374.8	-2.1	3.1	6401.1	1.0
Hover.OEI.LF1	LP_rotor					
Hover.OEI.LF1	RP_rotor					
Hover.OEI.LF1	RF_rotor	1329.4	-3.2	2.738	1990.0	1.0
Hover.OEI.LF1	RR_rotor	191.0	-2.2	2.738	11.7	29.902

Table C.2. Rotor metrics/outputs for the 6 Lift (Tractor) configuration (Part 2).

Condition	Rotor	Rotor RPM	Pitch (°)	Diameter (m)	Thrust (N)	Thrust margin
Hover.OEI.LF2	LF1_rotor	1394.0	-2.7	3.1	6946.9	1.0
Hover.OEI.LF2	RF1_rotor	1241.5	-2.7	3.1	5501.0	1.021
Hover.OEI.LF2	LF2_rotor	1375.2	-1.0	3.1	3352.0	1.91
Hover.OEI.LF2	RF2_rotor	1335.2	-1.0	3.1	6317.1	1.013
Hover.OEI.LF2	LP_rotor					
Hover.OEI.LF2	RP_rotor					
Hover.OEI.LF2	RF_rotor	1339.7	-3.4	2.738	1990.8	1.0
Hover.OEI.LF2	RR_rotor	670.2	-5.0	2.738	349.3	1.0
Hover.OEI.RF	LF1_rotor	1309.0	-4.8	3.1	5178.1	1.342
Hover.OEI.RF	RF1_rotor	1314.1	-4.8	3.1	5219.5	1.076
Hover.OEI.RF	LF2_rotor	1370.2	-2.9	3.1	6121.6	1.046
Hover.OEI.RF	RF2_rotor	1360.8	-2.9	3.1	6036.6	1.06
Hover.OEI.RF	LP_rotor					
Hover.OEI.RF	RP_rotor					
Hover.OEI.RF	RF_rotor	1526.3	-0.9	2.738	1561.9	1.275
Hover.OEI.RF	RR_rotor	590.9	0.5	2.738	339.5	1.029
Condition	Rotor	Rotor RPM	Pitch (°)	Diameter (m)	Thrust (N)	Thrust margin
Hover.OEI.RR	LF1_rotor	1178.0	-1.8	3.1	5277.4	1.316
Hover.OEI.RR	RF1_rotor	1175.4	-1.8	3.1	5254.2	1.069
Hover.OEI.RR	LF2_rotor	1365.1	-3.5	3.1	5910.4	1.083
Hover.OEI.RR	RF2_rotor	1370.6	-3.5	3.1	5958.1	1.074
Hover.OEI.RR	LP_rotor					
Hover.OEI.RR	RP_rotor					
Hover.OEI.RR	RF_rotor	1119.6	0.3	2.738	1875.5	1.062
Hover.OEI.RR	RR_rotor	624.3	0.2	2.738	181.6	1.924

Table C.3. Rotor metrics/outputs for the 6 Lift (Tractor) configuration (Part 3).

Condition	Rotor	Motor torque (Nm)	Torque margin	Power (kW)	Power margin	Efficiency (%)
Cruise	LF1_rotor					
Cruise	RF1_rotor					
Cruise	LF2_rotor					
Cruise	RF2_rotor					
Cruise	LP_rotor	107.9	1.379	142.2	1.103	72.6
Cruise	RP_rotor	107.9	1.379	142.2	1.103	72.6
Cruise	RF_rotor					
Cruise	RR_rotor					
Reserve	LF1_rotor					
Reserve	RF1_rotor					
Reserve	LF2_rotor					
Reserve	RF2_rotor					
Reserve	LP_rotor	148.7	1.0	156.8	1.0	69.0
Reserve	RP_rotor	148.7	1.0	156.8	1.0	69.0
Reserve	RF_rotor					
Reserve	RR_rotor					
Condition	Rotor	Motor torque (Nm)	Torque margin	Power (kW)	Power margin	Efficiency (%)
Hover	LF1_rotor	133.2	1.423	126.9	1.437	70.1
Hover	RF1_rotor	132.2	1.442	125.5	1.035	70.1
Hover	LF2_rotor	127.9	1.308	120.4	1.318	69.8
Hover	RF2_rotor	130.0	1.326	123.3	1.288	69.9
Hover	LP_rotor					
Hover	RP_rotor					
Hover	RF_rotor	30.1	1.148	27.7	1.003	77.1
Hover	RR_rotor	3.7	1.449	1.1	2.177	66.4
Hover.OEI.LF1	LF1_rotor	189.5	1.0	182.3	1.0	38.4
Hover.OEI.LF1	RF1_rotor	190.7	1.0	129.8	1.0	54.0
Hover.OEI.LF1	LF2_rotor	167.4	1.0	158.8	1.0	67.4
Hover.OEI.LF1	RF2_rotor	167.4	1.03	158.8	1.0	67.4
Hover.OEI.LF1	LP_rotor					
Hover.OEI.LF1	RP_rotor					
Hover.OEI.LF1	RF_rotor	30.3	1.14	27.8	1.0	77.0
Hover.OEI.LF1	RR_rotor	0.3	16.649	0.0	55.636	22.4

Table C.4. Rotor metrics/outputs for the 6 Lift (Tractor) configuration (Part 4).

Condition	Rotor	Motor torque (Nm)	Torque margin	Power (kW)	Power margin	Efficiency (%)
Hover.OEI.LF2	LF1_rotor	189.5	1.0	182.3	1.0	66.4
Hover.OEI.LF2	RF1_rotor	150.5	1.267	128.9	1.007	66.1
Hover.OEI.LF2	LF2_rotor	91.4	1.832	86.7	1.831	46.8
Hover.OEI.LF2	RF2_rotor	172.4	1.0	158.8	1.0	66.1
Hover.OEI.LF2	LP_rotor					
Hover.OEI.LF2	RP_rotor					
Hover.OEI.LF2	RF_rotor	30.0	1.149	27.8	1.0	77.1
Hover.OEI.LF2	RR_rotor	5.2	1.05	2.4	1.0	65.8
Hover.OEI.RF	LF1_rotor	123.8	1.531	111.8	1.63	69.6
Hover.OEI.RF	RF1_rotor	124.8	1.528	113.2	1.147	69.6
Hover.OEI.RF	LF2_rotor	155.1	1.079	146.6	1.083	68.3
Hover.OEI.RF	RF2_rotor	153.0	1.127	143.6	1.106	68.3
Hover.OEI.RF	LP_rotor					
Hover.OEI.RF	RP_rotor					
Hover.OEI.RF	RF_rotor	26.4	1.309	27.8	1.0	53.6
Hover.OEI.RF	RR_rotor	5.4	1.0	2.2	1.08	68.1
Condition	Rotor	Motor torque (Nm)	Torque margin	Power (kW)	Power margin	Efficiency (%)
Hover.OEI.RR	LF1_rotor	153.1	1.238	124.4	1.465	64.4
Hover.OEI.RR	RF1_rotor	152.4	1.251	123.6	1.051	64.4
Hover.OEI.RR	LF2_rotor	146.6	1.142	138.1	1.15	68.8
Hover.OEI.RR	RF2_rotor	147.8	1.167	139.7	1.136	68.8
Hover.OEI.RR	LP_rotor					
Hover.OEI.RR	RP_rotor					
Hover.OEI.RR	RF_rotor	34.5	1.0	26.7	1.042	73.4
Hover.OEI.RR	RR_rotor	2.9	1.904	1.2	1.946	48.0

Bibliography

[1] Christian Alba, Ali Elham, Leo LM Veldhuis, and Brian J German. A surrogate-based multi-disciplinary design optimization framework exploiting wing-propeller interaction. In *18th AIAA/ISSMO Multidisciplinary Analysis and Optimization Conference*, page 4329, 2017.

[2] Alessandro Bacchini and Enrico Cestino. Electric vtol configurations comparison. *Aerospace*, 6(3):26, 2019.

[3] Pierre-Marie Basset, Binh Dang Vu, Philippe Beaumier, Gabriel Reboul, and Biel Ortun. Models and methods at onera for the presizing of evtol hybrid aircraft including analysis of failure scenarios. 2018.

[4] Nicholas K Borer, Joseph M Derlaga, Karen A Deere, Melissa B Carter, Sally Viken, Michael D Patterson, Brandon Litherland, and Alex Stoll. Comparison of aero-propulsive performance predictions for distributed propulsion configurations. In *55th AIAA Aerospace Sciences Meeting*, page 0209, 2017.

[5] Nicholas K Borer and Mark D Moore. Integrated propeller-wing design exploration for distributed propulsion concepts. In *53rd AIAA Aerospace Sciences Meeting*, page 1672, 2015.

[6] John Brandt and Michael Selig. Propeller performance data at low reynolds numbers. In *49th AIAA Aerospace Sciences Meeting including the New Horizons Forum and Aerospace Exposition*, page 1255, 2011.

[7] Benjamin J Brelje and Joaquim RRA Martins. Electric, hybrid, and turboelectric fixed-wing aircraft: A review of concepts, models, and design approaches. *Progress in Aerospace Sciences*, 104:1–19, 2019.

[8] John T Conway. Analytical solutions for the actuator disk with variable radial distribution of load. *Journal of Fluid Mechanics*, 297:327–355, 1995.

[9] Christopher Courtin, Michael J Burton, Alison Yu, Patrick Butler, Parker D Vascik, and R John Hansman. Feasibility study of short takeoff and landing urban air mobility vehicles using geometric programming. In *2018 Aviation Technology, Integration, and Operations Conference*, page 4151, 2018.

[10] E. J. Cramer, J. E. Dennis, P. D. Frank, R. M. Lewis, and G. R. Shubin. Problem formulation for multidisciplinary optimization. *SIAM Journal on Optimization*, 4(4):754–776, 1994.

[11] Karen A Deere, Sally Viken, Melissa Carter, Jeffrey K Viken, Joseph M Derlaga, and Alex M Stoll. Comparison of high-fidelity computational tools for wing design of a distributed electric propulsion aircraft. In *35th AIAA Applied Aerodynamics Conference*, page 3925, 2017.

[12] Robert W Deters, Gavin Kumar Ananda Krishnan, and Michael S Selig. Reynolds number effects on the performance of small-scale propellers. In *32nd AIAA applied aerodynamics conference*, page 2151, 2014.

[13] Philip E Gill, Walter Murray, and Michael A Saunders. SNOPT: An sqp algorithm for large-scale constrained optimization. *SIAM review*, 47(1):99–131, 2005.

[14] Justin S. Gray, John T. Hwang, Joaquim R. R. A. Martins, Kenneth T. Moore, and Bret A. Naylor. OpenMDAO: An open-source framework for multidisciplinary design, analysis, and optimization. *Structural and Multidisciplinary Optimization*, 59(4):1075–1104, April 2019.

[15] Ohad Gur. Maximum propeller efficiency estimation. *Journal of aircraft*, 51(6):2035–2038, 2014.

[16] Tae Hyun Ha, Keunseok Lee, and John T Hwang. Large-scale design and economics optimization of evtol concepts for urban air mobility. In *2019 AIAA/ASCE/AHS/ASC Structures, Structural Dynamics, and Materials Conference*, 2019.

[17] Naourez Ben Hadj, Rihab Abdelmoula, Mohamed Chaieb, and Rafik Neji. Permanent magnet motor efficiency map calculation and small electric vehicle consumption optimization. *Journal of Electrical Systems*, 14(2):127–147, 2018.

[18] Andrew Hahn. Vehicle sketch pad: a parametric geometry modeler for conceptual aircraft design. In *48th AIAA Aerospace Sciences Meeting Including the New Horizons Forum and Aerospace Exposition*, page 657, 2010.

[19] John T. Hwang, John P. Jasa, and Joaquim R. R. A. Martins. High-fidelity design-allocation optimization of a commercial aircraft maximizing airline profit. *Journal of Aircraft*, pages 1–15, 2019.

[20] John T. Hwang and Joaquim R. R. A. Martins. A computational architecture for coupling heterogeneous numerical models and computing coupled derivatives. *ACM Trans. Math. Softw.*, 44(4):37:1–37:39, jun 2018.

[21] John T Hwang and Andrew Ning. Large-scale multidisciplinary optimization of an electric aircraft for on-demand mobility. In *2018 AIAA/ASCE/AHS/ASC Structures, Structural Dynamics, and Materials Conference*, 2018.

[22] John P. Jasa, John T. Hwang, and Joaquim R. R. A. Martins. Open-source coupled aerostructural optimization using python. *Structural and Multidisciplinary Optimization*, 57(4):1815–1827, Apr 2018.

[23] Wayne Johnson. Ndarc-nasa design and analysis of rotorcraft. 2015.

[24] Th Kármán, JM Burgers, and William Frederick Durand. *Aerodynamic Theory: A General Review of Progress Under a Grant of the Guggenheim Fund for the Promotion of Aeronautics*. Springer, 1935.

[25] Imke C Kleinbekman, Mihaela A Mitici, and Peng Wei. evtol arrival sequencing and scheduling for on-demand urban air mobility. In *2018 IEEE/AIAA 37th Digital Avionics Systems Conference (DASC)*, pages 1–7. IEEE, 2018.

[26] Trent W Lukaczyk, Andrew D Wendorff, Michael Colonno, Thomas D Economon, Juan J Alonso, Tarik H Orra, and Carlos Ilario. Suave: an open-source environment for multi-fidelity conceptual vehicle design. In *16th AIAA/ISSMO Multidisciplinary Analysis and Optimization Conference*, page 3087, 2015.

[27] Kevin R Moore and Andrew Ning. Distributed electric propulsion effects on existing aircraft through multidisciplinary optimization. In *2018 AIAA/ASCE/AHS/ASC Structures, Structural Dynamics, and Materials Conference*, page 1652, 2018.

[28] SA Ning. *CCBlade documentation*. National Renewable Energy Laboratory, 2013.

[29] Ruben E Perez, Peter W Jansen, and Joaquim RRA Martins. pyopt: a python-based object-oriented framework for nonlinear constrained optimization. *Structural and Multidisciplinary Optimization*, 45(1):101–118, 2012.

[30] Daniel P. Raymer. *Aircraft Design: A Conceptual Approach*. AIAA, 5th edition, 2012.

[31] Umberto Saetti, Jacob Enciu, and Joseph Francis Horn. Performance and design optimization of the f-helix evtol concept. In *Vertical Flight Society's 75th Annual Forum and Technology Display*, 2019.

[32] Christopher Silva, Wayne R Johnson, Eduardo Solis, Michael D Patterson, and Kevin R Antcliff. Vtol urban air mobility concept vehicles for technology development. In *2018 Aviation Technology, Integration, and Operations Conference*, page 3847, 2018.

[33] B-K Song, T Sun, J-P Hong, and J-J Lee. Hysteresis torque estimation by using iron-loss analysis in permanent magnet synchronous motor. *IET electric power applications*, 5(7):558–562, 2011.

[34] David P Thipphavong, Rafael Apaza, Bryan Barmore, Vernol Battiste, Barbara Burian, Quang Dao, Michael Feary, Susie Go, Kenneth H Goodrich, Jeffrey Homola, Husni R Idris, Parimal H Kopardekar, Joel B Lachter, Natasha A Neogi, Hok K Ng, Rosa M Oseguera-Lohr, Michael D Patterson, and Savita A Verma. Urban air mobility airspace integration concepts and considerations. In *2018 Aviation Technology, Integration, and Operations Conference*, page 3676, 2018.

[35] Julius M Vegh, Emilio Botero, Matthew Clarke, Jordan Smart, and Juan Alonso. Current capabilities and challenges of ndarc and suave for evtol aircraft design and analysis. In *AIAA Propulsion and Energy 2019 Forum*, page 4505, 2019.

[36] Leonardus L M Veldhuis. *Propeller Wing Aerodynamic Interference*. PhD thesis, Delft University of Technology, 2005.